UDK 621.3:(53+54+621+66)(05)(497.1)=00 ISSN 0352-9045

INFORMACIJE MIDEM

1 ○ 2006

Strokovno društvo za mikroelektroniko
elektronske sestavne dele in materiale

Strokovna revija za mikroelektroniko, elektronske sestavne dele in materiale
Journal of Microelectronics, Electronic Components and Materials

INFORMACIJE MIDEM, LETNIK 36, ŠT. 1(117), LJUBLJANA, marec 2006

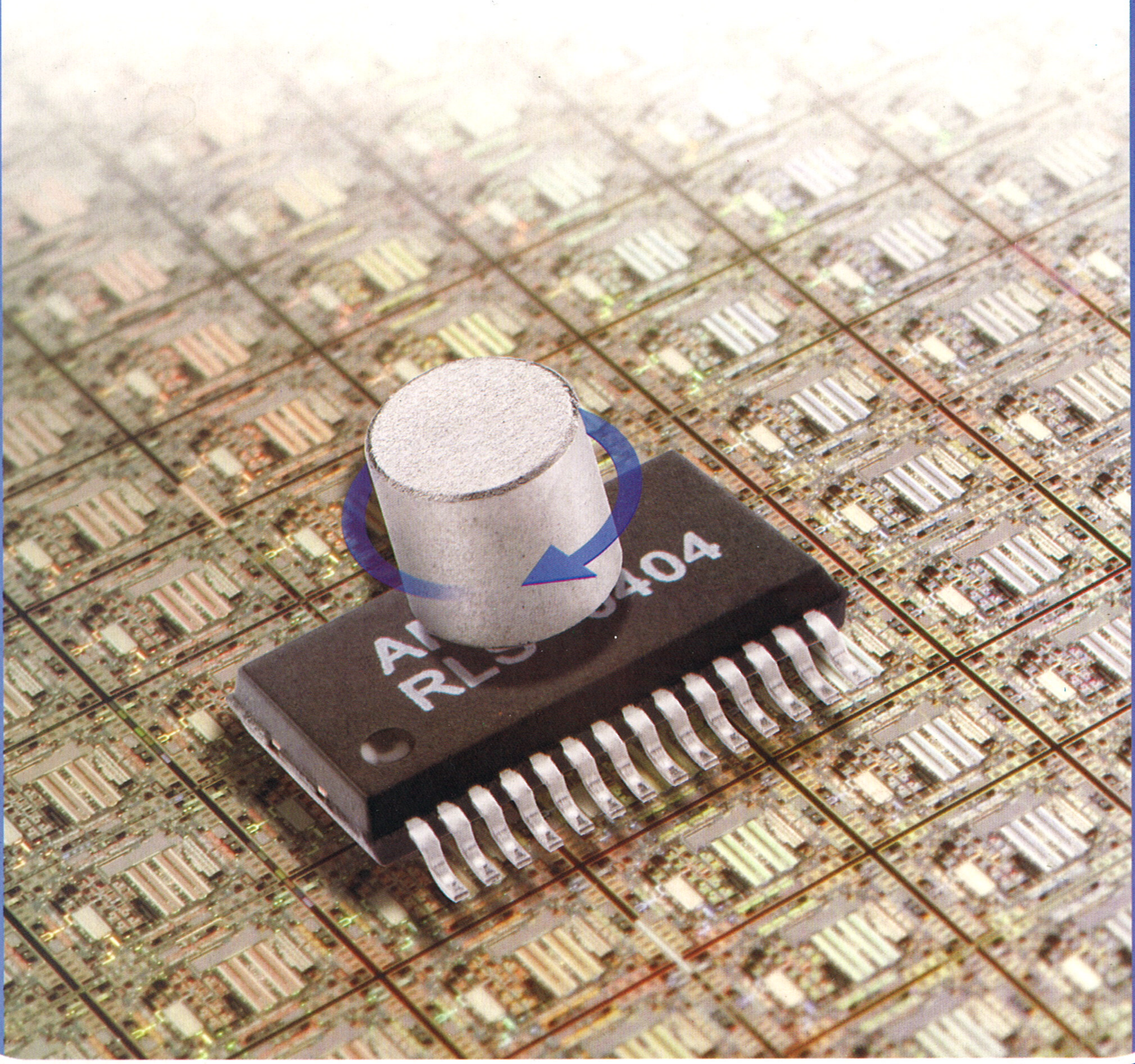

UDK 621.3:(53+54+621+66)(05)(497.1)=00 ISSN 0352-9045

INFORMACIJE MIDEM 1 ○ 2006

INFORMACIJE MIDEM LETNIK 36, ŠT. 1(117), LJUBLJANA, MAREC 2006

INFORMACIJE MIDEM VOLUME 36, NO. 1(117), LJUBLJANA, MARCH 2006

Revija izhaja trimesečno (marec, junij, september, december). Izdaja strokovno društvo za mikroelektroniko, elektronske sestavne dele in materiale - MIDEM.
Published quarterly (march, june, september, december) by Society for Microelectronics, Electronic Components and Materials - MIDEM.

Naslov uredništva
Headquarters

Uredništvo Informacije MIDEM
MIDEM pri MIKROIKS
Stegne 11, 1521 Ljubljana, Slovenija
tel.: + 386 (0)1 51 33 768
fax: + 386 (0)1 51 33 771
e-mail: Iztok.Sorli@guest.arnes.si
http://www.midem-drustvo.si/

Letna naročnina znaša 12.000,00 SIT, cena posamezne številke je 3000,00 SIT. Člani in sponzorji MIDEM prejemajo Informacije MIDEM brezplačno.
Annual subscription rate is EUR 100, separate issue is EUR 25. MIDEM members and Society sponsors receive Informacije MIDEM for free.

Znanstveni svet za tehnične vede I je podal pozitivno mnenje o reviji kot znanstveno strokovni reviji za mikroelektroniko, elektronske sestavne dele in materiale. Izdajo revije sofinancirajo ARRS in sponzorji društva.
Scientific Council for Technical Sciences of Slovene Research Agency has recognized Informacije MIDEM as scientific Journal for microelectronics, electronic components and materials.
Publishing of the Journal is financed by Slovene Research Agency and by Society sponsors.

Znanstveno strokovne prispevke objavljene v Informacijah MIDEM zajemamo v podatkovne baze COBISS in INSPEC.

Prispevke iz revije zajema ISI® v naslednje svoje produkte: Sci Search®, Research Alert® in Materials Science Citation Index™

Scientific and professional papers published in Informacije MIDEM are assessed into COBISS and INSPEC databases.

The Journal is indexed by ISI® for Sci Search®, Research Alert® and Material Science Citation Index™

Po mnenju Ministrstva za informiranje št.23/300-92 šteje glasilo Informacije MIDEM med proizvode informativnega značaja.

Grafična priprava in tisk
Printed by

BIRO M, Ljubljana

Naklada
Circulation

1000 izvodov
1000 issues

Poštnina plačana pri pošti 1102 Ljubljana
Slovenia Taxe Percue

UDK621.3:(53+54+621+66), ISSN0352-9045 Informacije MIDEM 36(2006)1, Ljubljana

VSEBINA **CONTENT**

Obnovitev članstva v strokovnem društvu MIDEM in iz tega izhajajoče ugodnosti in obveznosti

Spoštovani,

V svojem več desetletij dolgem obstoju in delovanju smo si prizadevali narediti društvo privlačno in koristno vsem članom.Z delovanjem društva ste se srečali tudi vi in se odločili, da se v društvo včlanite. Življenske poti, zaposlitev in strokovno zanimanje pa se z leti spreminjajo, najrazličnejši dogodki, izzivi in odločitve so vas morda usmerili v povsem druga področja in vaš interes za delovanje ali članstvo v društvu se je z leti močno spremenil, morda izginil. Morda pa vas aktivnosti društva kljub temu še vedno zanimajo, če ne drugače, kot spomin na prijetne čase, ki smo jih skupaj preživeli. Spremenili so se tudi naslovi in način komuniciranja.

Ker je seznam članstva postal dolg, očitno pa je, da mnogi nekdanji člani nimajo več interesa za sodelovanje v društvu, se je Izvršilni odbor društva odločil, da stanje članstva uredi in **vas zato prosi, da izpolnite in nam pošljete obrazec priložen na koncu revije.**

Naj vas ponovno spomnimo na ugodnosti, ki izhajajo iz vašega članstva. Kot član strokovnega društva prejemate revijo »Informacije MIDEM«, povabljeni ste na strokovne konference, kjer lahko predstavite svoje raziskovalne in razvojne dosežke ali srečate stare znance in nove, povabljene predavatelje s področja, ki vas zanima. O svojih dosežkih in problemih lahko poročate v strokovni reviji, ki ima ugleden IMPACT faktor.S svojimi predlogi lahko usmerjate delovanje društva.

Vaša obveza je plačilo članarine 25 EUR na leto. Članarino lahko plačate na transakcijski račun društva pri A-banki : 051008010631192. Pri nakazilu ne pozabite navesti svojega imena!

Upamo, da vas delovanje društva še vedno zanima in da boste članstvo obnovili. Žal pa bomo morali dosedanje člane, ki članstva ne boste obnovili do konca leta 2006, brisati iz seznama članstva.

Prijavnice pošljite na naslov:

MIDEM pri MIKROIKS

Stegne 11

1521 Ljubljana

Ljubljana, marec 2006

Izvršilni odbor društva

SILICON OPTICAL MICROSTRUCTURES BASED ON WET MICROMACHINING

D. Resnik, D. Vrtačnik, B. Batagelj*, U. Aljančič, M. Možek, S. Amon

University of Ljubljana, Faculty of Electrical Engineering, Laboratory of Microsensor Structures and Electronics, Ljubljana, Slovenia

*Radiation and Optics Laboratory, Ljubljana, Slovenia

Key words: silicon micromachining, surfactant, beam splitters, micro mirrors, roughness

Abstract: Optical microstructures were designed and fabricated with the purpose of out-of-plane and in-plane light beam manipulation. Microstructures were realized on {100} silicon with improved wet etching technique. Successful implementation of Triton-x-100 surfactant as an additive to the 25%TMAH-water etching system is reported, resulting in improved etching anisotropy and realization of smooth {110} silicon crystal planes, representing 45° mirrors. For in-plane reflections, thin {010} vertical walls were realized, serving as beam splitters or mirror reflectors. Fabricated microstructures were characterized in order to obtain information on the morphology of reflecting planes and their optical properties at three wavelengths.

Silicijeve optične mikrostrukture realizirane z mikroobdelavo

Kjučne besede: silicij, mikroobdelava, surfaktanti, mikrozrcala, delilniki, hrapavost

Izvleček: V prispevku so predstavljene optične mikrostrukture, realizirane na {100} siliciju s postopki anizotropnega mokrega jedkanja. Načrtane in izdelane so bile mikrostrukture, ki omogočajo manipulacijo svetlobnega žarka tako v {100} ravnini, kot tudi pravokotno navzven. Z dodatkom Triton-x-100 surfaktanta pri mokrem jedkanju silicija s 25%TMAH jedkalom smo dosegli izboljšanje anizotropije med posameznimi kristalnimi ravninami, kar nam je omogočilo realizacijo 45° zrcal z izredno gladkimi {110} površinami. Za manipulacijo žarka v ravnini so bila izdelana vertikalna zrcala, omejena z {010} kristalnimi ravninami, ki služijo kot odbojne površine ali polpropustni delilniki vpadnega žarka. Izvedena je bila optična in morfološka karakterizacija izdelanih mikrostruktur.

1. Introduction

Integration of MEMS and micro-optics has created a new class of microsystems, termed micro-opto-electro-mechanical systems (MOEMS), covering a very broad spectrum of microsystems and functionalities, from telecommunications and optical instrumentation to imaging systems. Excellent survey on the state of the art MOEMS was given recently by Motamedi /1/.

Optical communications require various types of light beam manipulations that can be realized monolithically on a single silicon optical bench. This approach enables integration of mechanical, electrical and optical components and functions in a single complex microstructure, resulting in improved performance and reduced cost. Furthermore, it is expected for the future that many electrical connections on/between chips will be replaced by optical waveguides.

In parallel optical communications, aligning of optical fibres to a second group of elements with low coupling losses is a demanding task. One segment of optical links where the losses can be optimized are reflecting mirrors, reflecting the in-plane to the out-of plane optical signal, or vice versa. Monolithic optical silicon benches with micromachined mirrors that meet demands for desired reflecting angle and low beam scattering, in conjunction with appropriate *U* or *V* shaped fibre aligning grooves are an attractive solution /2/. Compared to {111} crystal planes where mirror is under 54.74° with respect to the {100} surface, the {110} mirror planes with an angle of 45° toward surface allow more efficient coupling with single mode fibres having a small angle of acceptance /3,4/.

In our study, beside standard IPA additive to TMAH etchant, nonionic surfactant Triton-x-100 is investigated as an additive to the TMAH etching solution to improve the anisotropy ratio. Besides, Triton is also commonly used in the microelectronics processing. Another advantage over IPA is that the etching temperature can be increased due to higher boiling point of Triton. Our investigation was carried out by adding small amounts of Triton to the 25%TMAH-water etchant in the range of 0.1-1000ppm.

Monolithic optical benches were designed and fabricated to allow the characterization of etching parameters. Designed benches included 45° mirrors for out-of- plane reflection, corner splitters as well as vertical walls bounded by {010} planes for in-plane manipulation of light beam. Experimental validation of these planes was performed by measurement of angles and intensity profiles of reflected beams as well as by measuring the morphological parameters of reflecting planes.

By applying two step anisotropic etching (mask/maskless) we found a possibility of obtaining reflecting planes with very low angle. In this case the mirror planes are {311}, with the angle of 25.24° toward {100} surface. By implementing our original approach, it is also shown that a mirror composed of {111} and {311} plane can be fabricated, thus acting as a beam splitter.

Optical mirror planes are characterized by several quality factors, most important being the degree of reflectance and dispersion angle of reflected light. Dispersion of reflected light is a function of mirror surface microroughness which causes scattering, the fibre distance from the mirror and the numerical aperture of single mode fibre. Optimal conditions for implementation of Triton, such as agitation, etch rates, anisotropy and surface roughness were investigated.

2. Experimental work

The experimental work was carried out on a low resistivity (1-5Ohmcm), n-type, single side mechanically polished float zone (FZ) silicon wafers with <001> crystal orientation (Topsil). Silicon wafers were thermally oxidized at 975°C to grow 600nm of SiO_2 and some were additionally covered with 70nm of LPCVD nitride (Si_3N_4) deposited at 800°C, to provide accurate masking against aggressive etchants.

Chromium mask was designed to fabricate optical bench microstructures (10x10mm^2) with parallel fibre grooves of different widths (240-400μm) and 200μm pitch between them (see Fig.5). Designed *V* grooves were terminated with mirror at one side of the groove and with open end on the opposite side to insert the fibre. Mask orientation versus primary wafer flat determines the sidewall angle of the groove and the slope of end mirror toward the surface plane and was chosen according to the requirements of the microstructure functionality.

Wet anisotropic micromachining of photolithogaphically defined areas was performed in 25%TMAH -water solution (Honeywell) and also in 33%KOH-water solutions in some cases.

A new additive, which was used with TMAH in our experiments, the non-ionic surfactant (i.e. surface active agent) Triton-x-100, is a mild surfactant often used in biochemical applications. Chemically, this additive is a stable octylphenol-ethyleneoxide condensate (Union Carbide). Beside compatibility with CMOS processes, the advantage of Triton-x-100 is higher boiling temperature point compared to IPA. This enables etching at higher temperatures, thus reducing the etch time.

Samples were etched in a closed thermostated (±1°C) glass vessel with the total content of 500ml of etching solution, with agitation by a magnetic stirrer in the temperature range 70-100°C.

Geometrical dimensions and accordingly the etch rates were determined by measuring lateral distances under the microscope. Surface quality, described by average roughness *Ra*, was evaluated by Taylor-Hobson surface profiler and surface morphology was characterized by AFM, SEM and optical microscope.

Fabricated benches and mirrors were characterized optically by measuring the beam dispersion angle and by analyzing the intensity profile of reflected beam. Fibres used in characterization setup were standard single mode fibres with diameter 125μm and numerical aperture NA=0.12. The intensity of reflected beam was measured at three wavelengths: 632nm (HeNe laser), 1.33μm and 1.54μm (Fabry-Perot type laser diodes).

3. Results and discussion

3.1. The role of additives in the etching process

In a manner to reveal {110} crystal planes on commonly used (100) silicon wafers, two conditions have to be met simultaneously. The first is that the structures are oriented at 45° toward the <110> oriented wafer flat and secondly, additives to the anisotropic etchant are essential to properly adjust the anisotropy ratio.

It is known that IPA additive to KOH or TMAH /5,6/ does not affect significantly the {100} etch rate; however, it does decrease {111} and {110} etch rates and therefore also anisotropy. It was shown recently that not only IPA, but also other alcoholic moderators have similar effect /7/.

Another type of additives was reported by Sekimura /8/ showing that small amounts (0.2%) of added surfactant NCW-601 to 22% TMAH solution exhibits improved surface performances for fabricated {110} planes with roughness Ra=100nm. Anisotropy and convex corner underetching were improved in both cases as well as surface roughness of {100} and of {110} planes. Presented work is focused on detailed investigation of TMAH-Triton etching parameters in order to obtain smooth {110} crystal planes with good anisotropy.

3.2. Effect of Triton-x-100 additive

Surfactants generally tend to accumulate and/or adsorb at solid-liquid interface, thus decreasing the contact angle between solid (silicon) and aqueous phase (anisotropic etchant). Triton surfactant acts as modifier of etchant surface tension. It is also very likely that Triton enters also in the polymerization process of the etching products by surrounding the etching products with the hydrated layer. This layer acts as a steric barrier to particle coalescence /9/. It is presumed that these effects play also a role in the observed etching characteristics. Etching experiments were performed with Triton content in the range 1-1000 ppm added into the 25% TMAH-water solution and optical bench samples were finally etched in the temperature range from 70-100°C.

In our previous work /10/, significant increase of etching anisotropy ratio $R_{(100)}/R_{(110)}$ was found in the range 10-

200ppm of added Triton to 25%TMAH. Over three orders of magnitude of added Triton (1-1000 ppm) very small variations of {100} crystal plane etch rate $R_{\{100\}}$ were observed. Major contribution to the increased anisotropy is a reduction of lateral etch rate $R_{<100>}$ which is related to $R_{\{110\}}$ ($R_{\{110\}}=R_{<100>}/\sqrt{2}$).

Minor influence of Triton on the $R_{\{100\}}$ etching rate is comparable to IPA influence observed by Merlos /5/ in the case of TMAH-IPA (reduction of 10 %). Compared to pure 25 % TMAH-water system, it was found that the {100} etch rate difference at these three temperatures is less than 15%. It was determined that the anisotropy ratio also increases with the increased etch temperature, mainly due to smaller increase of $R_{\{110\}}$ compared to $R_{<100>}$. Anisotropy ratio of 3.6 is achievable, which is much higher than for TMAH-IPA or KOH-IPA (0.9 and 1.8, respectively).

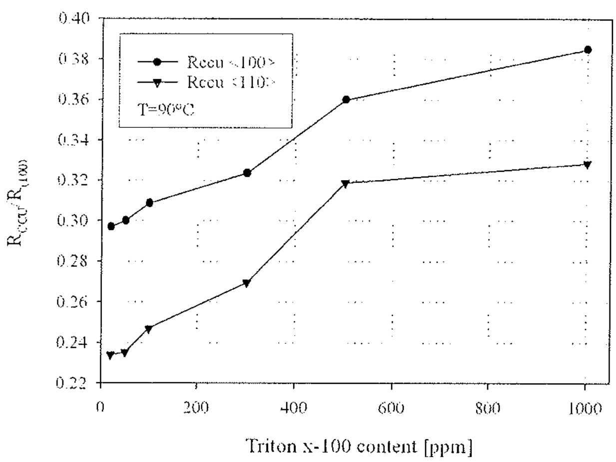

Fig.1. Normalized convex corner underetching for corners oriented in <110> and <100> direction for TMAH-Triton (50ppm) etching system.

Important figure of merit for an etching system in micromachining of silicon microstructures is low convex corner underetching. This phenomenon is more severe for structures having convex corners pointing in <100> direction compared to corners pointing in <110> direction. In our optical microstructures both directions are implemented and were investigated for TMAH-triton etchant. The corner underetching rate R_{CCU} was measured for both types of corners and then normalized by $R_{\{100\}}$ etch rate as shown in Fig.1. This ratio indicates how efficient is a specific etching system in preserving convex corners within the original shape during the etching process. Dependence of $R_{CCU}/R_{\{100\}}$ ratio on Triton content as presented in Fig.1 demonstrates that low content of Triton is favorable for decreasing the underetching in both cases. For the microstructures oriented in <100> direction having convex corners oriented in <110>, only etched bottom of corner is rounded while on the mask level, convex corner is completely preserved.

3.3. Influence of agitation on roughness (Ra) and etch rate R

To study the nature of etching mechanism in the presence of Triton and to distinguish whether the reaction is diffusion limited or surface reaction limited, the investigation was performed, how the agitation of the solution in the range from moderate (10rpm) to vigorous (900rpm) affects the etch rate of silicon. Therefore, etching in TMAH-triton (50ppm) at 90°C and equal etch time was chosen for all samples (60min). Results are shown in Fig.2. By measuring the {100} etch rates it was determined that the solution agitation does not influence severly the latter, and that the etching process is therefore almost surface reaction limited. However, lateral etch and therefore {110} plane etch rate $R_{\{110\}}$ show strong dependency on the agitation and points toward the diffusion controlled etching process in the presence of Triton. As well, convex corner underetching as a function of agitation was monitored for both directions, (<110> and <100>, respectively). Convex corners pointing in <110> direction were not influenced by agitation. However, corners pointing in <100> direction were significantly affected by agitation, i. e. corner high index crystal planes show diffusion limited behaviour.

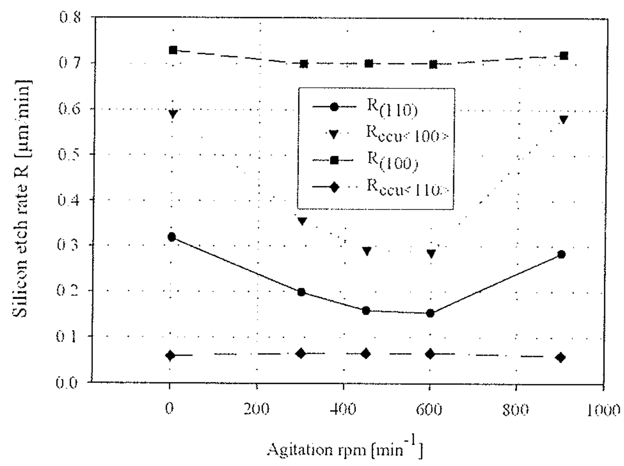

Fig.2. Dependency of vertical and lateral silicon etch rates on the agitation of TMAH-Triton (50ppm) solution at 90°C.

Regarding the surface quality of the reflecting {110} crystal planes etched by 25%TMAH-50ppm Triton-x-100, the agitation of the solution showed significant influence on *Ra*. Average roughness *Ra* is given by arithmetical mean value and was measured by surface profiler. At least four measurements on each sample were performed and etch experiments were repeated three times with fresh solutions. Therefore, results presented are an average of 12 measurements. It must be stressed that cut-off lenght (scan length) must be the same to obtain consistent results. Fig.3. shows that for the etching setup used, the most suitable range, where almost three times better {110} surface smoothness can be obtained is around 600rpm. Surface roughness appears as paralell elongated pits. Interplay beween the mechanism of fresh solution reaching the interface and disturbance of turbulent flow at the interface result in homogeneous etching with low *Ra*.

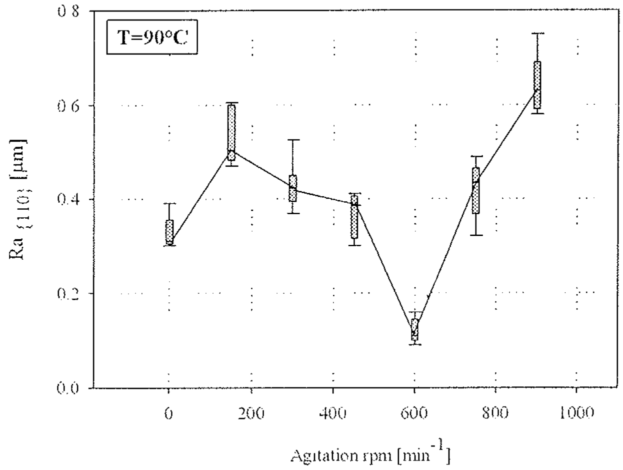

Fig.3. {110}crystal plane roughness vs. agitation of TMAH-Triton (50ppm) solution.

3.4. Activation energy of {110} and {100} plane

Beside TMAH-Triton, two other etching systems were taken into consideration, which also enable the formation of {110} planes. Activation energy for TMAH-Triton was established experimentally by measuring temperature dependence of etch rate for two planes of interest, i.e. {100} and {110}. The removal of silicon atoms is mainly a consequence of sufficient activation energy of the etching species. Arrhenius plot presented in Fig.4 shows the measured temperature dependency of etch rate for both crystal planes. From these plots activation energies for different etchants were derived, taking into account the well known Arrhenius expression (R=*k.exp(-Ea/RT)*). Here, R is the measured etch rate of specific crystal plane, *k* is the pre-exponential factor corresponding to the total number of the events and *Ea* is the activation energy. *Ea* is actually proportional to the number of molecules which are capable of removing Si atoms from the surface. This, so called, collision theory is, however, not sufficient to explain the activation energy differences when using different additives. By introducing activating complex theory, which is describing the transition state of the reaction, Ea corresponds to the molar enthalpy of the reaction and the factor *k* represents the molar entropy of the activation process /11/. Due to the fact that the reaction and transport take place in a solution, which affects events macroscopically, the explanation is even more complicated. Beside sufficient energy of reactant species, the orientation of species necessary for the reaction and the necessary distance is important as well.

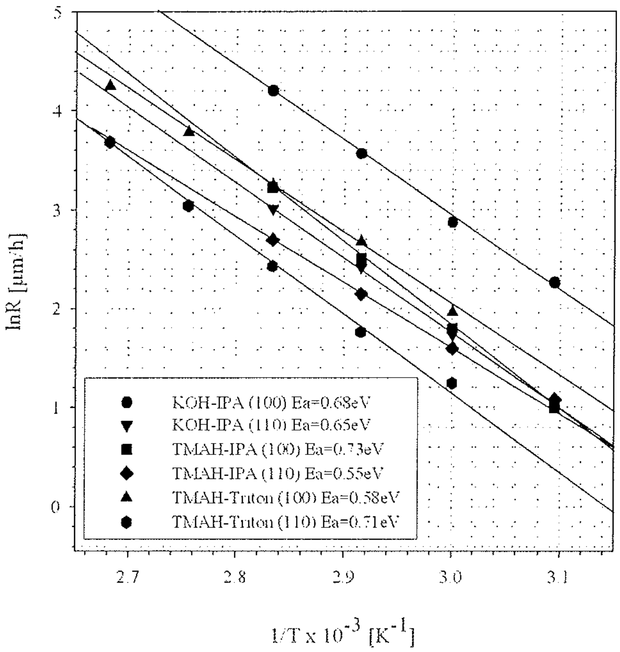

Fig.4. Arrhenius plot showing temperature dependency of etch rates of {110} and {100} planes, for three etchants.

Calculated highest activation energy for TMAH-Triton-50ppm (0.71eV) is in a good correlation with significant increase in anisotropy which is actually a consequence of reduced {110} etch rate. The lowest activation energy for {110} plane exhibits TMAH-IPA etching system, what complies with highest {110} etch rate. KOH-IPA activation energy is in-between, but with very rough surface (Ra>200nm). At lower temperatures it was observed that etch rates were inhibited, probably due to prevailed growth of passivation oxide layer. Table1 presents values of activation energies and preexponential factors, derived from measurements of etch rates for two crystal planes and three etching solutions of interest.

Triton is affecting the accessibility of etching species toward preferential crystal planes which have more open network structure, such as {110} and higher index planes. Probably it plays a role also in the removal of etching products at the interface of {110} plane more dominantly compared to {100} interface Additional factors, such as polarity effects of surfactant, which are connected to binding energy on the specific preferential planes, angle and type of bonds may also affect the characteristics of Triton-etchant-silicon system /12/.

Table 1: Calculated activation energies and pre-exponential factors

	KOH-IPA {100}	KOH-IPA {110}	TMAH-IPA {100}	TMAH-IPA {110}	TMAH-TRITON {100}	TMAH-TRITON {110}
Ea [eV]	.683	.651	.735	.553	.579	.709
Preexp.factor	3.74E11	3.94E10	7.56E11	1.14E9	4.64E9	1.47E11

3.5. Fabrication of optical benches

Three different types of optical benches were designed and fabricated on (100) silicon substrate. First optical bench was designed for aligning out-of-plane mirrors and optical fibres, where fibres enter the optical bench from the same direction (Fig.5a). Second optical bench was designed for optical fibres entering from both directions, where V grooves and the out-of-plane 45° mirrors are interdigitated (Fig.5b). In the third optical bench design, four optical functions were taken into considerations with in-plane light paths (Fig.5c). This optical bench enables function of corner beam splitter and function of retroreflection (reflecting light beam of 180°) in {100} plane. Furthermore, the structure of thin vertical {010} wall beam splitter should enable partial reflection and partial transmission of the input light signal, depending on the wavelength and angle of incidence. However, due to limitations in the etching process (anisotropy, roughness) it is not always possible to provide simultanousely good performances for all of the above functions in the same etching system.

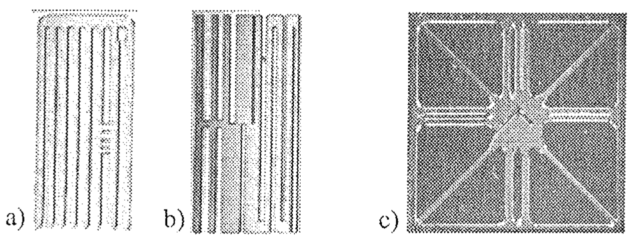

Fig.5. Three different designed and fabricated monolithic silicon optical benches with fibre grooves and reflecting mirrors (a,b-size 5x10mm^2, c-size 10x10mm^2).

3.5.1. {110} crystal plane mirrors

On the basis of etching experiments and measurements, optimal conditions were chosen for a fabrication of 45° mirrors. TMAH-Triton (50ppm) at temperature 90°C and agitation of 550rpm was selected. Fig.6a presents a detail of the fabricated groove terminating with a broad {110} mirror. Grooves are 130μm deep, sufficient to accommodate single mode fibres. The micromachined peninsulas formed by superposition of squares (convex corners in <110> direction) at each side of the groove are dedicated to limit the lateral movement of inserted fibre and can be well trimmed with etching process parameters

Additionally, in Fig.6b fibre and beam reflection is also illustrated to obtain clear view of light path and beam widening for the standard groove and mirror. Fig. 6c is presenting 45° mirror with recorded beam pattern of reflected 632nm light. Beam width angle b is estimated to 25°. Fibre with NA=.12 corresponds to beam width of 15.3°, thus the difference 10° is due to scattering. Surface roughness for TMAH-Triton system of these mirrors was measured by AFM. Average roughness *Ra* was between 6-14nm and the appearance of shallow, elongated pits is significantly minimized.

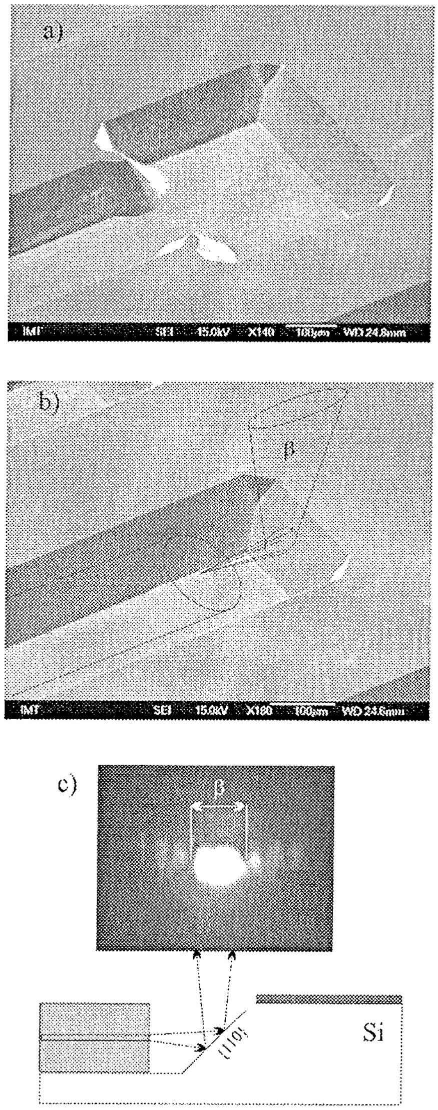

Fig.6. Detail of the groove, ending with {110} mirror plane (a) and design accompanied with a structure for precise horizontal aligning (b), etched by TMAH-Triton-x-100 (50ppm), while (c) shows pattern of the reflected out of plane beam.

In the mirror applications, reflectance is a dominant parameter. If mirror is perfectly flat, then only specular reflectivity, which is a function of material properties (refractive index *n* and extinction coefficient *k*), is expected. Specular reflectivity of bare Si is around 35% at 628nm (31%, 32% at 1.33 and 1.54μm, respectively). According to measurements made by Uenishi, reflectance increases with increasing angle of incident light; at incident angle of 45°, the reflectivity is around 0.5 /13/ and according to Zou /14/ around 0.4 at 632nm for bare silicon substrate. By covering the reflecting planes with highly reflective metals such as gold or aluminum, the reflectivity of mirror can be increased /14,15/. In our experiments, 50nm thick sputtered Au layer on the silicon mirror surface was used as reflective surface on 45° mirrors. This thickness exceeds greatly the required minimal skin depth. Au exhibits an overall specular reflectivity of 97.5% at 632nm and above for higher incident wavelengths /15/.

In reality, the reflective surface is rough by nature and this results in additional reflective component losses due to diffused reflection (light scattering). Light scattering is mainly determined by surface microroughness, incident angle and wavelength of incident light. To estimate the reduction of reflectivity due to scattering component, ratio of scattering component vs. total reflected light can be calculated by the following expression (1) from the scalar scattering theory /16/:

$$\frac{P_{scat}}{P_{tot}} = 1 - e^{-\left(\frac{4\pi Ra\cos\theta}{\lambda}\right)^2} .100 \text{ [\%]} \qquad (1)$$

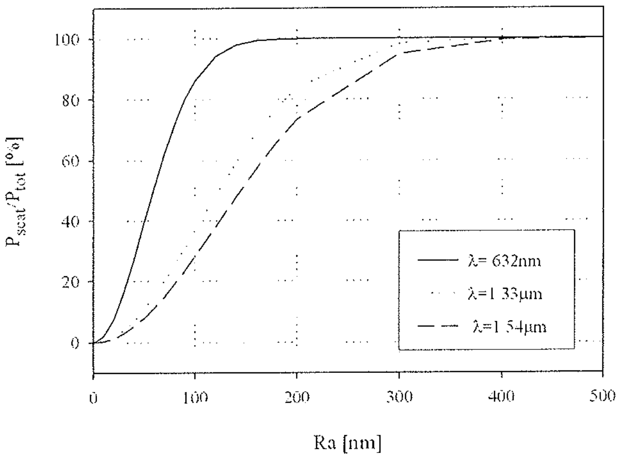

Fig. 7. Influence of mirror surface roughness Ra *on the scattering component of reflected light.*

According to Cochran /15/, *Ra* values that are three orders of magnitude less than operating wavelength are acceptable. Tradeoffs are needed between the mirror surface quality and compatible processes required to finalize the whole microstructure. Fig.7 shows the scattering light contribution with respect to increased mirror roughness *Ra* for three wavelengths taken into account in our study. Roughness is more severely involved in scattering toward lower wavelengths. For measured values of our samples, realized with optimal Triton conditions (*Ra* between 5-14nm), the expected scattering part should be below 5 % for the 632nm and even less for higher two wavelengths. The overall measured out-of-plane intensity for Au coated mirrors was about 73% of incident light at 632nm and 78 to 80% for 1.33μm and 1.55μm, respectively. Additional losses are attributed to air-fibre interface (6.8% according to Cochran /15/) and geometrical misalignment. According to measured intensities, roughness of some samples was probably higher than shown by AFM results on small scale.

3.5.2. *{111}/{311} crystal plane splitter*

When the microstructures are oriented in <110> direction, mirrors with angle 54.74° toward surface are obtained. Using two step etching (mask/maskless) with 25%TMAH etchant, also grooves and mirrors with {{311}} sidewalls and corresponding angle of 25.24° toward surface are viable /17/. Interesting features can be obtained by combining the {111} and {311} planes as a reflective slopes on (100) silicon bench.

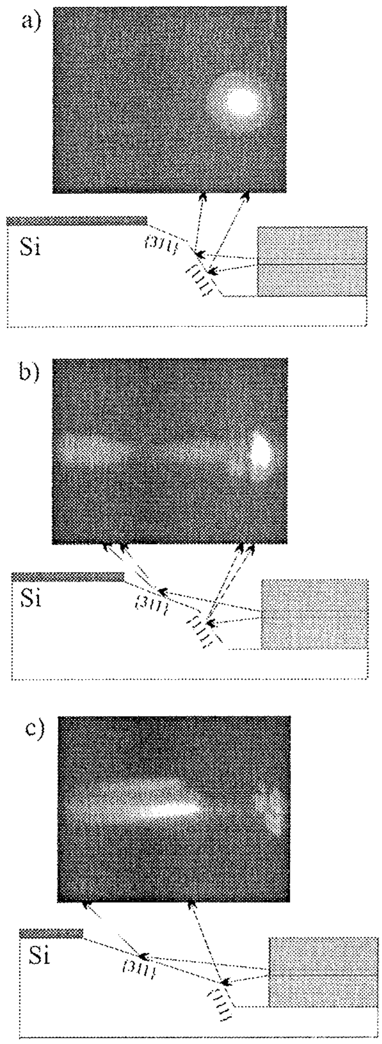

Fig.8. Beam patterns obtained from three different stages of micromachining combined {111}/{311} crystal plane splitter.

By implementing this approach, the incident beam can reflect from two slopes and two out-of-plane beams can be obtained. Fig.8 is presenting this principle together with images of reflected optical beam which is detected on transparent screen, located parallel and above the optical bench. Fig.8a corresponds to the situation where {311} is just formed and most of the slope is still {111} plane giving symmetrical Gaussian beam pattern. After further etching, {311} plane prevails by consuming the {111} plane. This is seen as reduced image from {111} and elongated image appears from {311} (Fig.8c). By accurate fabrication of the two planes in a desired height ratio, one can tailor the splitter by the actual requirements. AFM results for {311} and {111} planes are shown in Fig.9 and can be validated by means of *Ra* values.

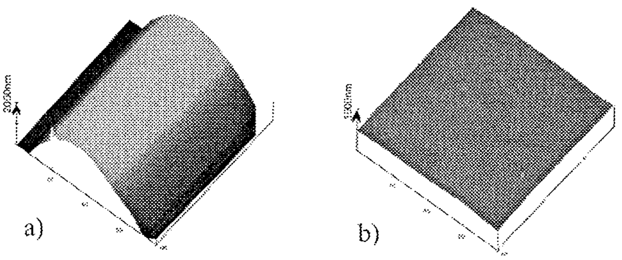

Fig 9. *AFM 3D image of 80x80 μm² mirror area of combined {111}/{311} crystal plane splitter (a) {311} plane with* Ra=*180nm and (b) {111} plane with* Ra=*2.9nm*

As reported earlier /17/, and shown as well on the AFM 3D plot (Fig.9), slightly convex shape is obtained, which causes the dispersion of reflected beam shown above. Consequently the optical losses are quite high. However, the distortion of reflected pattern from {311} is difficult to annulate. Beam width is proportional to the distance of fibre from the mirror and the numerical aperture of fibre. By correlating the screen pattern with AFM results, it is evident that the high scattering angle is the consequence of a pronounced convex contour rather than a local microroughness.

3.5.3. {010} wall beam splitter

To enable beam reflection in (100) plane, vertical mirrors are required. For such vertical {010} walls, design rules have to take into consideration all the predictive details determined earlier. To accomplish this kind of wall, KOH or TMAH anisotropic etchant have to be employed and mask must be oriented in <100> direction. To obtain partial reflection and partial transmission at particular wavelength, proper thickness has to be determined according to the material properties as will be shown in detail later in this section. Fig.10 shows SEM micrograph of fabricated central region of bench, showing vertical {010} wall, 15μm thick and 150μm high. SEM analysis have shown that wall fabricated by KOH reveals (010) plane with residuals on top and bottom level, while TMAH gives perfectly smooth {010} plane (see inset in Fig.10).

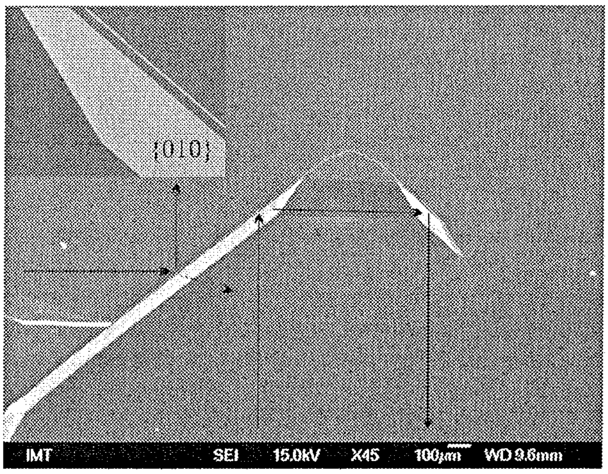

Fig.10. *SEM micrograph of smooth vertical {010} wall (15μm thick, 130μm high), fabricated by 25%TMAH.*

Fig.11 shows 90° reflection from silicon {010} vertical wall, with partial tranmission, depending on wall thickness and incident wavelength. Precise alignment of fibres is mainly a function of the design and is of utmost importance for minimizing optical losses.

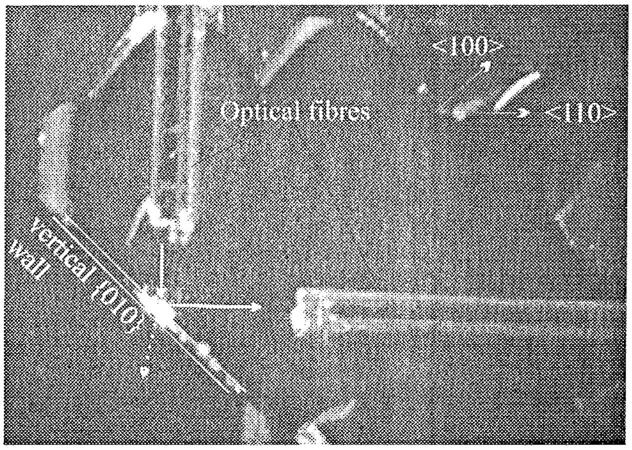

Fig.11. *Detail of optical bench with designed in-plane beam 90° reflection from (010) wall*

For the wavelengths in the range of 1.1-2.5μm, the absorption in silicon is very low. Therefore increased transmittance is governed by the following equation given by /18/ for the normal angle of incidence.

$$T = \frac{(1-R^2)e^{-\left(\frac{4\pi k x}{\lambda}\right)}}{1-R^2 e^{-\left(\frac{8\pi k x}{\lambda}\right)}} \tag{2}$$

where *R* is the reflectivity of Si, *k* is the extinction coefficient of Si, *l* is the wavelength of incident light and *x* is the thickness of Si {010} wall. According to the calculated dependency of transmittance vs. silicon thickness, as shown in Fig.12, vertical wall can act as an attenuator. Small amount of attenuation is expected for higher two wavelengts and

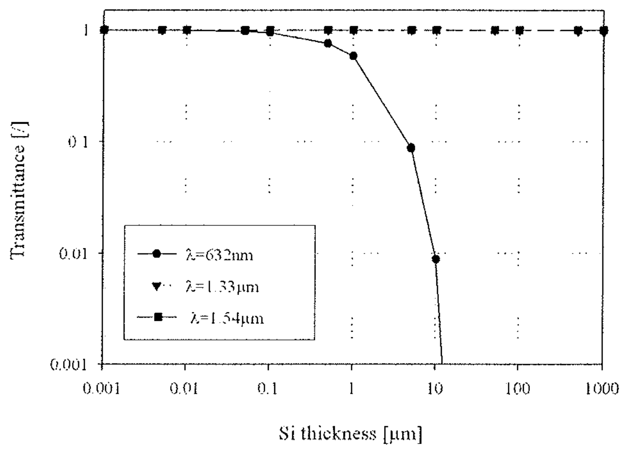

Fig.12. *Calculated dependency of transmittance vs. silicon thickness, for three wavelengths (according to eq.2).*

higher for 632nm (here, transmittance is reduced due to increased reflectivity and absorption). Attenuating configuration on the fabricated optical bench is presented in Fig.13. In this case, 15μm thick silicon transmits less than 0.1% of incident light intensity, what correlates well with the results of Uenishi /13/.

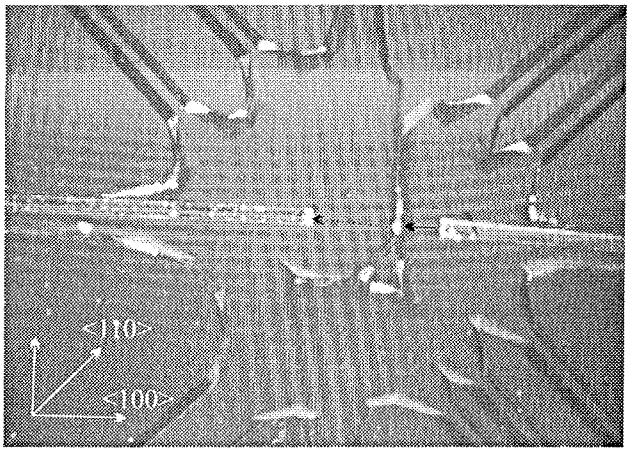

Fig.13. Detail of optical bench with designed in-plane attenuation through (010) wall.

3.5.4. Corner beam splitter

Optical microstructure, enabling in-plane division of incident beam, is also corner splitter, presented in Fig.14. To elaborate vertical {010} walls, meeting at right angle thus forming sharp convex corner, structure must be oriented in <100> direction. To avoid underetching, we designed square shaped compensation structure that resulted in relatively sharp convex corners. Two different etching solutions were investigated to obtain a sharp convex corner, which would provide perfect beam splitting without out-of-plane beam losses. By applying the TMAH etchant in the fabrication, the splitter convex corner was greatly improved compared to KOH. The optical paths for splitter microstructure were designed for 50μm wide and 130μm high {010} vertical wall. In this case the insertion loses between input and output fibres should be minimized. To obtain the ideal splitter 50:50, convex corner of two orthogonal {010} planes should have perfect edge and the fibres must be carefully aligned in the proximity of corner, which is in practice a very demanding task. Results of our measurements on this particular corner beam splitter as shown in Fig.14, showed that each of output fibres received only 20-25% of incident intensity at 632nm. According to Rosengren /19/, this corresponds to 3-4dB of optical losses. To minimize losses, improved compensation structure has to be designed, which will improve the corner quality even further. For quantitative evaluations, additional efforts are required also in terms of reduced misalignment of fibres.

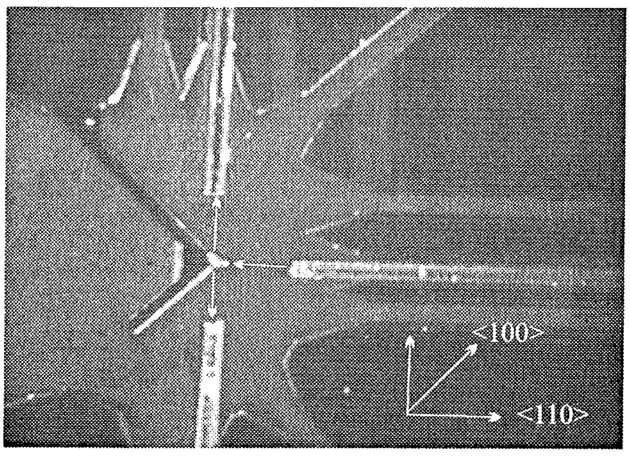

Fig.14. Detail of optical bench with corner beam splitter and inserted fibres.

3.6. Optical characterization of reflecting {110} mirrors

The setup for optical characterization of 45° mirrors at three wavelenghts consisted of light sources, collimator, *xyz* adjusting micromanipulators to achieve maximal coupling between the source and the optical fibre guide, detector and a microscope with CCD camera to enable precise fibre insertion in the grooves of optical bench (Fig.15).

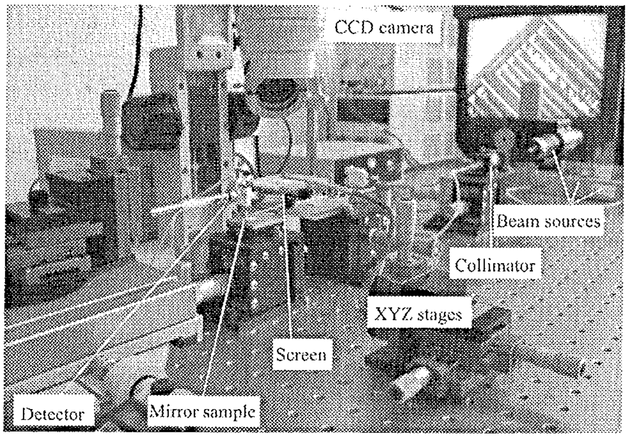

Fig.15. Optical characterization setup.

For 45° silicon mirrors, optical measurements with visible 632nm wavelength beam were first accomplished. Reflected light beam pattern, displayed on semitransparent screen positioned perpendicularly to the output beam at a fixed distance from the optical mirror, provided information about scattering angle, angle of out-of-plane deflection and also morphology of reflecting mirror, as shown in Fig.6c and Fig.8.

Mirrors were further characterized by scanning the *xy* plane perpendicular to the direction of the reflected beam by Si calibrated reference photodiode. Intensity of illuminated photodiode detector was measured with HP 3457A multimeter. In case of 1.33μm and 1.54μm wavelengths, Fabry-Perot type laser diode light sources were used and reflected beam intensity was determined by measuring the response of InGaAs photodetector.

Fig. 16 presents measured intensity profiles of reflected beam from {110} mirror (made by TMAH-Triton (50 ppm)) for three incident wavelengths. At 632nm, mirror has a very wide spatial response with FWHM value of angle nearly 35° and thus lower peak. The proportions of FWHM values are in a reasonable agreement with the results presented in Fig.6c where beam pattern was recorded on the semitransparent screen.

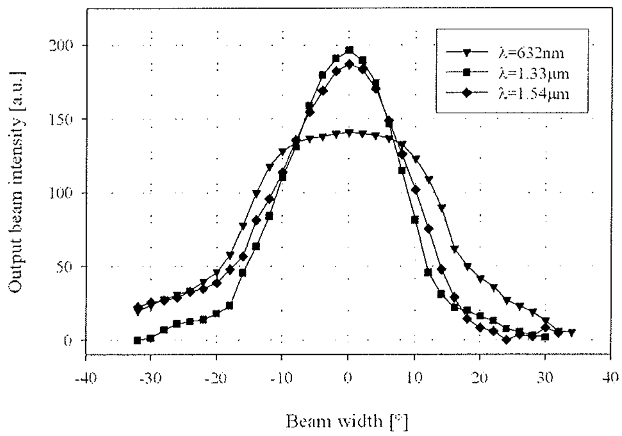

Fig.16. Intensity profiles of reflected output beams from {110} crystal planes. Mirrors were covered by 50nm of Au layer.

In case of incident beam wavelengths of 1.33μm and 1.54μm, what is substantially higher than the average roughness of reflecting crystal plane, it was expected, according to Fig.7, that microroughness does not play such a severe role as at lower wavelengths ($Ra \ll \lambda$). By analyzing the profiles it can be seen that FWHM were decreased to values around 19° for both cases. Profiles are not fully symmetrical due to geometrical errors of fibre misalignment or *xy* scanning setup.

By correlating the results at 1.54μm and 1.33μm to those at 632nm wavelength, minor differences were revealed concerning reflected beam scattering angle at the two higher wavelengths. On the other hand, significant scattering was determined at the lowest wavelength, higher than expected from Fig.7. It is believed that this is due to poor endface finish of the fibre (increased return losses) and due to additional modes present at 632nm wavelength.

Further work is needed to decrease optical losses, particularly those originating from mechanical misalignment (longitudinal, axial and angular) and from return losses due to poor fibre cut.

4 Conclusions

In the proposed study, optical microstructures realized on (100) silicon substrates with wet anisotropic etching were investigated. The implementation of Triton-x-100 surfactant in the range of 1-1000ppm to the 25% TMAH etchant is found to increase the anisotropy by decreasing the {110} etch rate and retaining the {100} etch rate. It was shown that surface roughness of {110} planes used as 45° optical mirrors is also greatly improved (*Ra*=6-14nm). In addition, convex corner underetching is strongly reduced. It was shown that TMAH-Triton system enables the formation of {110} mirror and fibre groove simultaneously. Optimal conditions for added content of Triton (50ppm) and stirring conditions (550rpm) were established to achieve smooth {110} mirrors. Activation energies of 0.58eV and 0.71eV for {100} and {110} planes, respectively, were determined.

Three types of optical microbenches were fabricated by wet micromachining, enabling out-of-plane and in-plane manipulation of light beam. Besides, important parameters such as roughness of reflecting mirror surfaces, transmittance of thin silicon {010} walls and spatial intensity distribution of reflecting beam were determined. Optical characterization of microbenches with incident light at wavelengths of 632 nm, 1.33 μm and 1.54 μm confirmed the functionality of the designed and presented microstructures.

Acknowledgments: This work was supported by Ministry of Higher Education, Science and technology of Republic of Slovenia.

References

/1./ M.E. Motamedi, editor, MOEMS, Micro-Opto-Electro-mechanical Systems, *SPIE Press*, Bellingham, USA, 2005.

/2./ M. Hoffmann, E. Voges, Bulk silicon micromachining for MEMS in optical communication system, *J. Micromech. Microeng.* 12, 349-360, 2002.

/3./ D. Sadler, M.J. Garter, C.H. Ahn, S. Koh, A.L. Cook, Optical reflectivity of micromachined {111} oriented silicon mirrors for optical input-output couplers, *J. Micromech. Microeng.* 7, 263-269, 1997.

/4./ C. Strandman, L. Rosengren, H.G.A. Elderstig, Y. Backlund, Fabrication of 45ş mirrors together with well defined V-grooves using wet anisotropic etching of silicon, *J. of Microelectromechanical Systems*, Vol. No. 4, December 213-219, 1995.

/5./ A. Merlos, M. Acero, M. H. Bao, J. Bausells, J. Esteve, TMAH-IPA anisotropic etching characteristics, *Sensors Actuators* A37-38, 737-743, 1993.

/6./ H. Seidel, L. Csepregi, A. Heuerberger and H.A. Baumgartel, Anisotropic etching of crystalline silicon in alkaline solutions, *J. Electrochem. Soc.* 11, 3612-3625, 1990.

/7./ W-J. Cho, W-K. Chin and C-T. Kuo, Effects of alcoholic moderators on anisotropic etching of silicon in aqueous potassium hydroxide solutions, *Sensors Actuators* **A** 116, 357-368, 2004.

/8./ M. Sekimura, Anisotropic etching of surfactant-added TMAH solution, *Proc. 21th IEEE Micro-Electro-Mech. Syst. Conf. (MEMS'99)* Orlando FL, Jan 17-21 650-55,1999.

/9./ A. Karagunduz, K.D. Pennel and M. Young, Influence of a nonionic surfactant on the water retention properties of unsaturated soils, *Soil Sci. Soc. of America J.* 65 1392-1399, 2001.

/10./ D. Resnik, D. Vrtacnik, U. Aljancic, M.Mozek, S. Amon, The role of Triton surfactant in anisotropic etching of {110} reflective planes on (100) silicon, *J. Microm. Microeng.*, 15, pp. 1174-1183, 2005.

/11./ P.W.Atkins, Physical Chemistry, Third edition, *Oxford University press*, 1986.

/12./ I. Zubel, The influence of atomic configuration of (*hkl*) planes on adsorption processes associated with anisotropic etching of silicon, *Sensors Actuators* A94, 76-86, 2001.

/13./ Y. Uenishi, T. Masahiro, M. Mehregany, Micro-opto-mechanical devices fabricated by anisotropic etching of (110) silicon, *J. Microm. Microeng.*, 5, pp. 306-312, 1995.

/14./ J. Zou, M. Balberg, C. Byrne, C.Liu, D.J. Brady, Optical properties of surface micromachined mirrors with etched hole, *J. Micromech. Microeng.* 8, 1999.

/15./ K.R. Cochran, L. Fan, D.L. DeVoe, Moving reflector type microoptical switch for high-power transfer in a MEMS- based safety and arming system, *J. Micromech. Microeng.* 14 2004.

/16./ M-Y. Jung, H. Ryu, M-L. Lee, C-H. Jun, Y.T. Kim, A novel process for high reflectivity of Al sidewalls of optical mirrors using KrF excimer laser annealing, *Proceed. of SPIE, Micromach. and microfabr. process technol. VII, 22-24.Oct S Francisco* 4557 111-118, 2001.

/17./ D. Resnik, D. Vrtacnik, S. Amon, Morphological study of {311} crystal planes anisotropically etched in (100) silicon: role of etchants and etching parameters, *J. Microm. Microeng.*, 10, pp. 430-439, 2000.

/18./ S.M. Sze, Physics of semiconductor devices, 2nd edition, *J.Wiley and sons*, N.Y. 1981

/19./ L. Rosengren, L. Smith, Y. Backlund, Micromachined optical planes and reflectors in silicon", *Sensors and Actuators*, A 41-42, 330-333, 1994.

doc.dr. Drago Resnik
doc.dr. Danilo Vrtačnik
*doc.dr. Boštjan Batagelj**
mag. Uroš Aljančič
mag. Matej Možek
prof.dr. Slavko Amon
University of Ljubljana, Faculty of Electrical Engineering, Laboratory of Microsensor Structures and Electronics

**Radiation and Optics Laboratory*
Trzaska 25, Ljubljana 1000, SLOVENIA
E-mail: Drago.Resnik@fe.uni-lj.si

Prispelo (Arrived): 03. 01. 2006; Sprejeto (Accepted): 30. 01. 2006

LIMIT CYCLES IN HIGH ORDER ΣΔ MODULATORS

D.Strle

University of Ljubljana, Faculty for Electrical Engineering, Ljubljana, Slovenia

Key words: ΣΔ modulators, limit ajcles, dithoring

Abstract: Limit-cycles generated in ΣΔ modulators are analysed and discussed in this paper. Simulation results of two high order modulators are presented together with techniques to reduce limit cycles. The procedure is limited to general single loop ΣΔ modulators. Simulations are based on a general state-space description, which is applicable to general single loop architecture with one or multi bit internal ADC and/or DAC. Simulation results prove that high order modulators are as susceptible to limit-cycles as low order modulators are, which is in contrast to what is generally believed. To reduce the probability of the appereance of limit cycles a method called dithering is used to reach ultimate performance. Simulation results of 2nd and 5th order modulators are presented, and the method's efficiency is discussed.

Limitni cikli pri ΣΔ modulatorjih visokega reda

Kjučne besede: ΣΔ modulatorji, limitni cikli, tresenje

Izvleček: V prispevku analiziramo in prikažemo limitne cikle, ki se generirajo v ΣΔ modulatorjih višjega reda. Predstavljeni so simulacijski rezultati modulatorja 2. in 5. reda skupaj z metodo eliminacije limitnih cilkov. Metoda analize je primerna za splošne modulatorje prvega reda z enim filtorm v zanki. Simulacije bazirajo na splošnem opisu v prostoru stanj, ki ga lahko uporabimo za poljuben modulator višjega reda z eno ali več bitnim notranjim kvantizatorjem in D/A pretvornikom. Simulacijski rezultati kažejo, da tudi modulatorji visokega reda niso imuni na tvorbo limitnih cilklov, kar je v nasprotju s splošnim prepričanjem. Da bi zmanjšali verjetnost pojava limitnih ciklov pri ekstremnih zahtevah uporabimo metodo tresenja (dither). Simulacijski rezultati dokazujejo uporabnost metode za modulatorje višjega reda.

1. Introduction

Over-sampling and noise shaping are efficient techniques for increasing the resolution of a quantizer by trading the quantizer's accuracy for circuit speed, possibly resulting in a high resolution A/D or D/A converter using only a 1-bit quantizer /1/. The resulting circuitry is simple, robust and has very good distortion properties, so it is very suitable for numerous integrated applications mainly because of modest matching requirements. This principle has been known for a long time but the modulator models' theoretical concepts are restricted. Usually linearization of a quantizer is used to understand basic principles and behaviour. Unfortunately, such simplification blurs some important aspects of the behaviour, so it is supplemented by long term time domain simulations of a nonlinear model and an FFT, which uncover some aspects of the behaviour but do not give a general overview of the problem. Because of the system's nonlinearity and complexity, an analytic solution exists only for a 1st order modulator /2/ and partly for a 2nd order /3/, while for higher order modulators only approximate analytical models exist. None of them gives a complete qualitative and quantitative understanding of the behaviour. In reality the modulator is not an ideal A/D converter because of non-ideal circuit effects and because of the appearance of limit cycles, which lead to undesirable tonal behaviour of a bit-stream and state variables. This article will analyse the appearance of limit cycles using long term time domain simulations of a nonlinear model of a modulator and an FFT.

It is well known that a 1st order modulator has tonal quantization noise spectra /2/. It was believed that for high order modulators (N≥2) the in-band tones inside the quantization noise are reduced by the loop filter's high-pass noise transfer function (NTF). However, limit-cycles are formed because of the quantizer's nonlinearity. They have very high amplitudes close to $f_s/2$ and a still unacceptable level in the base-band. In addition they may live only for a short time due to some special conditions that may exist due to different circuit conditions (offset voltage, input DC voltage, AC voltage of high or small amplitudes, etc.). Empirical observations of a 2nd order modulator show that tones with frequencies dependent on DC input voltage are generated with frequencies f_T and amplitudes attenuated with NTF of a loop-filter /1/:

$$f_T(n)=\frac{n\, f_s\left|A_{DC}\right|}{2\Delta} \qquad n=\{0,1,2,...\} \tag{1.1}$$

Tones at low and high frequencies are dangerous because they may reduce the S/N ratio. Those in the base-band are attenuated by NTF. Their rms values may be higher than noise in a base-band and thus directly reduce the S/N ratio. The tones close to $f_s/2$ usually have very high amplitudes and may be eventually translated to the base-band by some nonlinear process, sampling or cross-talk; especially dangerous to the references is cross-talk. It is therefore necessary to understand the behaviour as well as possible to be able to predict the tones and to use an appropriate technique for minimizing the probability of tone formation and existence. For ultimate performance modulators limit-cycles must be broken by adding an appropriately shaped dither signal. If an A/D converter is to be used for any "acoustic device" or for very narrow-band signal conversion, than the smallest number of tones that are even smaller than the level of total noise in the base-band could reduce the S/N ratio considerably /4/. Generally the in-band tones with rms values below the rms noise level in the whole band are not dangerous. Unfortunately, out-of-band spectral components coupled with the reference voltage through substrate connection or supply voltage are very dangerous because they are not attenuated and have very large amplitudes; they can be easily transferred to the base-band by some nonlinear process or cross-talk.

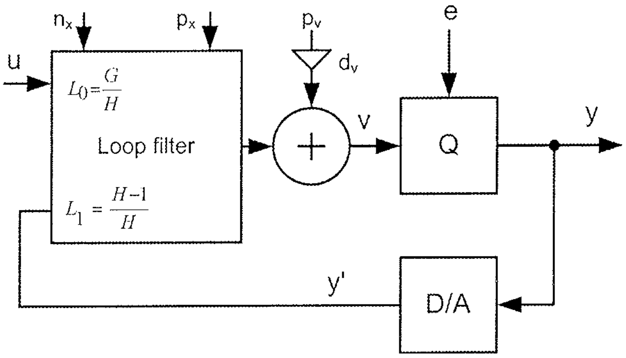

Figure 1: *State-space model of a modulator*

The paper is organised as follows. Section 2 presents a state-space model of a general single loop modulator. It includes circuit noise sources and dithering inputs. Section 3 presents some simulation results for 2nd and 5th order modulators showing tonal behaviour in the base-band and at high frequencies close to $f_s/2$ as a function of different conditions. Section 4 summarises the results and concludes the paper.

2. State-space model of a modulator

A discrete-time modulator can be efficiently represented by its state-space model shown in Figure 1 and described by equation using integrator outputs x(n) as state-variables, v(n) as the loop filter's output, y(n) as a quantizer's output (bit-stream of a one bit modulator) and u(n) as the input signal. The topology is defined by state transition matrix **A**, vector of input signal connections **b** and vector of reference connections **r**, while vector **c** defines the linear combination of state-variables forming the loop filter's output v(n). Different dither signals can be added to the model: p_v is a pseudo-random signal with an appropriate PDF connected to a quantizer's input through weight d_v and $\mathbf{p}_x$ is a vector of different dither signals possibly connected to the state variables through diagonal matrix $\mathbf{Id}_x$. For S-C implementation the kT/C noise sources are added through noise vector $\mathbf{n}_x$ and connected to state-variables through matrix $\mathbf{N}_x$ /5/.

$$
\begin{aligned}
v(n) &= \mathbf{c}^{\mathrm{T}}\mathbf{x}(n) + d_v p_v(n) \\
\mathbf{x}(n+1) &= \mathbf{A}\mathbf{x}(n) + \mathbf{b}u(n) + \mathbf{r}y(n) + \\
&\quad + \mathbf{Id}_x\mathbf{p}_x(n) + \mathbf{N}_x\mathbf{n}_x(n) \qquad (2.1) \\
y(n) &= Q\{v(n)\}
\end{aligned}
$$

No other constraints limit the modulator's topology in Figure 1 except that the D/A converter is for now assumed ideal and therefore $y' = y$. An analytical solution, which would give general and qualitative results of this nonlinear system does not exist at the moment and is beyond the scope of this paper. The formulation above is used only for efficient simulations of a general, high order, single loop modulator with a one bit quantizer. The next section presents simulation results and tonal behaviour of 2nd and 5th order modulators using a state-space description defined in equation (2.1).

3. Simulation results

3.1. LP 2nd order modulator:

Let us start with a known 1-bit 2nd order modulator with f_{OVS} = 4MHz. We are interested in the spectral components and the S/N ratio as functions of input DC voltage, the state variables' initial conditions, dither signal, presence and level of circuit noise and level of AC input signal voltage amplitude. Simulation of a standard 2nd order modulator implemented with the S-C technique is performed here. An AC signal with amplitude of a_{in} = 58μV and frequency f_{in} = 3.7 kHz is connected to the input to have a reference, while DC input voltage is swept from approx. -4.5mV to +4.5mV in 51 steps. The PSD of y(n) is calculated using the FFT of 2^{18} (262,144) samples. Noise sources (dither and kT/C) are switched on or off to generate two different groups of results. The dither signal used is a binary, pseudo-random signal with weight 0.5 and length L = 2^{16}. It is connected to a quantizer's input. The results in Figure 2 present a 3D plot of a PSD of bit-stream y(n) in the base-band when dither and kT/C noise sources are switched off. The frequency is plotted on the x-axis, DC input voltage on the y-axis and PSD relative to 1Vrms on the z-axis. As expected we observed many tones whose amplitudes and frequencies depended on the DC input voltage. These tones have sufficient energy in the base-band to be able to corrupt the S/N ratio.

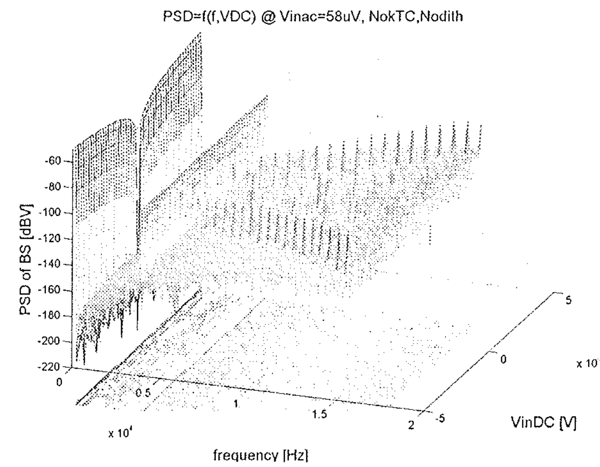

Figure 2: *PSD of a Mod2 bit-stream: no dither and no kT/C*

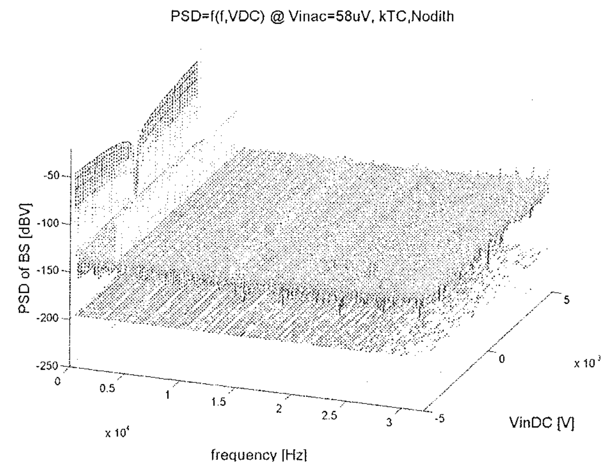

Figure 3: *PSD of a Mod2 bit-stream: no dither, kT/C noise included*

Figure 3 shows the same modulator when the dither signal is switched off but circuit noise and kT/C noise sources corresponding to the S-C implementation are switched on. We could immediately see that the low frequency portion of the spectrum was covered with "thermal" noise, but tones in higher frequencies in the base-band are not affected; they are approximately the same in frequency and power as before. The message from that experiment is that only kT/C noise cannot decorrelate low frequency (and also high frequency) tones. It would be possible to "cover" the base-band tones by increasing the kT/C noise level but this would decrease the S/N ratio in the base-band, so this approach is of little benefit. In addition, high frequency tones remain unchanged as will be shown in the next subsection. Adding the dither signal efficiently decorrelates limit-cycles in the base-band as shown in Figure 4.

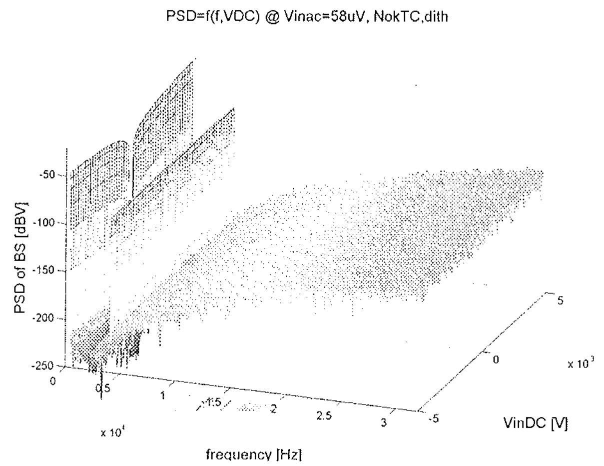

Figure 4: *PSD of a Mod2 bit-stream: dither included, no kT/C noise*

A dither signal has a flat spectrum and is connected to a quantizer's input or it could be HP shaped and connected to a second integrator's input. We can see that the tones' peak amplitudes are reduced for more than 10dB at high frequencies and even more at low frequencies, but at the same time the base-band noise floor has increased slightly. Additionally, the modulator's S/N ratio is reduced by approximately 3dB because part of the second integrator's voltage range has been consumed by dither "noise." Decorrelation of tones at high frequencies close to fs/2 is even more dramatic, as will be shown later.

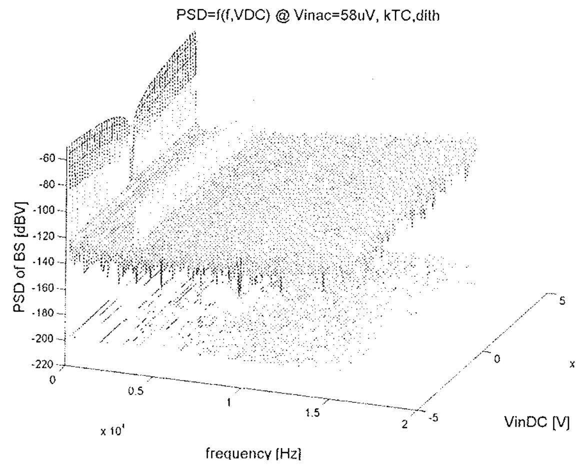

Figure 5: *PSD of a Mod2 bit-stream: dither included, kT/C noise included*

Figure 5 shows a bit-stream's real spectrum when a dither signal is applied and all circuit noise sources are switched on. The noise floor in that case is approximately flat in the base-band and tones are almost completely eliminated in the base-band and also at high frequencies close to $f_s/2$, so the chance of cross-talk is greatly reduced.

The conclusion from this experiment is that kT/C noise alone is not sufficient to eliminate tones in the base-band and at high frequencies for a 2nd order modulator. A suitable dither signal must be used to achieve that goal. The improvement is much more dramatic for a smaller bandwidth where the tone power's relative contribution might be much bigger than the noise floor's power. Because integrators are analogue modules with unpredictable offsets that change with stress, temperature, supply voltage, etc., "tones" can move around the base-band as a function of external conditions and may corrupt the A/D conversion process. It is therefore important to eliminate or at least reduce the potentially harmful tonal behaviour of any ΣΔ modulator using appropriate techniques.

To further investigate a mod2's behaviour with regard to its tonal behaviour under different conditions, a mod2 was simulated using different DC and AC input voltages. The maximum possible Signal to Noise and Distortion ratio (SNDR) has been calculated and plotted on a 3D plot shown in Figure 6. Dither and kT/C noise have been switched on. Noise level in the base-band is measured for each pair of AC and DC input voltages and is compared to the maximum possible input signal's rms voltage before overload starts to reduce the SNDR. For input signals around signal ground with amplitudes from 0 up to ~$0.58V_{ref}$, the SNDR is more

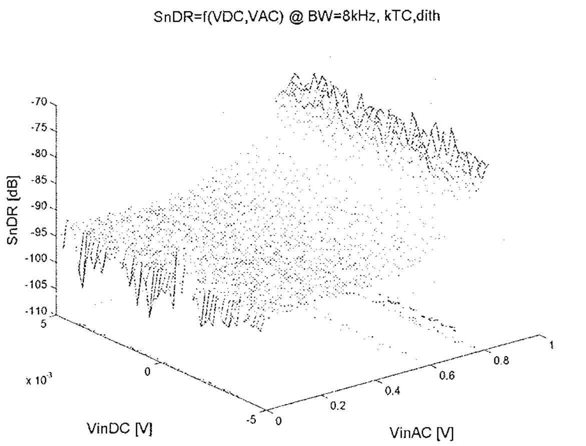

Figure 6: *PSD=f (DC, AC); dither and kT/C included*

than 90dB in the 8 kHz bandwidth. Tones in the base-band have been eliminated or at least reduced below the noise floor. In addition, the noise level is approximately constant for all amplitudes up to 0.7V, while the noise level starts to increase at higher input voltages, which suggests the biggest useful input voltage taking into consideration the integrator model that includes the limitation of the state variable voltages due to real circuit behaviour.

The major limitations to reaching better performance are quantization noise and kT/C noise. Both can be improved; the first one by increasing the over-sampling ratio and the second by increasing the capacitances of input switched capacitors.

In the literature /1/ we saw many statements that the limit-cycles depend also on the state variables' initial conditions. To test that we performed simulations and analysis of a 2nd order modulator at a fixed DC input voltage (V_{ref}/1024), fixed AC input voltage of a_{in} = 58μV and different conditions regarding kT/C noise and dither, changing the initial conditions. The same experiment was performed first with a 2nd order modulator and then also with a 5th order modulator. The same initial conditions for all state-variables were used, which varied from -3.3V_{ref} to +3.3V_{ref}. A bit-stream's PSD is observed and plotted on a 3D plot with frequency on the x-axis, initial condition voltage on the y-axis and PSD on the z axis for different combinations of dither and circuit noise. The results are presented in Figure 7 through10.

The analysis of simulation results shows that at least for the stated conditions (60uV AC input signal and fixed DC input voltage V_{ref}/1024) the tones' frequencies and amplitudes do not depend on the initial conditions. As before, we can see that by using appropriate dither and circuit noise the tones can be almost completely eliminated as shown on Figure 10. The remaining tones seem independent of the initial conditions. Unfortunately these experiments do not prove that limit cycles are independent of initial conditions because we could not test all possible combinations of different conditions.

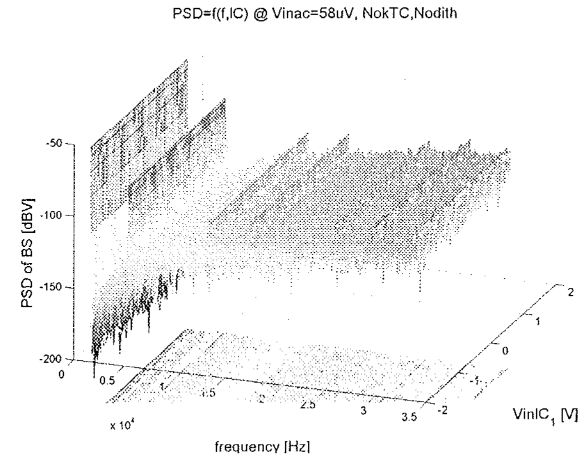

Figure 7: *Tones as a function of initial conditions (IC); no dither, no kT/C*

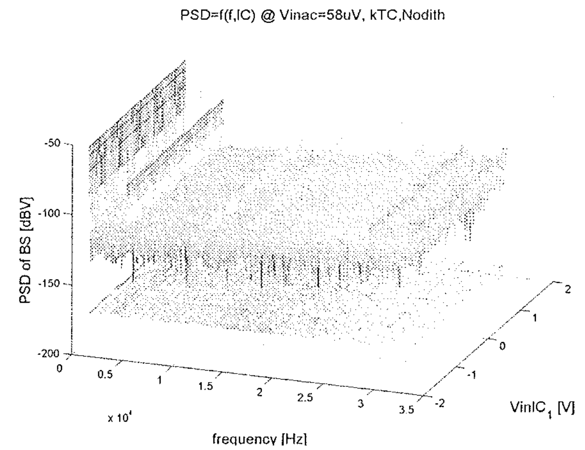

Figure 8: *Tones as a function of initial conditions (IC); no dither, kT/C*

As we mentioned previously, very dangerous tones are generated at high frequencies close to (f_s/2). These types of limit cycles are formed for any kind of input signal even in the presence of a high amplitude AC input signal. They are not

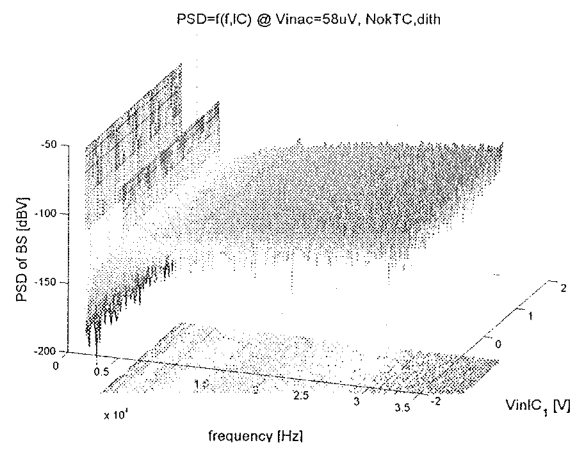

Figure 9: *Tones as a function of initial conditions (IC); dither, no kT/C*

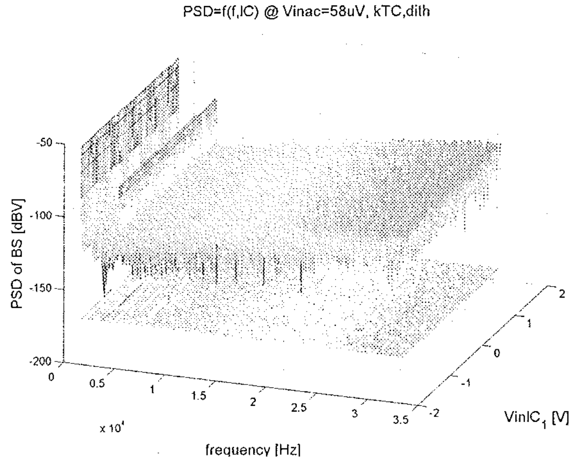

Figure 10: *Tones as a function of initial conditions (IC); dither, kT/C*

dangerous by themselves because they are out of the band and are attenuated by the decimation filter. Unfortunately, they may be transferred back to the base-band by some nonlinear process or by cross-talk to the input or, for example, through the references. Simulations of a standard 2nd order modulator were performed with sine-wave signals having amplitudes from 1uV to maximum input voltage of $V_{ref} / \sqrt{2}$.

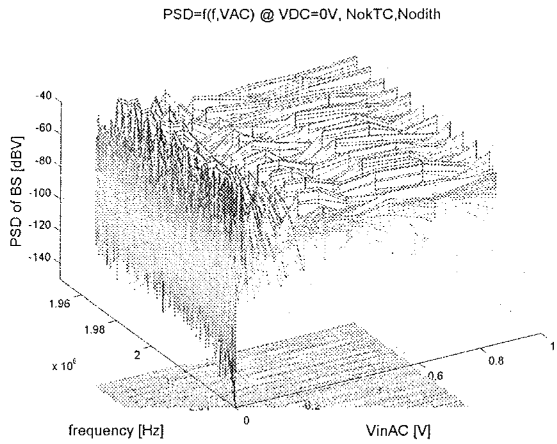

Figure 11: *PSD of y (n) at high frequencies; no dither, no kT/C*

A bit-stream's PSD is observed in a band between $(f_s/2)$ - 80kHz and $(f_s/2)$ as a function of frequency and input signal amplitude at a fixed DC input voltage of $(V_{ref}/1024)$.

The results are presented on four 3D plots shown in Figure 11 through Figure 14. In all cases the x-axis is the frequency, the y-axis represents the amplitude of a sine wave and the z-axis shows the bit-stream's PSD.

It is obvious that when dither is switched off many tones at high frequency are present (Figure 11). Their amplitudes are higher than the level of quantization noise, and the frequencies and amplitudes depend on the input AC signal's amplitude.

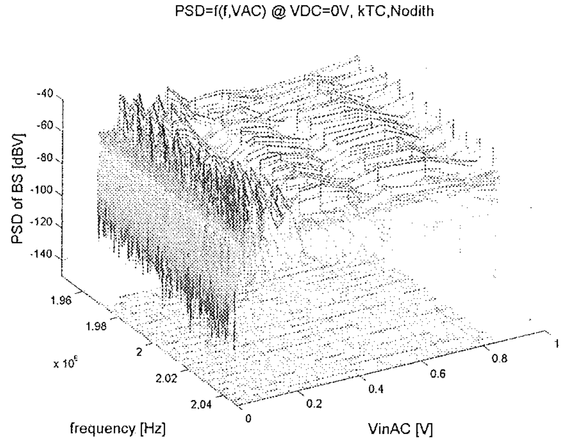

Figure 12: *PSD of y (n) at high frequencies; no dither, kT/C*

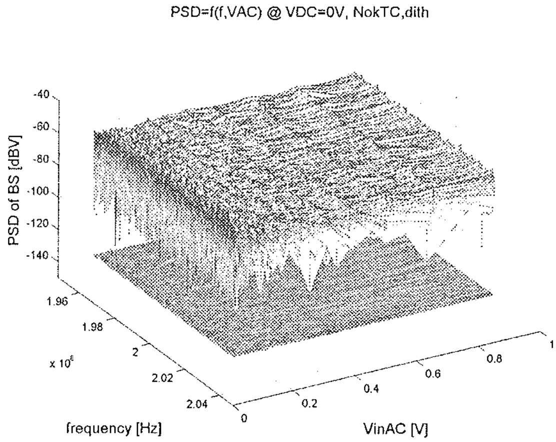

Figure 13: *PSD of y (n) at high frequencies; dither, no kT/C*

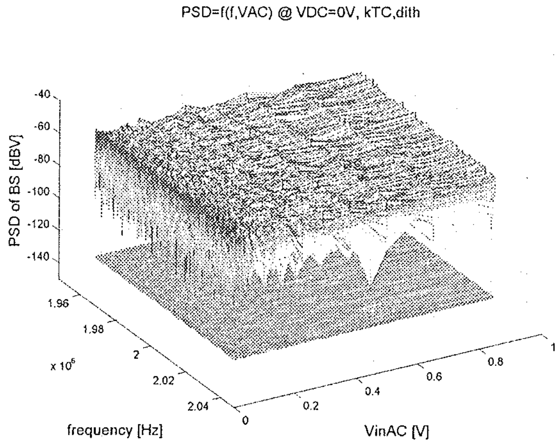

Figure 14: *PSD of y (n) at high frequencies; dither, kT/C*

The addition of kT/C and thermal noise to the structure, which corresponds to S-C stages, does not break the HF limit cycles or improve the tonal behaviour as demonstrated in Figure 12. The HF tonal behaviour is greatly improved if a dither signal is applied to a quantizer's input, independent of kT/C noise as shown in Figure 13 and Figure 14.

From these simulations and analyses we can conclude that applying an appropriate dither signal and an appropriate level of circuit noise almost completely removes tones in the base-band as well as at high frequencies. The price paid is a small reduction in the maximum achievable SNR ratio because part of the last integrator's voltage range is occupied by the dither signal; this loss is in the range of 2 to 3dB.

3.2 LP 5th order modulator:

The same technique used for the 2nd order modulator is used for the 5th order modulator with a 1 bit quantizer. Again, simulations of an ideal modulator demonstrate tones in the base-band dependent on DC input voltage as shown in Figure 15. Adding kT/C noise just covers low frequency tones. Higher frequency base-band tones remain unchanged as can be observed in Figure 16. Therefore, without using a dither signal it does not make sense to decrease the input switched capacitors' kT/C noise too much because sooner or later the tones in the base-band will limit the (S/N) ratio.

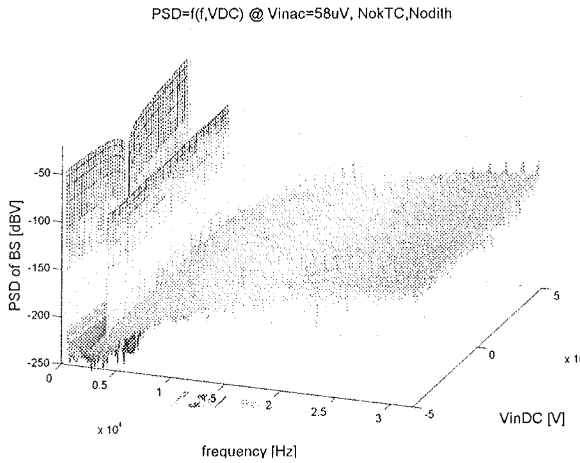

Figure 15: *PSD of a mod5; no dither, no kT/C*

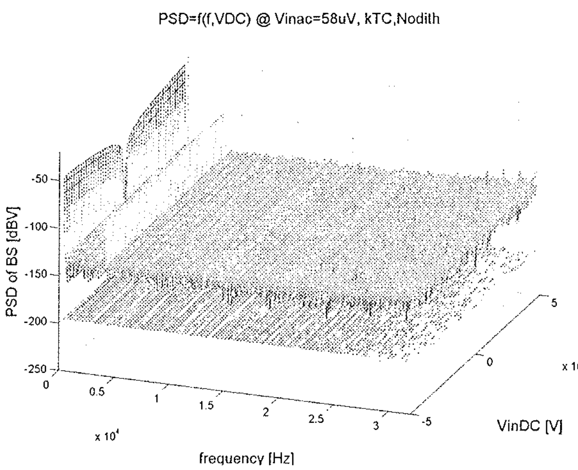

Figure 16: *PSD of a mod5; no dither, kT/C*

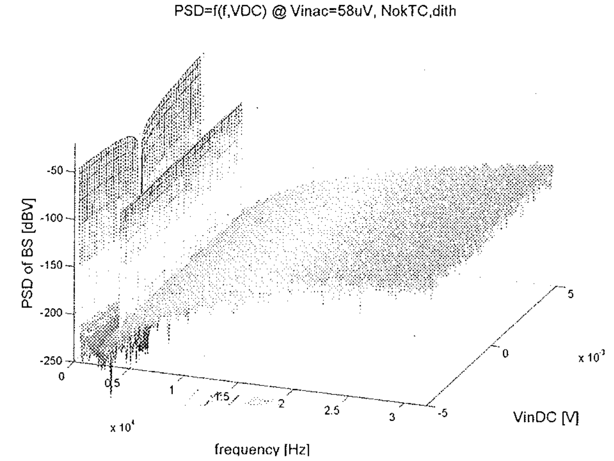

Figure 17: *PSD of a mod5; dither, no kT/C*

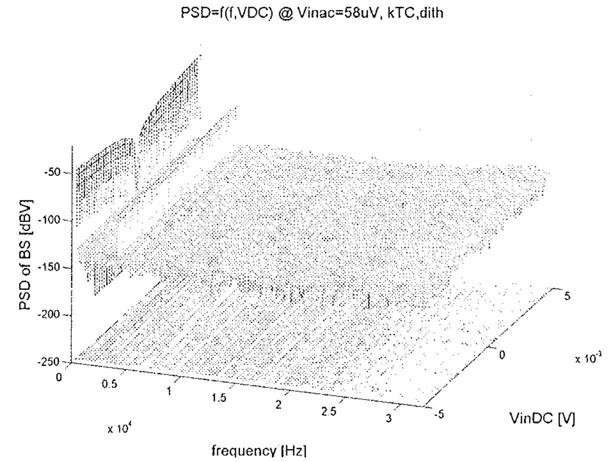

Figure 18: *PSD of a mod5; dither, kT/C*

Adding a dither signal to a quantizer's input efficiently decorrelates limit-cycles in the base-band as shown in Figure 17. A real situation including dither and kT/C noise is depicted in Figure 18, which looks similar to Figure 16 with the important difference that in this case tones at higher frequencies of a base-band are eliminated.

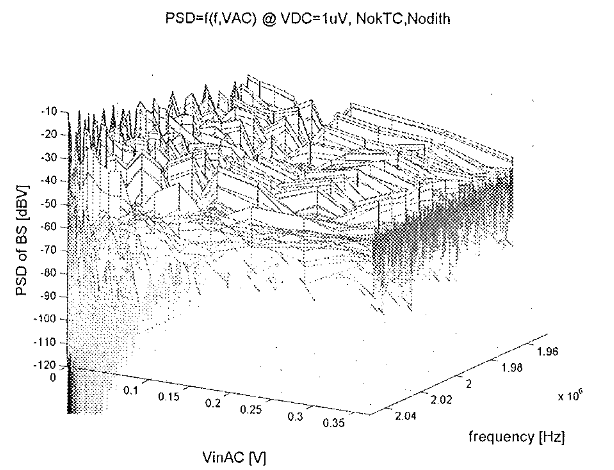

Figure 19: *PSD of a mod5 at HF; no dither, no kT/C*

In-band tones of a 5th order modulator have less power in general than a 2nd order modulator because the NTF has greater attenuation of quantization noise in the base-band; unfortunately the demands for the S/N ratio are bigger. Again, tones can be eliminated using dither and kT/C noise. As before, not only base-band tones are dangerous but also high frequency tones because they could be translated to the base-band by some nonlinear process or, for example, a cross-talk mechanism.

The high frequency behaviour of an ideal 5th order modulator is presented in Figure 19 through Figure 22. The PSD of a quantization noise in a band 80 kHz away from $f_S/2$ is presented as a function of AC input voltage. All 3D plots have input signal amplitudes on the x-axis, frequency on the y-axis and the bit-stream's PSD on the z-axis.

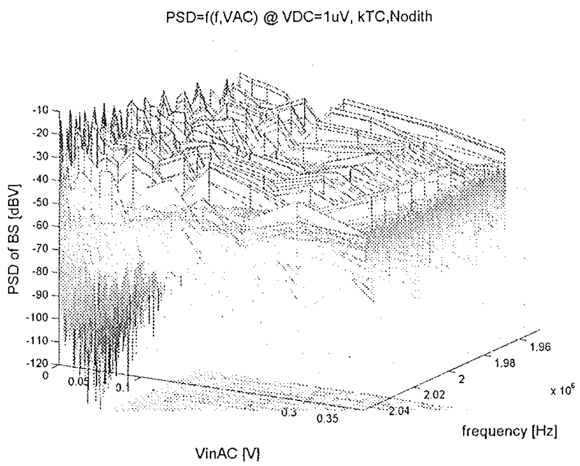

Figure 20: *PSD of a mod5 at HF; no dither, kT/C*

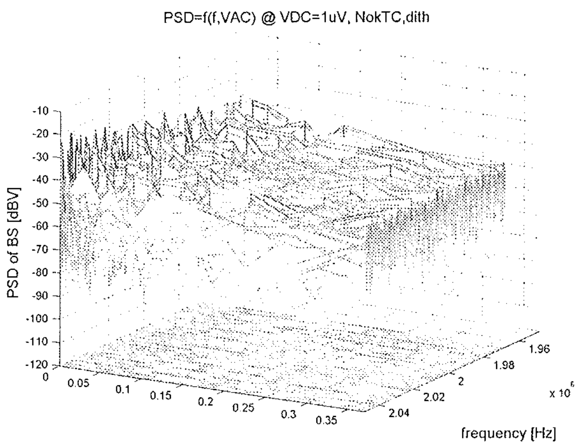

Figure 21: *PSD of a mod5 at HF; dither, no kT/C*

As before, the kT/C noise alone does not change HF limit-cycles as we can see from Figure 19 and Figure 20. Their frequencies and amplitudes depend on the applied amplitude of the AC signal. The most dangerous tones are those with frequency close to $f_S/2$ because they can be aliased to the base-band; their amplitudes are very big compared to the level of the signal, so even the smallest cross-talk, which has, for example, 100dB of attenuation, will degrade the performance.

Applying a dither signal to a quantizer's input reduces the amplitudes of tones at HF by more than 10db. This is a significant improvement, while the penalty in SnR is only ~3dB. Further reduction of HF tones is possible by applying a frequency shaped dither signal to the modulator.

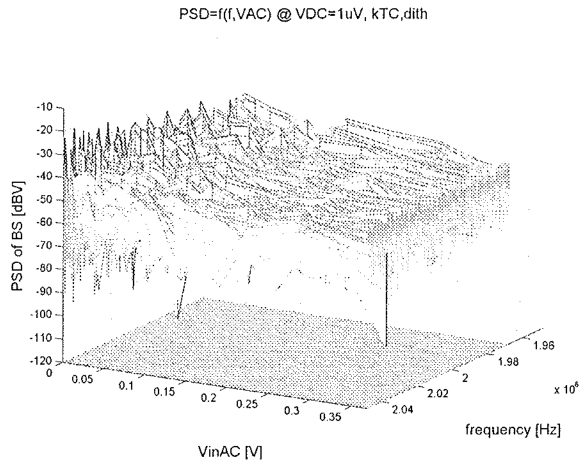

Figure 22: *PSD of a mod5 at HF; dither, kT/C*

4. Conclusion

A new state-space model of a general single loop ΣΔ modulator including kT/C noise sources and dither inputs and sources has been developed and used. Thanks to modern computers' high computing power it is fairly easy to simulate the tonal behaviour of any single loop modulator in a short time. For a 2nd order modulator it is proven that the quantization noise spectrum consists of tones whose frequencies depend on DC input voltage. They can be greatly reduced by applying appropriate dither to the modulators' state variables. Thermal and kT/C noise alone cannot decorrelate the modulators' tonal behaviour, so an appropriate dither signal is needed. Describtion of dither signal is beyond this paper's scope. A dither signal's effect is even greater on the quantization noise's HF part, which reduces the chance of HF tones appearing in the base-band due to some cross-talk mechanism. Further research will focus on an analytical solution and the study of tonal behaviour as a function of different parameters, signals and dither signals connected to the modulators' loop filter's state-variables.

5. References

/1/ R. Schreier, G.C. Temes, "Understanding Delta-Sigma Data Converters," Wiley Interscience, 2005

/2/ R.M.Gray, "Quantization Noise Spectra," IEEE Trans. Inform. Theory, Nov. 1990.

/3/ S.Mann, D.Taylor, "Limit Cycle behaviour in the double loop band-pass Sigma-Delta A/D converter," IEEE Trans CAS.II, Analogue and digital Signal Processing, vol .46, Aug.1999.

/4/ C. Dunner and M. Sandler, "A comparison of Dithered and Chaotic Sigma-Delta Modulators," J. Audio Eng. Soc., VOl. 44, No. 4, pp.227-244, Apr. 1996.

/5/ D.Strle, "Capacitor-area and power-consumption optimization of high order Ó-Ä modulators," Inf. MIDEM, 2001.

D.Strle,
University of Ljubljana, Faculty for Electrical Engineering, Tržaška 25, Ljubljana, Slovenia

Prispelo (Arrived): 03. 01. 2006; Sprejeto (Accepted): 30. 01. 2006

UDK621.3:(53+54+621+66), ISSN0352-9045 Informacije MIDEM 36(2006)1, Ljubljana

EFFICIENT SUBSET SELECTION FROM PHONETICALLY TRANSCRIBED TEXT CORPORA FOR CONCATENATION-BASED EMBEDDED TEXT-TO-SPEECH SYNTHESIS

Aleš Mihelič[1], Jerneja Žganec Gros[1], Nikola Pavešić[2], Mario Žganec[1]

[1]Alpineon, Ljubljana, Slovenia

[2] Faculty of Electrical Engineering, University of Ljubljana, Slovenia

Key words: embedded text-to-speech synthesis, speech corpus design, sentence subset selection

Abstract: In this paper we describe the design concept of a corpus-based concatenation text-to-speech (TTS) system for Slovenian, suitable for implementation in embedded applications. Because memory and processing power requirements are important factors when designing TTS systems for embedded devices, lexica and speech corpora need to be reduced. We describe a simple and efficient implementation of a greedy subset selection algorithm that extracts a compact subset of high coverage text sentences out of a larger set of sentences. The experiment on the Slovenian text corpus showed that the subset selection algorithm produced a compact sentence subset with a small redundancy. We conclude that the proposed sentence selection algorithm is capable of selecting a rather modest subset of sentences out of the reference text corpus, and the resulting sentence subset covers the most frequent collocations, words, quadphones and triphones in a given language.

Postopek za izbor podmnožice stavkov iz besedilnega korpusa za sintezo govora v vgrajenih sistemih

Kjučne besede: vgrajena sinteza govora, govorne podatkovne zbirke, izbira reprezentativne podmnožice stavkov

Izvleček: V članku opisujemo postopek zasnove in tvorjenja govorne zbirke za korpusno sintezo slovenskega govora, ki je primerna za implementacijo v vgrajenih sistemih. Postopek obsega izbiro besedila, snemanje in segmentacijo ter označevanje govornega gradiva. Sprva smo izvedli frekvenčno analizo pogostosti pojavljanja glasovnih sklopov za slovenski jezik nad obsežnim vhodnim besedilom, ki smo ga predhodno pretvorili v fonetični prepis. Nadalje opisujemo postopek, ki iz množice besedil v pisni obliki izbere kompaktno podmnožico stavkov, ki vsebujejo vsa želena pogosta zaporedja glasov v danem jeziku. Sledi snemanje ter polsamodejno označevanje posnetega govornega gradiva. Članek sklenemo z rezultati preskusa naravnosti in razumljivosti sintetizatorja govora.

1. Introduction

A vital part of speech technology applications in modern human-machine user interfaces is a text-to-speech (TTS) engine. Text-to-speech synthesis enables automatic conversion into spoken form of any available textual information. Despite its considerable promise, text-to-speech synthesis is still not being used on a wide-scale basis in public service contexts. Wider acceptance of TTS devices will depend on three factors: better quality, smaller footprints, and more attractive pricing.

With the evolution of small portable devices, porting of high quality text-to-speech engines to embedded platforms has been made possible /1/, /2/. Many applications in mobile telephony and portable computing require high-quality speech synthesis systems with a very modest computational and memory footprint.

TTS systems, which are using a corpus-based concatenative approach, yield close-to-natural sounding speech /3/, /4/, /5/. However, the linguistic resources required to build embedded TTS modules need to be scaled down to meet the hardware specifications of the embedded devices. The major memory and processing power consuming linguistic resources that need to be reduced are lexica and speech corpora /6/, /7/. The application of these reductions to Slovenian is demonstrated in the paper by utilizing efficient exception lexicon and speech corpus reductions. They were performed on the baseline full-size AlpSynth TTS system /8/, which uses a 95 Mb read speech corpus. A new, compressed speech corpus with a reduced set of read sentences was designed, which covers the most frequent allophone sequences in the language. The sentence subset has been selected from a large phonetically transcribed text corpus. The goal was to extract a sentence subset with high phonetic coverage and small size.

First an overview of the AlpSynth TTS components is given. We continue to describe the small-footprint speech corpus design process, with an emphasis on the sentence subset selection method. The quality of the synthesized speech was assessed in a listening experiment in terms of intelligibility and naturalness of pronunciation, whereby the small-footprint TTS system was compared against the baseline full-size AlpSynth TTS system. We conclude the paper by discussing the evaluation results and outlining plans for future work and concept implementation (Figure 1).

2. Concatenation-based TTS

In the AlpSynth TTS system, input text is transformed into its spoken equivalent by a series of modules: a grapheme-to-phoneme module produces strings of phonetic symbols based on information in the written text; a prosodic generator assigns pitch and duration values to individual phones; final speech synthesis is based on speech unit concatenation, where the elemental units are selected from a prerecorded and annotated speech corpus and later concatenated using a pitch-synchronous overlap-and-add technique. The linguistic front-end speech synthesis phases used in the system are described in the following two subsections.

2.1. Grapheme-to-allophone conversion

Input to the TTS system is unrestricted Slovenian text. It is translated into a series of allophones in two consecutive steps. First, input text tokenization and token-to-word conversions are performed. Abbreviations are expanded to form equivalent full words using a special list of lexical entries. The text normalizer converts further special formats, such as numbers or dates, into standard grapheme strings. The rest of the text is segmented into individual words and basic punctuation marks.

Next, phonetization or grapheme-to-phoneme conversion is performed. Word pronunciations are derived based on a user-extensible pronunciation dictionary and letter-to-sound rules. We constructed a dictionary that covers over 1,400,000 Slovenian inflected word forms. When dictionary derivation fails, words are transcribed using automatic lexical stress assignment and letter-to-sound rules. The use of rules enables the TTS system to generate a first attempt at pronunciations of neologisms and named entities.

To further reduce the memory footprint of the grapheme-to-allophone conversion module, we compiled an exception dictionary that contains only the differences from the phonetic transcriptions obtained by applying the letter-to-sound rule set. Similar to /7/, a compression factor of ten was

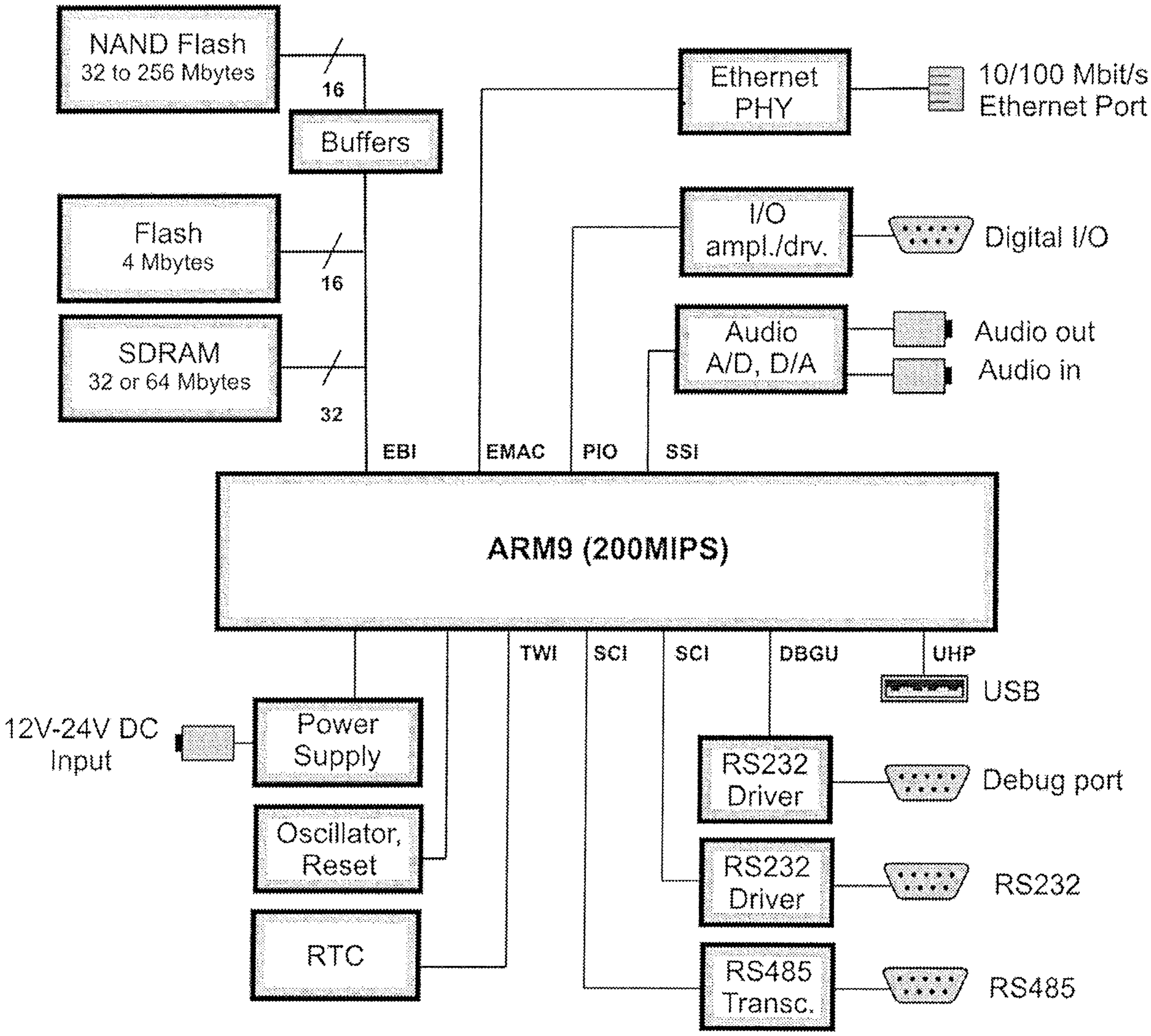

Fig. 1: Outline of hardware implementation of the reduced-footprint TTS system.

achieved, compared to the baseline full-lexicon representation, without sacrificing transcription accuracy. Further lexicon size reductions were achieved by modeling the exception lexicon in form of a decision tree, as proposed by /9/. We intend to test more approaches for efficient lexicon representation, among them finite-state transducers, which have already been applied for coding of language resources /10/, including Slovenian /11/.

2.2. Prosody Modeling

Corpus-based prosody modeling yields high-quality and close-to-natural sounding prosody parameter prediction; however, it requires a large amount of linguistic information upon which to rely. We used a compact rule-based prediction method to determine the target prosodic parameters in four phases: intrinsic duration assignment, extrinsic duration assignment, modeling of the intra word F0 contour, and assignment of a global intonation contour /8/.

Regardless of whether the duration units are words, syllables, or phonetic segments, contextual effects on duration are complex and involve multiple factors. A two-level duration model first determines the words' intrinsic duration, taking into account factors relating to the phone segmental duration, such as: segmental identity, phone context, syllabic stress, and syllable type: open or closed syllable /12/. Further, the extrinsic duration of a word is predicted, according to higher-level rhythmic and structural constraints of a phrase, operating at the syllable level and above. Here the following factors are considered: the chosen speaking rate, the number of syllables within a word and the word's position within a phrase, which may be isolated, phrase-initial, phrase-final or nested within the phrase.

Finally, intrinsic segment duration is modified, so that the entire word acquires its predetermined extrinsic duration. It is to be noted that stretching and squeezing does not apply to all segments equally. Stop consonants, for example, are much less subject to temporal modification than other types of segments, such as vowels or fricatives. Therefore, a method for segment duration prediction was used, which adapts a word with an intrinsic duration t_i to the determined extrinsic duration t_e, taking into account how stretching and squeezing apply to the duration of individual segments /12/.

Slovenian is a language with pitch accent, therefore special attention was paid to the prediction of tonemic accents for individual words. First, initial vowel fundamental frequencies were determined according to the parameters obtained from prior prosody measurements, creating the F0 backbone. Each stressed word was assigned one of the two tonemic accents characteristic for Slovenian. The acute accent is mostly realized by a rise on the post-tonic syllable, whereas with the circumflex the tonal peak usually occurs within the tonic.

3. Speech Corpus Design

For unit-selection and other types of concatenation-based text-to-speech synthesis, a speech corpus of recorded and annotated elemental speech units is required /4/. The quality of the output synthetic speech depends crucially on the quality of the speech corpus. The longer elemental speech units are used, the better and more natural-sounding synthetic speech the TTS system can yield.

However, with longer elemental speech units the corpus size increases dramatically, as do the recording and annotation costs. Therefore, a compromise between the size of the speech corpus and the quality of the resulting speech has to be taken /13/ that is even more pronounced for embedded TTS.

If the corpus selection method is unbalanced or random, the recorded data may lack critical phone transitions and may be full of redundancies. Various corpus reduction methods have been reported, from those optimizing and reducing the contents of the prerecorded and annotated speech corpora to those that try to compress the initial text corpus to be recorded /14/, /15/, /16/, /17/, /18/. Often sentence pair exchanges are calculated using diphone and triphone entropies. In /14/, the unit coverage is maximized using prosody information. In /15/, a modified greedy algorithm is applied that maximizes the hit-rate and covering-rate for sentence selection criteria. A two-stage sentence recording script design presented in /17/ takes into account the balance of acoustic speech parts to provide variations in short-time speech features, and the linguistic parts provide long-time speech features, such as words or frequent word sequences.

We wanted the most frequent allophone sequences in a given language to be represented in the final sentence set, and therefore we implemented a greedy algorithm, similar to the one described in /15/, to reduce the initial text sentence set to a compact and efficient subset. The process of designing a speech corpus for concatenation-based TTS was divided into three phases:

- Representative sentence set selection,
- Recording of selected texts, and
- Segmentation and annotation of the recorded speech material.

3.1. Sentence subset selection algorithm

Initially, we collected a large corpus of texts covering various text styles, ranging from newspaper articles to fiction. All sentences shorter than five words or longer than 25 words were discarded from further analysis. The remaining reference text corpus contained 500,000 different sentences, corresponding to 50 Mb of text in ASCII format.

The text corpus was processed by a grapheme-to-allophone converter from the TTS system in order to obtain an allophone transcription of the text corpus. A statistical analysis of frequent phone sequences of allophones, diphones, triphones and quadphones was performed on this corpus. It provided us with information about how frequently certain phone combinations occur in spoken Slovenian. In addition, the analysis has shown that only a few triphones have frequent occurrences.

Therefore, it makes sense to select only the most frequent triphones to be represented in the final speech corpus. We opted for the first 1,000 triphones: these represent 1% of the complete triphone set but cover almost 50% of all triphones in the transcribed reference text corpus. In a similar way, the 500 most frequent quadphones were selected.

To synthesize high-quality speech, the speech corpus was required to contain a wide variety of speech parts: from collocations and words to diphones and sub-phoneme parts. With the most frequent triphones and quadphones selected, we wanted to select an optimal compact subset of corpus sentences that cover all the chosen allophone sequences, including most frequent collocations and words in a given language.

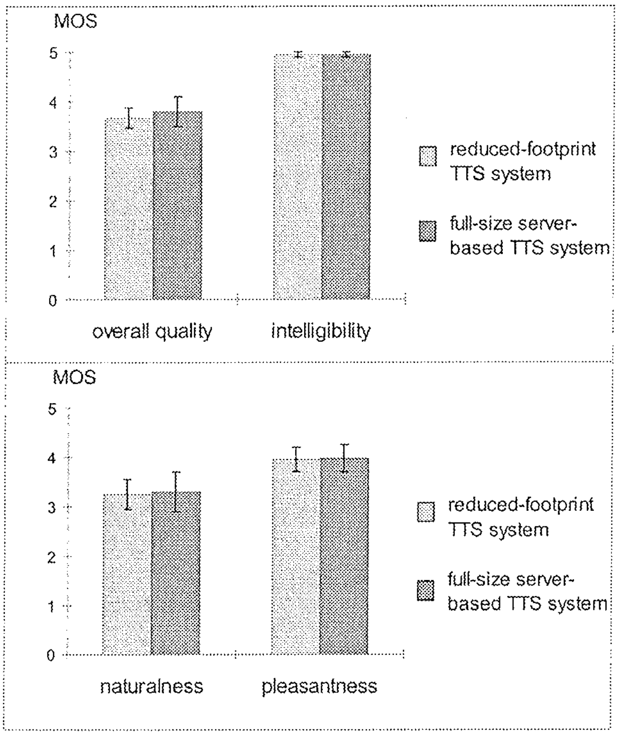

Fig. 2: Subjective evaluation results of the listening tests for both tested TTS systems. The results are given as MOS (Mean Opinion Score) ratings for the following categories: overall quality, intelligibility, naturalness, and voice pleasantness.

A greedy sentence selection algorithm was implemented for this purpose. Each sentence in the reference text corpus was equipped with a cost attribute based on the amount of the preselected frequent allophone sequences they contained. The highest cost value was attributed to a rare preselected quadphone or collocation, and the lowest to a frequent preselected triphone. In order to avoid the selection of long sentences, which contain more allophone sequences than shorter sentences, the cost value was normalized by the total number of allophones within the sentence.

The sentence with the highest score was selected for the final text corpus. The preselected allophone sequences covered by this sentence were eliminated from the list. Then the cost derivation and sentence selection process was performed for this new set of preselected allophone sequences and a new sentence was chosen for the final text corpus. The same process was repeated in a loop until all of the initial preselected allophone sequences were covered in the resulting corpus of selected sentences.

The sentence-selection algorithm was capable of selecting a rather modest subset of sentences out of the reference text corpus that cover the most frequent collocations, words, quadphones and triphones in the given language. A total of 299 sentences were selected out of the initial 500,000 sentences from the reference text corpus. The phonetic transcription of the selected sentence set covered all preselected most-frequent triphones and quadphones.

3.2. Recording and Segmentation

The selected sentence subset was recorded along with logatoms containing all phonetically possible diphone combinations for spoken Slovenian. The speaker was instructed to read the phonetically transcribed sentences and logatoms in supervised recording sessions.

The recorded speech material was segmented and annotated. A semi-automatic procedure was used for segmentation of elemental speech units. A dynamic time-warping acoustic alignment procedure between the synthesized voice and the recordings /19/ was used to obtain preliminary phone boundaries because it performed better in detecting consonant segment boundaries than the HMM approach /20/. The performance of the acoustical clustering plus dynamic time-warping method was upgraded along with boundary specific corrections by means of a decision tree, as recently proposed by /21/. Manual corrections were needed on consonant boundaries within some consonant clusters.

The final speech corpus contains read sentences with 1,993 words. In addition, 1,635 logatoms were recorded. For use in embedded devices, the speech corpus was compressed. Several compression techniques, outlined in /22/, were examined. Finally, a 14.1:1 corpus size reduction was chosen by using Ogg Vorbis encoding, without noticeably degrading the quality of the output speech signal. The resulting footprint of the compressed speech corpus was just below 2 Mb.

4. Evaluation Results

Over recent years, various guidelines have been proposed for evaluating the quality of text-to-speech systems. Yet there are still no existing standards for their evaluation, although a number of different methods have been tried and it has been pointed out that the test results they yielded were often inconsistent /23/.

The adequacy of the resulting concatenation-based TTS system was evaluated in terms of acceptability and intelligibility. The objective of the test was to compare the quality of the small-footprint TTS system to the baseline full-blown large-footprint unit-selection server-based TTS system /8/.

The experiment was performed in laboratory conditions with 51 test subjects. It was designed according to ITU-T Recommendations P.81 and P.85, describing methods for subjective performance assessment of the quality of voice output devices. The evaluators were selected from a wide range of professional backgrounds, and they were in general not familiar with synthetic voice quality. The test was divided into two sessions, neither lasting more than 20 minutes, in order to reduce the fatigue of the evaluators. The synthesis output was directed to a loudspeaker. Each test speech was presented only once.

The first part served to evaluate whether the intelligibility and the quality of the synthetic speech were sufficiently high for a real application of the system in a potential embedded-system application, simulating spoken directions provided by a car-navigation system. The subjects were asked to fill in different application-specific templates based on the information they heard. Each message consisted of a fixed part, which was specific to the task, and a variable part, which was different in all the produced messages. The intelligibility for both systems, when spelling errors are ignored, was nearly 100%. Over 95% of the listeners estimated that both TTS systems were mature enough for deployment in a car-navigation system.

In the second part of the test, the performance of both TTS systems was evaluated by the listeners with grades on a five-point MOS (Mean Opinion Score) scale. For the test, the sentences were synthesized by both TTS systems and presented to the listeners in random order. The listeners were asked to evaluate the overall quality, intelligibility, naturalness, and voice pleasantness. The results are provided in Figure 2. In terms of overall quality MOS grades, the full-size server-based TTS outperformed the reduced-footprint version by only a small margin of 0.15. The majority of the test subjects evaluated the reduced-footprint (as well as the large-footprint) synthetic speech produced by the TTS system as pleasant and quite natural-sounding, sufficiently rapid and not over-articulated.

5. Conclusions

The memory and computational resources in TTS applications on embedded portable devices are inherently limited. Various footprint reduction considerations for embedded TTS implementation are discussed in the paper. We concentrated on shrinking the speech corpus while maintaining high coverage of the frequent allophone sequences in a given language: our goal was to extract a sentence subset with high coverage and small size. The sentence subset was selected from a large phonetically transcribed text corpus.

The greedy sentence selection algorithm implementation described in the paper was capable of selecting a rather modest subset of sentences out of the reference text corpus that covers the most frequent collocations, words, quadphones, and triphones in a given language. A total of 299 sentences were selected out of the initial 500,000-sentence text corpus. The phonetic transcription of the selected sentence subset covered all of the preselected most-frequent triphones and quadphones, words, and collocations.

An implementation of the proposed sentence subset selection method for Slovenian has resulted in a small-footprint TTS system yielding intelligible and sufficiently natural-sounding speech, so that the system is ready for deployment in embedded applications. Listening experiments proved that the TTS system gives satisfactory performance in phonetization and speech concatenation quality with considerably reduced memory resources. The system is implemented in ANSI-C and runs on several operating systems. The object code size of the small-footprint TTS system is 98 Kb, while the size of the language resources used by the system is just below 2Mb. Using the designed compact speech database, the program's current version runs 300 times faster than real time on a Pentium 2 GHz personal computer. At run-time, the program code requires 472 Kb, minimum RAM requirement is 3,500 Kb, while the minimum disc or flash memory requirement is 5,560 Kb.

In order to further compress exception lexica, alternative lexicon representation approaches will be examined, such as /11/. An initial implementation of the described methods on an embedded TTS Unix platform built around an ARM9 processor with an AT91RM9200 core (Figure 1) is under development.

6. Acknowledgements

The authors wish to thank the Slovenian Ministry of Higher Education, Science, and Technology and the Slovenian Research Agency for co-funding this work under contract no. V2-0896.

7. References

/1/ Black, A.W. and Lenzo, K.A., "Flite: a small fast run-time speech synthesis engine", In Proceedings of the 4th ISCA Workshop on Speech Synthesis, 2001, pp. 204-207.

/2/ Tomokoyo, M.L., Black, W.A. and Lenzo, A.K., "Arabic in my hand: small footprint synthesis of Egyptian Arabic", In Proceedings of the Eurospeech'03, Geneva, Switzerland, 2003, pp. 2049-2052.

/3/ Campbell, N., "CHATR: a high-definition speech resequencing system", In Proceedings of the 3rd ASA/ASJ Joint Meeting, 1996, pp. 1223-1228.

/4/ Beutnagel, M., Conkie, A., Schroeter, J. and Stylianou, Y., "The AT&T Next-Gen TTS System", in Proceedings of the 137th Meeting of the Acoustic Society of America, 2000.

/5/ Möbius, B. "The Bell Labs German text-to-speech system", Computer Speech and Language, Vol. 13, 1999. pp. 319-358.

/6/ Tian, J., Nurminen, J. and Kiss, I., "Optimal subset selection from text databases", In Proceedings of the ICASSP'05, PA, USA, 2005.

/7/ Meron, J. and Veprek, P., "Compression of exception lexicons for small footprint grapheme-to-phoneme conversion", In Proceedings of the ICASSP'05, PA, USA, 2005.

/8/ Žganec Gros, J., Mihelič, A., Pavešić, N., Žganec, M., Gruden, S., "AlpSynth - concatenation-based speech synthesis for the Slovenian language", In Proceedings of ELMAR'05, Zadar, Croatia, 2005, pp. 213-216.

/9/ Šef, T. "A two level lexical stress assignment model for highly inflected Slovenian language", In Proceedings of the International Conference on Information Technology and Applications, Sydney, Australia, 2005, pp. 347-351.

/10/ Mohri, M., "On some applications of finite/state automata theory to natural language processing", Natural Language Engineering I, Cambridge University Press, 1996.

/11/ Rojc, M., Kačič, Z., Kramberger, I., "Hardware implementation of language resources for embedded systems". Inf. MIDEM, Vol. 32, No. 3, 2002, pp. 199-203.

/12/ Gros, J., Pavešić, N. and Mihelič, F., "Speech timing in Slovenian TTS", Proceedings of the Eurospeech'97, Rhodes, Greece, 1997, pp. 323-326.

/13/ Van Santen, J.P.H., "Methods for optimal text selection", In Proceedings of the Eurospeech'97, Rhodes, Greece, 1997, pp. 553-556.

/14/ Kawai, H., Yamamoto and Shimizu, T., "A design method of speech corpus for text-to-speech synthesis taking into account prosody", in Proceedings of the ICSLP'00, 2000, pp. 420-425.

/15/ Kuo, C. and Huang, J., "Efficient and scalable methods for text script generation in corpus-based TTS design", in Proceedings of the ICSLP'02, 2002, pp. 121-124.

/16/ Bozkurt, B., Ozturk, O. and Dutoit, T., "Text design for TTS speech corpus building using a modified greedy selection", in Proceedings of the Eurospeech'05, Geneva, Switzerland, 2003, pp. 277-180.

/17/ Isogai, M., Mizuno, M. and Mano, K., "Recording script design for corpus-based TTS system based on coverage of various phonetic elements", In Proceedings of the ICASSP'05, PA, USA, March 18-23, 2005.

/18/ Rojc, M. and Kačič, Z., "Design of optimal Slovenian speech corpus for use in the concatenative speech synthesis system", In Proceedings of the LREC'00, Athens, Greece, 2000, pp. 321-325.

/19/ Malfrčre, F. and Dutoit, T., "High quality speech synthesis for phonetic speech segmentation", In Proceedings of the Eurospeech'97, Rhodes, Greece, 1997, pp. 2631-2634.

/20/ Mihelič, F., Gros, J., Dobrišek, S., Žibert, J. and Pavešić, N., "Spoken language resources at LUKS of the University of Ljubljana", International Journal on Speech Technologies, Vol. 6, No. 3, 2003, pp. 221-232.

/21/ Xydas, G. and Kouroupetroglou, G., "An intonation model for embedded devices based on natural F0 samples", In Proceedings of the Interspeech'04, Korea, 2004, pp. 801-804.

/22/ Hoffmann, J., Jokisch, O., Hirschfeld, D., Strecha, G., Kruschke, G., Kordon, U. and Koloska, U., "A multilingual TTS system with less than 1 Mbyte footprint for embedded applications", In Proceedings of the ICASSP'03, Hong Kong, 2003.

/23/ Alvarez, Y. and Huckvale, M., "The reliability of the ITU-T P.85 standard for the evaluation of text-to-speech systems", In Proceedings of the ICSLP'02, Denver, CO, 2002, pp. 329-332.

mag. Aleš Mihelič, dr. Jerneja Žganec Gros,
dr. Mario Žganec
Alpineon, Ulica Iga Grudna 15, SI-1000 Ljubljana,
Slovenia
info@alpineon.com
tel +386 1 423 9440
tel +386 1 423 9445

prof. dr. Nikola Pavešić
Faculty of Electrical Engineering, University of Ljubljana
Tržaška 25, SI-1000 Ljubljana, Slovenia
nikolap@fe.uni-lj.si
tel +386 1 476 8840
tel +386 1 476 8319

Prispelo (Arrived): 03. 01. 2006; Sprejeto (Accepted): 30. 01. 2006

ZMANJŠANJE POMNILNIŠKEGA PROSTORA ZA PRIMERE NEREKURZIVNIH SIT Z LINEARNIM POTEKOM FAZE V KLASIČNI IN MODIFICIRANI OBLIKI PORAZDELJENE ARITMETIKE

Bojan Jarc, Rudolf Babič

Univerza v Mariboru, Fakulteta za elektrotehniko računalništvo in informatiko, Maribor, Slovenija

Kjučne besede: digitalna obdelava signalov, digitalna sita z omejenim trajanjem impulznega odziva, porazdeljena aritmetika, modificirana porazdeljena aritmetika, zmanjšanje pomnilniškega prostora

Izvleček: Porazdeljena aritmetika (PA) predstavlja bitno-serijski postopek izračuna aritmetične vsote produktov brez uporabe množilnikov. Zaradi svoje homogene strukture je primerna za implementacijo v vezjih FPGA in VLSI. Izvedba digitalnih sit je eden izmed možnih načinov uporabe PA. V prispevku smo se omejili na izvedbo digitalnih sit FIR z linearnim potekom faze, ki ne vnašajo fazne popačitve v izhodni signal in so za področje digitalne obdelave signalov še posebej zanimiva. Njihova posebnost so simetrični koeficienti impulznega odziva. Osnovni problem strukture v porazdeljeni aritmetiki predstavlja velikost pomnilniškega prostora za shranjevanje delnih vsot, ki narašča eksponentno s številom produktov oz. koeficientov sita FIR. Zato v našem prispevki podajamo pristop za zmanjšanje velikosti pomnilniškega prostora v katerem smo izkoristili simetričnost koeficientov impulznega odziva in nasprotno simetrični zapis delnih vsot. Zaradi simetrije koeficientov lahko pomnilniški prostor zmanjšamo iz 2^N na $2^{N/2}$ potrebnih naslovov. Z združitvijo tega pristopa z nasprotnosimetričnim zapisom delnih vsot lahko pomnilniški prostor zmanjšamo na $2^{N/2-1}$ naslovov. Redukcijo pomnilniškega prostora iz 2^N na $2^{N/2}$ potrebnih naslovov lahko dosežemo tudi v modificirani PA. Pravilnost predstavljenih struktur smo potrdili z rezultati simulacij. Izkaže se, da redukcija pomnilnika iz 2^N na $2^{N/2}$ naslovov negativno vpliva razmerje signal-šum izhodnega signala, kar pa v nekaterih primerih uspemo kompenzirati z nasprotnosimetričnim zapisom delnih vsot.

The memory reduction for linear phase FIR filters in classic and modified distributed arithmetic form

Key words: digital signal processing, finite impulse response digital filters, hardware realization, distributed arithmetic, modified distributed arithmetic, memory size reduction

Abstract: Distributed arithmetic (DA) is a parallel serial implementation of the sum of products with no multipliers needed. Because of its structure homogeneity it is suitable for implementation in FPGA and VLSI circuits. Realization of digital filters is one of the fields of DA usage. In this article we have restricted ourselves on the implementation of digital FIR filters with linear phase response. Linear phase filters do not distort phase of output signal and are therefore common choice in the field of digital signal processing. Their property of symmetric impulse response coefficients can be efficiently used in memory reduction process. One of the main problems of DA structure is the quantity of memory, needed for memorizing the precalculated sums of coefficients. The required memory increases exponentially with the number of filter coefficients. This is why in this article we present an approach in which we have token the advantage of impulse response coefficients symmetry and anti-symmetrical presentation of the sums of coefficients. For the FIR filters with odd symmetry we can achieve memory reduction from 2^N to $2^{N/2}$ memory locations. Anti-symmetrical presentation of the sums of coefficients allows us to half the memory from 2^N to 2^{N-1} memory locations. We propose the conjunction of both approaches and thus we manage to achieve the reduction from 2^N to $2^{N/2-1}$ memory addresses. With the simulation results the correctness of proposed structure was confirmed. Since DA is fixed point arithmetic we have also analysed the influence of finite input word length and word length of sums of coefficients on signal-to-noise ratio (SNR). Simulation results show that the procedure of memory reduction from 2^N to $2^{N/2}$ have negative influence on SNR. To achieve the same SNR, the number of bits for sums of coefficients should be increased by one. Approach with anti-symmetrical sums of coefficients allows more appropriate normalization of coefficients and thus improvement of SNR. Consequently we achieve the same level of SNR as in basic DA without memory reduction. The memory reduction approach was also introduced in modified DA. Modified DA utilizes bipolar presentation of unipolar input signal to simplify the arithmetic-logic unit. In modified DA the reduction from 2^N to $2^{N/2}$ memory addresses was achieved. Same decrease of SNR was noticed as at the basic DA structure.

1. Uvod

Porazdeljena aritmetika (PA) predstavlja bitno-serijski postopek izračuna aritmetične vsote produktov z operacijo seštevanja vnaprej izračunanih delnih vsot (DV) shranjenih v pomnilniku. Koncept PA sta omenila že Anderson /1/ in Zohar /2/. Številne funkcije za digitalno procesiranje signalov lahko zapišemo v obliki aritmetične vsote. Med njimi tudi rekurzivna (IIR - *Infinite Impulse Response*) in nerekurzivna (FIR - *Finite Impulse Response*) digitalna sita. Zaradi primernosti za implementacijo v vezjih FPGA in VLSI je bil bitno-serijski postopek uporabljen v različnih aplikacijah /3, 5, 6, 7/.

Konvolucijska vsota digitalnega sita FIR predstavlja tipično vsoto produktov. Osnovni problem sit FIR v obliki PA predstavlja velikost pomnilniškega prostora za shranjevanje delnih vsot. V osnovni obliki PA mora imeti pomnilnik 2^N naslovov, kjer N predstavlja števili koeficientov sita. Tako že pri sitih z N = 30 potrebujemo pomnilnik z 109 naslovi. Iz tega vidika so smiselna prizadevanja za zmanjšanje potrebnega pomnilniškega prostora.

Eden izmed znanih načinov zmanjšanja potrebnega števila pomnilniških lokacij je uporaba nasprotno simetričnih delnih vsot /3/. Pristop omogoča prepolovitev pomnilniškega prostora. Za primere simetričnih sit FIR lahko učinkoviteje zmanjšamo potreben pomnilniški prostor /4, 5/. Na račun dodatne zakasnitve zaradi dvojnega naslavljanja pomnilnika, število naslovnih linij prepolovimo.

Modificirana oblika PA je bila prvič predstavljena v /8/ in podrobneje opisana v /9/. Modificirana PA temelji na unipolarni predstavitvi bipolarnega vhodnega signala $x[n]$ oz. premaknitvi iz območja vrednosti [-1, 1) v območje [0, 2). Zaradi nasprotno simetrične narave DV omogoča prepolovitev pomnilniškega prostora.

Ta prispevek je organiziran kot sledi. V drugem poglavju je opisana osnovna oblika sita FIR v PA, v tretjem poglavju je opisana predlagana struktura za primere simetričnih sit z zmanjšanjem pomnilniškega prostora iz 2^N na $2^{N/2-1}$ naslovov. Četrto poglavje predstavlja postopek zmanjšanja pomnilniškega prostora v modificirani PA. V poglavju 5 so predstavljeni rezultati in v poglavju 6 zaključek.

2. Klasična oblika porazdeljene aritmetike

Konvolucijsko vsoto digitalnega sita FIR zapišemo z:

$$y[n] = \sum_{k=0}^{N-1} h[k]x[n-k]. \tag{1}$$

Pri tem je $h[k]$ k-ti koeficienti impulznega odziva, N predstavlja število koeficientov $h[k]$, z $x[n]$ ter $y[n]$ smo označili vhodno in izhodno zaporedje sita, ter n je časovni indeks. Predpostavimo, da so vrednosti vhodnega zaporedja $x[n]$ omejene v polodprtem intervalu [-1, 1). Posamezni element zaporedja predstavimo z dvojiškim komplementom kot:

$$x[n] = -b_0[n] + \sum_{i=1}^{Bx-1} b_i[n]2^{-i}. \tag{2}$$

Pri tem je Bx število bitov za zapis $x[n]$ in $b_i[n]$ so binarne spremenljivke, ki lahko zavzamejo vrednost 0 ali 1. $b_0[n]$ predstavlja predznak in $b_{Bx-1}[n]$ najmanj utežni bit z utežno vrednostjo $2^{-(Bx-1)}$. Upoštevajoč (2) zapišemo (1) z:

$$y[n] = -v_0[n] + \sum_{i=1}^{Bx-1} v_i[n]2^{-i}, \tag{3}$$

pri tem so $v_i[n]$ delne vsote, ki jih izračunamo z:

$$v_i[n] = \sum_{k=0}^{N-1} h[k]b_i[n-k]. \tag{4}$$

Za izračun trenutne izhodne vrednosti potrebujemo le operacijo seštevanja in množenja z 2^{-i}. Množenje z 2^{-i} predstavlja pomik vsebine akumulatorja za i bitov na desno. Odštevanje zadnje delne vsote v_0 je izvedeno s prištevanjem dvojiškega komplementa v_0. Delne vsote izračunamo vnaprej in jih zapišemo v pomnilnik velikosti $B_v \times 2^N$, kjer B_v predstavlja število bitov za zapis delnih vsot in N je število koeficientov $h[k]$. Izvedbo digitalnega sita v PA prikazuje slika 1.

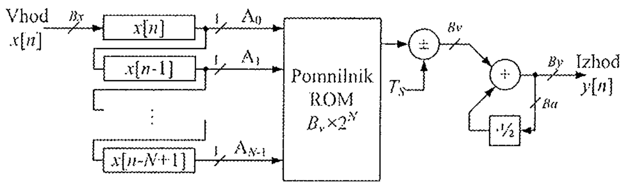

Slika 1: Izvedba digitalnega sita FIR v PA.

T_S na sliki 1 predstavlja kontrolni signal za spremembo predznaka v_0.

3. PA in sita FIR z linearnim potekom faze

V osnovi lahko imajo sita FIR poljuben amplitudni in fazni spekter. Posebnost so sita z linearnim potekom faze, ki so za področje digitalne obdelave signalov posebej zanimiva saj ne vnašajo dodatne fazne popačitve v izhodni signal. Posledično imajo takšna sita simetrične koeficiente $h[k]$. Glede na to ali imamo opravka s sodim ali lihim številom koeficientov govorimo o sodi ali lihi simetriji. Za oba primera simetrije velja:

$$h[k] = h[N-1-k], \qquad k = 0, 1, \ldots, N-1, \tag{5}$$

pri tem je N število koeficientov $h[k]$. Pri lihi simetriji centralni koeficient nima svojega simetričnega para. V obeh primerih sit je fazna zakasnitev $\Theta(\omega)$ linearno odvisna od frekvence in je:

$$\theta(\omega) = \frac{N-1}{2}\omega. \tag{6}$$

Za sita s sodo simetrijo ob upoštevanju (5) zapišemo (4) z:

$$\begin{aligned} v_i[n] &= \sum_{k=0}^{N/2-1} h[k]\big(b_i[n-k] + b_i[n-N+1+k]\big) \\ &= \sum_{k=0}^{N/2-1} h[k]\big(b_{i,S}[n-k] + 2b_{i,C}[n-k]\big) \\ &= v_{i,S}[n] + 2v_{i,C}[n]. \end{aligned} \tag{7}$$

Pri tem sta b_i binarni spremenljivki vrednosti 0 ali 1. S seštevanjem dobimo bit vsote $b_{i,S}$ in bit prenosa $b_{i,C}$ ter odgovarjajoči delni vsoti $v_{i,S}$ in $v_{i,C}$ izračunani vnaprej iz polovice koeficientov po:

$$v_{i,z}[n] = \sum_{k=0}^{N/2-1} h[k] b_{i,z}[n-k]. \quad (8)$$

Pri tem smo z "z" označili S ali C. Ker ima $b_{i,C}$ za dvakrat večjo utežno vrednost od $b_{i,S}$ moramo $v_{i,C}$ pomnožiti z dve. Na račun zmanjšanja pomnilniškega prostora, moramo za izračun ene delne vsote v_i pomnilnik naslavljati dvakrat. Ustrezno blokovno shemo sita v PA s prepolovljenim številom naslovnih linij prikazuje slika (2).

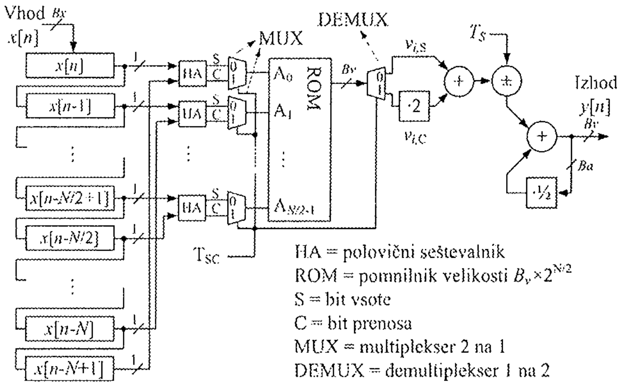

Slika 2: Zmanjšanje pomnilniškega prostora za sita FIR s sodo simetrijo koeficientov iz 2^N na $2^{N/2}$ naslovov.

Pri tem sta T_S in T_{SC} kontrola signala za zamenjavo predznaka v_0 oz. za naslavljanje $v_{i,S}$ in $v_{i,C}$.

3.1 Nasprotno simetrični zapis delnih vsot

Kot smo dejali uvodoma lahko, v klasični PA, z nasprotno simetričnim zapisom delnih vsot prepolovimo potreben pomnilniški prostor. Mi predlagamo dodatno prepolovitev pomnilniškega prostora za sito FIR s prepolovljenim številom naslovnih linij (glej sliko 2). Delne vsote polovice koeficientov izračunane po (8) zapišemo nasprotno simetrično z:

$$s_i[n] = \sum_{k=0}^{N/2-1} h[k] b_i[n-k] - \frac{1}{2} \sum_{k=0}^{N/2-1} h[k] \quad (9)$$

Primerjavo tako izračunanih in klasičnih delnih vsot prikazuje tabela 1.

Tabela 1: Klasične in nasprotno simetrične delne vsote iz polovice koeficientov s sodo simetrijo.

Naslov	v	s
00...000	0	½(-h[N/2-1]-...-h[1]-h[0])
00...001	h[0]	½(-h[N/2-1]-...-h[1]+h[0])
.	.	.
01...111	h[N/2-2]+...+h[1]+h[0]	½(-h[N/2-1]+...+h[1]+h[0])
10...000	h[N/2-1]	½(+h[N/2-1]-...-h[1]-h[0])
.	.	.
11...110	h[N/2-1]+...+h[2]+h[1]	½(+h[N/2-1]+...+h[1]-h[0])
11...111	h[N/2-1]+...+h[1]+h[0]	½(+h[N/2-1]+...+h[1]+h[0])

Nasprotno simetrične delne vsote povzročijo konstantno odstopanje izhoda y, kar izračunamo z:

$$\begin{aligned}\hat{y} &= -s_{0,S} + \sum_{i=1}^{Bx-1} s_{i,S} 2^{-i} - 2s_{0,C} + 2\sum_{i=1}^{Bx-1} s_{i,C} 2^{-i} \\ &= -v_{0,S} - 2v_{0,C} + \sum_{i=1}^{Bx-1} (v_{i,S} + 2v_{i,C}) 2^{-i} + \frac{3}{2} \sum_{k=0}^{N/2-1} h[k] 2^{-Bx+1} \\ &= y + \frac{3}{2} \sum_{k=0}^{N/2-1} h[k] 2^{-Bx+1}\end{aligned} \quad (10)$$

Pri tem sta $\hat{y}$ ter y dejanska in želena izhodna vrednost. Zaradi preglednost smo v enačbi (10) izpustili časovni indeks n. Odstopanje $\hat{y}$ od y lahko kompenziramo, če v register aritmetične enote zapišemo začetno vrednost:

$$K = -\frac{3}{2} \sum_{k=0}^{N/2-1} h[k]. \quad (11)$$

Začetna vrednost se prišteva le prvi delni vsoti v_{Bx-1}. V postopku iterativnega seštevanja in deljenja delnih vsot se začetna vrednost deli z $2^{(Bx-1)}$ in tako v celoti kompenzira odstopanje izhodnih vrednosti. Zaradi nasprotno simetričnega zapisa, v pomnilniku pomnimo le prvo polovico delnih vsot "s" v tabeli 1. Drugo polovico generiramo iz obstoječih delnih vsot z negiranjem bitov naslovnega vektorja $[A_0, A_1, \ldots, A_{N/2-2}]^T$ in zamenjavo predznaka tako naslovljene delne vsote. Ustrezno blokovno shemo sita prikazuje slika (3).

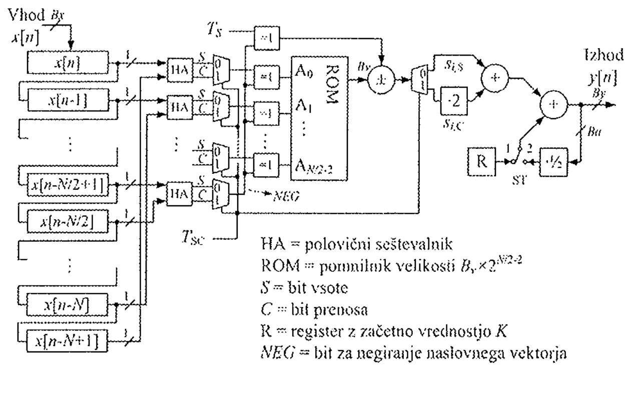

Slika 3: Sito v PA z zmanjšanjem pomnilniškega prostora iz 2^N na $2^{N/2-1}$ naslovov.

Pri tem sta T_S in T_{SC} kontrolna signala za zamenjavo predznaka delnih vsot s_0 oz. za naslavljanje delnih vsot $s_{i,S}$ in $s_{i,C}$. Z vrati ekskluzivni ALI tvorimo eniški komplement naslovnega vektorja za primere, ko se DV nahaja v drugi polovici tabele 1 (*NEG* =1). S tem naslovimo ustrezno DV v prvi polovici tabele 1, ki pa ji moramo zamenjati še predznak (tvorimo dvojiški komplement). Predznak zamenjamo tudi delnim vsotam s_0, zato T_S in *NEG* preko funkcije ekskluzivni ALI krmilita vezje za generiranje dvojiškega komplementa števila. Dvojiški komplement DV tvorimo, če ima T_S ali *NEG* vrednost 1. Prva delna vsota $s_{Bx-1,S}+2s_{Bx-1,C}$ je korigirana z začetno vrednostjo K shranjeno v registru R s katero kompenziramo odstopanje y zaradi nasprotno simetričnega zapisa DV. Stikalo ST je v položaju 1. Za ostale primere je stikalo ST v položaju 2.

4. Modificirana PA in sita FIR z linearnim potekom faze

Kot sledi iz /8, 9/ temelji modificirana PA na premaknitvi območja vrednosti vhoda x iz intervala [-1, 1) v interval [0, 2). Ker so vrednosti x predstavljene binarno v dvojiškem komplementu, je premaknitev območja vrednosti enostavno izvedljiva s komplementom bita za predznak. V binarni obliki x sedaj zapišemo z:

$$x[n]=\sum_{i=0}^{Bx-1} b_i[n]2^{-i}. \tag{12}$$

Ker ni bita za predznak oz. ima vrednost nič, izhod y izračunavamo le z operacijo seštevanja:

$$y[n]=\sum_{i=0}^{Bx-1} g_i[n]2^{-i}. \tag{13}$$

Pri tem je g modificirana DV izračunana z:

$$\begin{aligned} g_i &= v_i-\frac{1}{2}\sum_{k=0}^{N-1} h[k]\left[1+\frac{2^{-Bx}}{1-2^{-Bx}}\right] \\ &= v_i-K_1 \end{aligned} \tag{14}$$

in je v_i klasična DV izračunana s (4). Z modifikacijo v_i v (14) kompenziramo premaknitev vhoda x in zagotovimo območje izhodnih vrednosti v intervalu [-1, 1).

V poglavju 5 opisan postopek prepolovitve števila naslovnih linij lahko vpeljemo tudi v vezje modificirane PA. Glede na to, da se sedaj DV izračunava z vektorjem bitov vsot S in bitov prenosov C v dveh korakih, zapišemo (14) z:

$$\begin{aligned} g_i &= v_{i,S}+2v_{i,C}-K_1 \\ &= \left(v_{i,S}-\frac{K_1}{3}\right)+2\left(v_{i,C}-\frac{K_1}{3}\right). \end{aligned} \tag{15}$$

Pri tem sta $v_{i,S}$ in $v_{i,C}$ klasični delni vsoti izračunani iz polovice koeficientov z (8) in je K_1 konstanta iz (14) s katero kompenziramo premaknitev x. V pomnilniku pomnimo torej delne vsote polovice koeficientov izračunane z:

$$\begin{aligned} g_{i,z} &= v_{i,z}-\frac{1}{6}\left(1+\frac{2^{-Bx}}{1-2^{-Bx}}\right)\sum_{k=0}^{N-1} h[k] \\ &= v_{i,z}-K_2 \end{aligned} \tag{16}$$

Pri tem smo z "z" označili S ali C ter so $v_{i,z}$ klasične DV iz polovice koeficientov $h[k]$ izračunane z (8). Prikazuje jih tabela 2.

Tabela 2: Klasične in modificirane delne vsote iz polovice koeficientov s sodo simetrijo.

Naslov	$v_{i,S}$, $v_{i,C}$	$g_{i,S}$, $g_{i,C}$
00...000	0	$-K_2$
00...001	$h[0]$	$h[0]-K_2$
.	.	.
.	.	.
11...111	$h[N/2-1]+\ldots+h[1]+h[0]$	$h[N/2-1]+\ldots+h[1]+h[0]-K_2$

Ustrezno blokovno shemo sita v modificirani PA in s prepolovljenim številom naslovnih linij prikazuje slika 4.

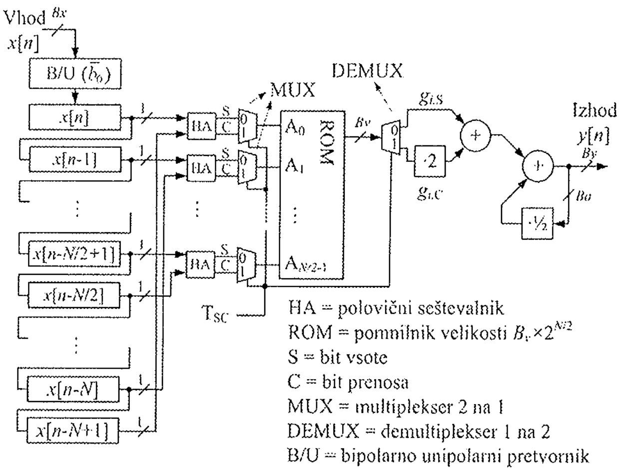

Slika 4: Sito v modificirani PA z zmanjšanjem pomnilniškega prostora iz 2^N na $2^{N/2}$ naslovov.

Za razliko od vezja s klasično PA na sliki 2 v vezju z modificirano PA ni odštevanja zadnje delne vsote, kar pomeni, da ne potrebujemo vezja za tvorjenje dvojiškega komplementa in vezja za generiranje kontrolnega signala T_S.

5. Rezultati

Z matematičnim orodjem Matlab smo zgradili simulacijske modele treh sit v PA:

- klasična PA (PA),
- klasična PA s prepolovljenim številom naslovnih linij (PA 1),
- klasična PA s prepolovljenim številom naslovnih linij in nasprotno simetričnimi zapisom DV (PA 2),

ter dveh sit v modificirani PA:

- modificirana PA (MPA),
- modificirana PA s prepolovljenim številom naslovnih linij (MPA 1).

V modelih smo zajeli vplive kvantizacije vhodnega signala, delnih vsot, aritmetične enote in izhodnega signala.

Za primerjavo smo izbrali optimalno minimaks nizko-prepustno sito stopnje N-1 = 29, s prepustnim pasom od 0 do 0,2f_v in zapornim pasom od 0,3f_v do 0,5f_v. Pri tem je f_v frekvenca vzorčenja. Koeficiente impulznega odziva smo izračunali z Remez menjalnim algoritmom in normirali na maksimalno amplitudo frekvenčnega odziva vrednosti ena. Referenčne vrednosti osnovnih frekvenčnih parametrov omenjenega sita so:

- ojačenje v prepustnem pasu PBG = 0,9993,
- slabljenje v zapornem pasu SBA = - 43,76 dB,
- slabljenje sita A = 43,76 dB.

Amplitudni spekter sita prikazuje slika 5.

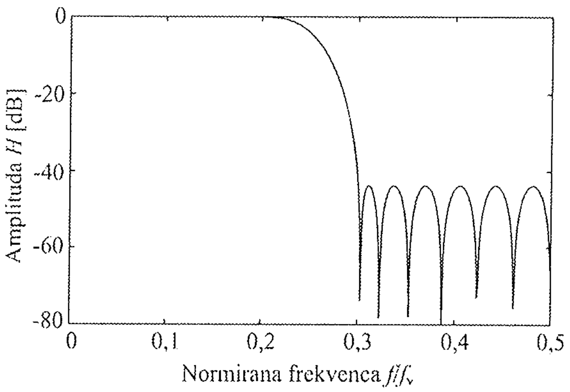

Slika 5: Amplitudni spekter nizko-prepustnega sita stopnje 29.

Ker gre v PA za celoštevilsko aritmetiko, je potrebno koeficiente $h[n]$ oz. delne vsote ustrezno normirati, da preprečimo prekoračitev območja izhodnega signala [-1, 1). Kot je bilo zapisano v /9/ se normiranje h izvaja na maksimalno absolutno vrednost frekvenčnega odziva H z:

$$h_{norm}[n]=\frac{h[n](1-Q_y)}{\max|H(e^{j\omega})|}, \quad n=0,1,...,N-1. \qquad (17)$$

Pri tem je Q_y stopnja kvantizacije izhodnega signala in je $Q_y = 2^{-(By-1)}$. Tudi pri zapisu DV smo omejeni s končno dolžino besede in maksimalna DV ne sme preseči območja za zapis DV. Zato DV delimo z 2^i, kjer i predstavlja najmanjše pozitivno celo število pri katerem je izpolnjen pogoj maksimalne DV. S tem smo zmanjšali dinamično območje y, kar delno kompenziramo z zamikom podatkovnih linij aritmetične enote, ki jih vodimo na izhod, za i bitov v levo. Kompenzacija je smiselna ob pogoju, da je $B_a \geq B_y+i$. Pri tem sta B_a dolžina aritmetične enote in B_y je dolžina izhodne besede.

Za primere, ko so koeficienti $h[n]$ izrazito pozitivni ali negativni[1], nasprotno simetrični zapis DV bolje izkoristi omejeno območje za zapis vrednosti. Posledično so normirane DV in dinamično območje y večje. Tudi za realizirane oblike sit se je, kot v /9/, pokazala prednost modificirane PA. Za siti v modificirani PA, kakor tudi za sito v klasični PA z nasprotno simetričnimi DV, so bili normirani koeficienti $h[n]$ dvakrat večji od tistih v klasični PA. Ustrezne koeficiente normiranja 2^i, za posamezno sito prikazuje tabela 3.

Tabela 3: Koeficienti normiranja za posamezno aritmetiko.

Aritmetika	Koeficient normiranja 2^i
PA	4
PA 1	4
PA 2	2
MPA	2
MPA1	2

Opazovali smo časovne odzive struktur na beli šum. Iz odstopanj med kvantiziranimi in referenčnimi odzivi smo določili šum izhodnega signala ter izračunali razmerje signal-šum (razmerje SNR). Razen velikosti pomnilniškega prostora se posamezne strukture bistveno razlikujejo predvsem po delnih vsotah. Zato smo ločeno opazovali vpliv kvantizacije vhodnega signala in delnih vsot, vrednosti v aritmetični enoti in izhodne vrednosti pa smo zapisali z 32 biti. Vpliv omejene dolžine vhoda in DV na razmerje SNR prikazujeta sliki 6 a) in b).

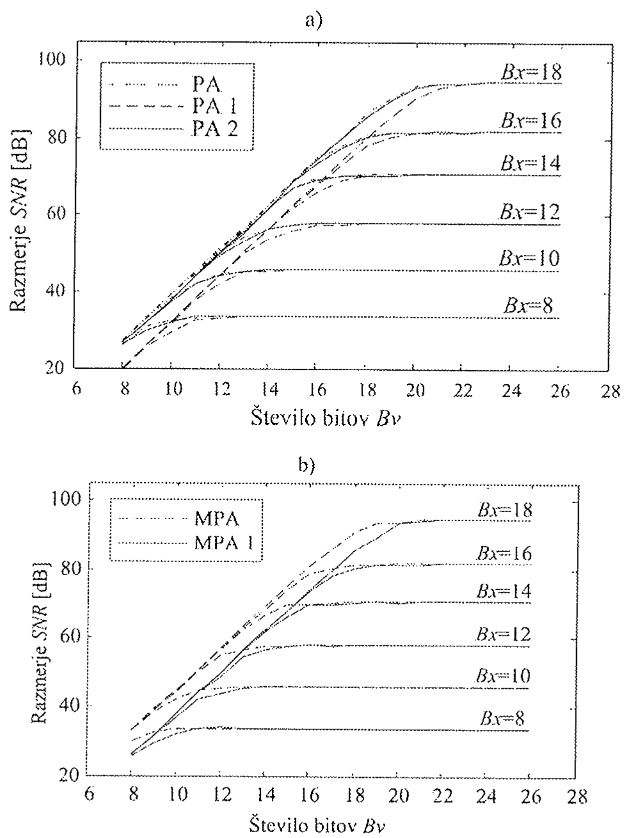

Slika 6: Potek razmerja SNR v odvisnosti od števila bitov B_v, B_x je parameter (PA – klasična PA, PA 1 - PA s prepolovljenim številom naslovnih linij, PA2 - PA s prepolovljenim številom naslovnih linij in nasprotno simetričnimi zapisom DV, MPA – modificirana PA,MPA 1 - modificirana PA s prepolovljenim številom naslovnih linij).

[1] *To je lastnost predvsem nizkoprepustnih sit.*

Iz primerjave poteka krivulj PA in PA 1 na sliki 6 a) je razvidno zmanjšanje razmerja SNR za sito s prepolovljenim številom naslovnih linij (PA 1) pri enaki stopnji kvantizacije. V obeh primerih je koeficient normiranja enak, zatorej gre zmanjšanje razmerja SNR na račun izračuna DV v dveh korakih, ki je posledica postopka zmanjšanja pomnilniškega prostora. Z nasprotno simetričnim zapisom DV lahko, predvsem za nizko-prepustna sita, uporabimo ugodnejše normiranje DV in tako dosežemo razmerja SNR, ki so primerljiva s klasično PA. Tak primer prikazuje potek krivulj PA 2 na sliki 6. a). Negativen vpliv postopka izračunavanja DV v dveh korakih na razmerje SNR je razviden tudi iz poteka krivulj MPA in MPA 1 na sliki 6 b). Zaradi postopka prepolovitve števila naslovnih linij moramo torej bitno število B_V povečati za ena, če želimo obdržati enako razmerje SNR. Zaradi ugodnejšega normiranja (glej tabelo 3) dosegamo, ob enaki stopnji kvantizacije, z modificirano PA večje razmerje SNR glede na klasično PA (glej poteke krivulj PA in MPA na sliki 6. a oz. b). Z uporabo postopka prepolovitve števila naslovnih linij v modificirani PA dosegamo podobno razmerje SNR kot v klasični PA (glej poteke krivulj PA in MPA 1 na sliki 6. a) oz. b).

6. Zaključek

V prispevku smo predstavili načine zmanjšanja potrebnega pomnilniškega prostora za shranjevanje DV digitalnih sit v klasični in modificirani PA. Pri delu smo se omejili na sita z linearnim potekom faze, katerih posebnost je simetrija koeficientov impulznega odziva. Zaradi simetrije je dovolj, če v pomnilniku pomnimo delne vsote polovice koeficientov impulznega odziva. Postopek omogoča zmanjšanje pomnilniškega prostora iz 2^N na $2^{N/2}$ naslovov. Drug pristop temelji na nasprotno simetričnem zapisu delnih vsot. V pomnilniku pomnimo le prvo polovico nasprotno simetričnih DV. Drugo polovico generiramo iz prve z ustreznim naslavljanjem in spremembo predznaka. S tem dosežemo zmanjšanje pomnilniškega prostora iz 2^N na 2^{N-1} naslovov. V prispevku predlagamo združitev obeh pristopov. Nasprotno simetrične delne vsote generiramo sedaj le iz polovice simetričnih koeficientov $h[n]$. Za primer sita s sodo simetrijo tako dosežemo zmanjšanje pomnilniškega prostora iz 2^N na $2^{N/2-1}$. Zaradi dvojnega naslavljanja pomnilnika v procesu izračunavanja ene DV, se poveča minimalno potrebno število bitov B_V, pri katerem dosežemo maksimalno možno razmerje SNR. Z uporabo nasprotno simetričnih DV uspemo, za sita z izrazito pozitivnimi ali negativnimi koeficienti, doseči enako razmerje SNR kot v klasični PA.

Modificirana oblika PA že v osnovi prinaša dve prednosti v primerjavi s klasično PA: manj kompleksno vezje in večje dinamično območje izhoda y. Posledično tudi večje razmerje SNR pri enaki stopnji kvantizacije. Slednje je prisotno pri sitih z izrazito pozitivnimi ali negativnimi koeficienti. Z vpeljavo postopka razpolovitve števila naslovnih linij v modificirano PA se razmerje SNR sicer zmanjša, vendar še zmeraj dosega nivo klasične PA.

7. Literatura

/1/ E. Anderson, "A digital filter implemented in parallel form", presented at the 1971 Symp. Digital Filtering, Imperial College, London, England, Aug. 1971.q

/2/ S. Zohar, "New hardware realizations on nonrecursive digital filters", IEEE Trans. Comput., vol. C-22, pp. 328-347, Apr. 1973.

/3/ Stenley A. White, Applications of Distributed Arithmetic to Digital Signal Processing: A Tutorial Review, *IEEE ASSP Magazine*, pages 4-19, Jul. 1989.

/4/ L. Mintzer, "FIR Filters with Filed-Programmable Gate Arrays," *Journal of VLSI Signal Processing,* 6, 119 - 127 (1993).

/5/ A. Chorevas, D. Reisis, "Efficient Systolic Array Mapping of FIR Filters Used in PAM-QAM Modulators," *Journal of VLSI Signal Processing Systems*, v.35 n.2, p.179-186, September 2003.

/6/ D. Osebik, B. Kostanjevec, B. Jarc, M. Solar, R. Babič, "Izvedba nerekurzivnega digitalnega sita s programirljivim poljem logičnih vezij v strukturi porazdeljene aritmetike" *Informacije MIDEM, št. 3* (1997), str. 195-202.

/7/ D. Osebik, R. Babič, Rudolf, M. Solar, "Adaptivna struktura s polji programirnih vezij za izvedbo nerekurzivnih digitalnih sit," *Informacije MIDEM*, september 2003, letn. 33, št. 3(107), str. 170-177.

/8/ B. Jarc, R. Babič, M. Solar, M. Brumec, "Modificirana obli-ka porazdeljene aritmetike," *Zbornik pete Elektrotehniške in računalniške konference ERK '96*, 19. - 21. september 1996, Portorož, Slovenija, Str. A/113-116.

/9/ R. Babič, B. Jarc, "Uporaba modificirane oblike porazdelje-ne aritmetike za osnovno in kaskadno izvedbo digitalnih sit," Informacije MIDEM, 1999, let. 29, št. 3, str. 136-142.

doc. dr. Bojan JARC,
izr. prof. dr. Rudolf BABIČ,
oba UNIVERZA V MARIBORU,
FAKULTETA ZA ELEKTROTEHNIKO,
RAČUNALNIŠTVO IN INFORMATIKO
2000 Maribor, Smetanova 17.
Email: bojan.jarc@uni-mb.si,
rudolf.babic@uni-mb.si
tel. (02) 220 7235, fax. (02) 251 1178

Prispelo (Arrived): 19. 12. 2005; Sprejeto (Accepted): 30. 01. 2006

THE ELECTROTHERMAL MACROMODEL OF ZCS RESONANT CONVERTER CONTROLLERS FOR SPICE

Krzysztof Górecki, Janusz Zarębski

Gdynia Maritime University, Department of Marine Electronics

Key words: ZCS converter controllers, SPICE, electrothermal macromodels

Abstract: The main aim of this paper is to propose a new electrothermal (including selfheating) macromodel of the MC34066 ZCS resonant converter controller for SPICE. The macromodel structure results both from the controller block diagram presented by the producer in the catalogue data and the principle of its operation. This macromodel formed in the network form describes the fundamental and the most important features of the considered IC. The proposed macromodel was verified experimentally. The majority of the macromodel parameter values have been obtained from the measured characteristics.

SPICE elektrotermični model ZCS resonančnih pretvornikov

Kjučne besede: ZCS pretvornik, SPICE, elektrotermični model

Izvleček: V prispevku predlagamo nov SPICE elektrotermični model za MC34066 ZCS resonančni pretvornik. Makromodel je nastal na osnovi blok diagrama proizvajalca, kakor tudi na osnovi principa delovanja. Makromodel v obliki blok vezja opise najbolj pomembne lastnosti integriranega vezja. Predlagani model smo preverili tudi eksperimentalno. Večino parametrov makromodela smo določili na osnovi merjenih karakteristik

1. Introduction

The resonant converters switching at zero voltage (ZVS) or at zero current (ZCS) /1, 2, 3/ are more and more popular circuits which belong to the class of Switch Mode Power Supplies (SMPS).

In the process of designing such a class of converters, fully credible models describing the converter components (diodes, transistors, etc.), or describing the whole circuit, play a fundamental role and the proper computer tools are necessary as well. Today, SPICE along with the built-in models and worked out by the producers macromodels of some devices such as: diodes, transistors, inductors, transformers and the large class of ICs is such a convenient tool. For example, the macromodels of controllers dedicated to dc-dc converters are available in the SWIT_REG.LIB library /4/ and in the libraries attached to the Basso book /5/. Unfortunately, there are no models or macromodels of resonant converter controllers available for SPICE users. The preliminary versions of ZVS and ZCS converter controller macromodels elaborated earlier by the authors can be found in the papers /6, 7/. The macromodels, presented in the cited papers are the isothermal ones and in these macromodels selfheating in semiconductor devices is omitted.

Due to the selfheating existing in IC, the electrical power is changed into heat, which in the non-ideal conditions of heat removing to the surrounding results in an increase of the inner temperature T_j. In turn, due to an increase of the device inner temperature both a change of d.c. characteristics and a decrease of device reliability are observed /8, 9/.

To include the selfheating phenomena in the computer-aided design and the analysis of SMPS the special kind of models, called the electrothermal ones should be used.

In the literature the electrothermal models of semiconductor devices for SPICE, e.g. /10, 11, 12/ are proposed, but there is no information about electrothermal models of monolithic integrated circuits.

The aim of the paper is to present a new electrothermal macromodel of the MC34066 controller dedicated for SPICE. In the macromodel construction process the modelling idea, used by the authors for the first time in the case of PWM controller electrothermal macromodel formulation /13/, has been adopted.

The monolithic controller MC34066 made by ONSemiconductor is dedicated for the class of resonant ZCS switched mode power supplies. By means of this controller the frequency modulation of the output signal is realised.

The considered controller can operate with the constant or variable value of the pulse duration time (on-time or off-time mode). The combination of both the modes of operation is also possible /14/.

At the outputs of MC34066 one can get two signals of the frequency from 40 kHz to 1.2 MHz and the high value of the current efficiency.

According to the catalogue data /14/ the output frequency signals can be changed a thousand times, and the frequency band of the error amplifier is equal to 5 MHz. The undervoltage and overcurrent protection, as well as the soft-starting circuit, are included in the considered IC.

The time duration of the high level at the generator output as well as the maximum value of the output signal period are determined by the external RC elements. The value of the output signal period depends on the voltage existing at the output of the error amplifier.

In Chapter 3, the proposed macromodel form of the MC34066 controller is shown and described, whereas Chapter 4 presents the results of the measurements and calculations of two important parameters, such as the pulse time duration and the period of the output signals of the considered controller working in the special test circuit with different values of the external RC elements.

3. The Macromodel Structure

The macromodel structure results from the controller block diagram presented by the producer in the catalogue data /9/, the principle of operation of the controller of the ZCS converter as well as the roles of formulating the device electrothermal models /15/. This macromodel, presented in Fig.1 in the network form, describes the fundamental and the most important features of the considered IC. The efficiencies of the controlled sources are given both as the logic expressions resulting from the IC structure and as the functions formulated on the measurement data.

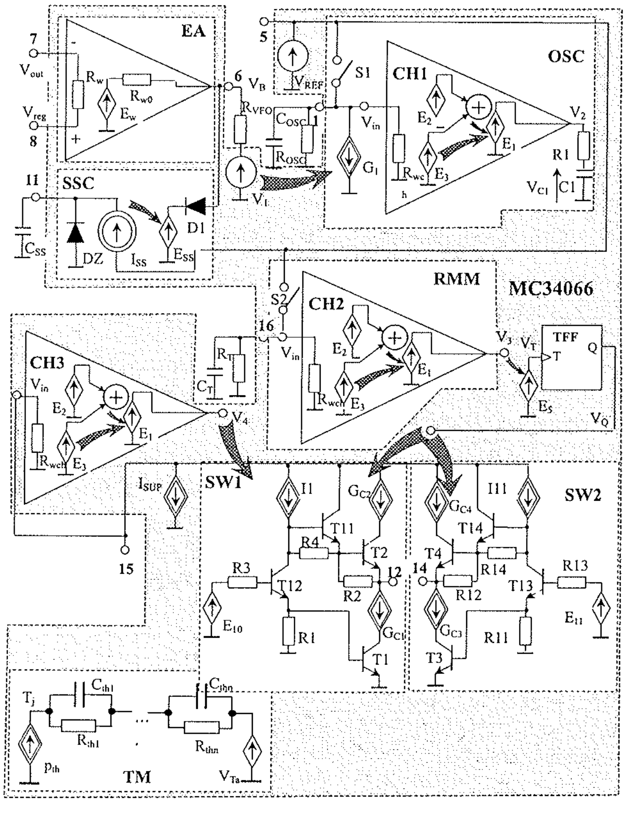

Fig.1. The macromodel diagram of the ZCS controller

Ten essential blocks: reference voltage source (V_{REF}), error amplifier (EA), oscillator (OSC), retrigerrable monostable multivibrator (RMM), T flip-flop (TFF), soft-start circuit (SS), under-voltage protection (CH3), two identical output stages (SW1 and SW2) and the thermal model (TM) can be distinguished in the macromodel.

The error amplifier is described as a quasi-ideal operation amplifier in which the efficiency of the voltage control source E_W given by

$$E_w = K_u \cdot \left(V_{reg} - V_{out}\right) \qquad (1)$$

is proportional to the open loop amplification factor (K_u) and the amplifier differential input voltage (V_{reg} - V_{out}), whereas R_W and R_{WO} represent the input and output amplifier resistances, respectively.

As it is seen from Fig.2, the inputs of the considered error amplifier are excited by the control voltage (V_{reg}) and the feedback voltage V_{out}, respectively. Its output controls the discharging current of the auxiliary capacitor C_{OSC}.

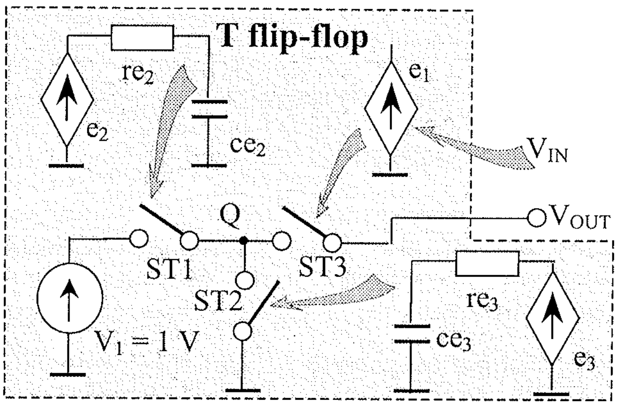

Fig.2. The network representation of the T flip-flop circuit

In the macromodel the typical catalogue values of the parameters R_W = 5 MΩ, R_{WO} = 75 Ω, and $K_u = 10^5$ have been taken into account.

The two-terminal network consisting of the resistor R_T and the capacitor C_T is used for programming the pulse time duration. In turn, the second two-terminal network composed of C_{OSC} capacitor and R_{OSC} resistor determines the minimum oscillation frequency, whereas the main task of the current source of the efficiency G_1 controlled by voltage V_B, is to discharge C_{OSC} capacitance. The efficiency of this source is described by

$$G_1 = LIMIT\left(\frac{V_B - V_1 \cdot \left(1 - a_T \cdot (T - T_0)\right)}{R_{VFO}}, \frac{V_2}{R_{VFO}}, \frac{V_3}{R_{VFO}}\right) \qquad (2)$$

where LIMIT denotes the built-in function of SPICE, T is the temperature, V_1, V_2, V_3, a_T are the model parameters, and T_0 is the reference temperature, at which parameter values have been estimated.

Two switches - S1 and S2 controlled by the signal existing at the output of the comparator with hysteresis (CH1) are switched on when the value of the voltage across C_{OSC} capacitance decreases below 3.6 V. On the contrary, they are switched off in the case when this voltage increases up to 5.1 V.

The comparator with hysteresis is modelled by means of three voltage controlled sources E_1, E_2, E_3 of the efficiences given by /16/

$$E_1 = LIMIT(x,1,0) \tag{3}$$

where: LIMIT denotes the standard SPICE function and x is given by

$$x = \begin{cases} E2 \;\; for \;\; V_{in} < V_{\min} \;\; and \;\; V_{in} > V_{\max} \\ E2 + E3 \;\; for \;\; V_{\min} < V_{in} < V_{\max} \end{cases} \tag{4}$$

$$E2 = \begin{cases} 1 \;\; for \;\; V_{in} < V_{\min} \\ \dfrac{1}{V_{mx} - V_{\min}} \cdot \left(V_{in} - V_{\min}\right) \;\; for \;\; V_{\min} < V_{in} < V_{mx} \\ 0 \;\; for \;\; V_{in} > V_{mx} \end{cases} \tag{5}$$

$$E3 = \begin{cases} 0 \;\; for \;\; dV_{in}/dt < 0 \\ dV_{in}/dt \;\; for \;\; 0 < dV_{in}/dt < 1 \\ 1 \;\; for \;\; dV_{in}/dt > 1 \end{cases} \tag{6}$$

where V_{min} and V_{max} denote the values of the bottom and the upper boundary of the hysteresis loop. In the model V_{min} = 3.5 V, V_{mx} = 3.51 V and V_{max} = 4.9 V were assumed.

The input of the T flip-flop circuit (TFF) is controlled by the logic sum of the output signals of both the comparators. In turn, the output of the flip-flop circuit controls the output block consisting of two BJTs, operating in the emitter follower circuits.

The efficiency of the source E_5 is

$$E_5 = LIMIT\left(V_2 + V_3, 1, 0\right) \tag{7}$$

where V_2 and V_3 denote the voltages at the outputs of the comparators CH1 and CH2, respectively.

In the soft-start circuit (SSC) the current source I_{SS}, whose efficiency is described by a Heaviside's jump of the value equal to 9 μA /9/, charges the auxiliary capacitor C_{SS}. The Zener diode DZ limits the voltage on this capacitor to 3 V. The efficiency of the controlled voltage source E_{SS} is equal to the voltage on the capacitor C_{SS}. Because of the use of the diode D1, the slew rate of the error amplifier (EA), after switching on the power supply, is limited by the slew rate of C_{SS} capacitor voltage and the controller starts working with the minimum switching frequency.

The undervoltage lockout is realised by the use of the comparator with histeresis CH3. If the supply voltage of controller decreases under 9 V, the comparator output voltage V_4 decreases to a low stage. The change of this voltage to a high stage requires an increase of the supply voltage to 16 V. The low stage of the output of the considered block causes the low stage on both the outputs of the MC34066 controller.

The output stage consists of two identical blocks: SW1 and SW2. In turn, each of them is composed of four bipolar transistors (BJT), four resistors and one current source. The shunt resistors are connected parallelly to BJT's base-to-emitter junctions in order to accelerate the transistors switching-off process /1/.

The bipolar transistors are described by their SPICE built-in model. The value of the series collector resistance is estimated according to the rate of the transistors switching-on.

The controlled current sources G_{C1}, G_{C2}, G_{C3} and G_{C4} model the temperature dependence of the collector resistance of the transistors T1, T2, T3, T4 operating in the output stage. These sources are described by the formulae

$$G_{Ci} = \frac{V_{GCi}}{R_C \cdot \alpha_{RC} \cdot \left(T - T_0\right)} \tag{8}$$

where i = 1, 2, 3, 4, V_{GCi} is the voltage on the i-th source, R_C is the collector series resistance for T = T_0, whereas α_{RC} denotes the temperature coefficient of R_C resistance.

The efficiency of two voltage sources E_{10} and E_{11} controlling the output stages depends on the input V_T and output V_Q voltages of T flip-flop. The considered sources are described by

$$E_{10} = \left(1 - V_Q\right) \cdot \left(1 - V_T\right) \cdot V_{CC} \tag{9}$$

$$E_{11} = V_Q \cdot \left(1 - V_T\right) \cdot V_{CC} \tag{10}$$

where V_{CC} denotes the supply voltage of the controller.

The efficiency of I_{SUP1} current source describes the current value consumed by the controller (without the output stage) from the source of the supply voltage. The obtained from the measurements values of I_{SUP1} are equal to 22.1 mA.

The pulse time duration both at the controller output and the output of the flip-flop are equal to each other. The flip-flop is modelled by means of the circuit shown in Fig.2.

The voltage controlled sources e_1, e_2 and e_3 are of the efficiency equal 0 or 1, depending on the logic state at the input (V_{IN}) and the output (V_{OUT}) of the flip-flop. The essential role of the resistances re_2, re_3 and capacitances ce_2, ce_3 is to delay properly the signals controlling switches S1 and S2 in such a way which ensures that both the switches are not switched on at the same time.

The efficiency of the source e_2 equals 1, when at the input (output) of the flip-flop the signal increases (low state) or when at its input (output) the voltage is constant (high state).

In turn, the efficiency of the source e_3, similarly to what was described above, is equal to 1 when at the input (output) of the flip-flop the signal increases (high state exists) or when at its input (output) the voltage is constant (low state exists).

The switch ST1 is switched on when the voltage at the capacitance ce_2 is greater than 0.5 V, whereas the switch ST2 is switched on when the voltage across the capacitance ce_3 is greater than 0.5 V. The switch ST3 is switched on while the control signal is increasing, otherwise it is switched off.

The thermal model (TM) consists of the controlled current source p_{th} of the efficiency equal to the dissipated power in the controller, the RC network, representing the transient thermal impedance of the controller and independent voltage source V_{Ta}, whose efficiency corresponds to the ambient temperature. The efficiency of the p_{th} source is given by

$$p_{th} = V_{CC} \cdot I_{SUP1} + \sum_{i=1}^{4} i_{Ci} \cdot v_{CEi} \tag{11}$$

where i_{Ci} and v_{CEi} denote the collector current and the collector-to-emitter voltage of the transistor Ti (i = 1, 2, 3, 4), respectively.

4. Verification of the Macromodel

The proposed macromodel has been verified experimentally. For the investigated device (MC34066) the test circuit (TC) with the resistance load and without a feedback loop has been proposed by the authors (Fig.3). Some measurements for the various values of the ambient temperature, supply voltage, and the load resistance as well as for some values of RC elements connected to the oscillator terminals and determining the period and the dead time of the output signals have been performed in TC.

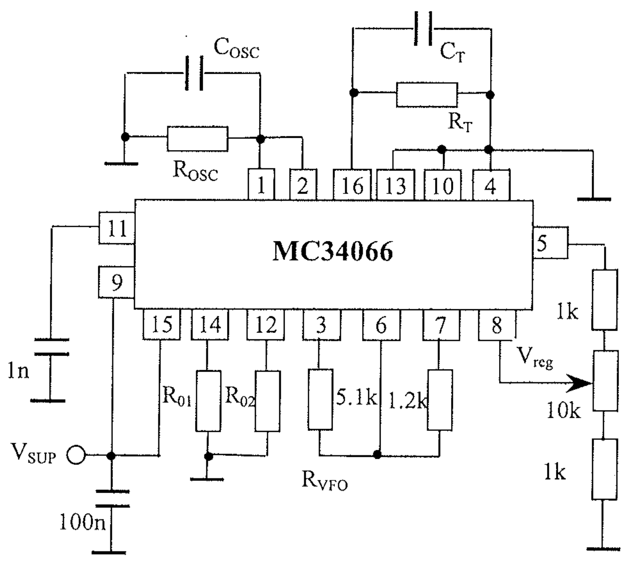

Fig.3. The test circuit

As an example, in Fig.4 the results of the simulations (lines) and measurements (squares) of the period of the output signal T_S on the regulation voltage V_{reg} for two values of temperature and different values of external RC elements are presented. In both cases the identical values of R_{OSC} = 89.45 kΩ and R_T = 14.86 kΩ are used, whereas the other elements are of the following values:

a) for the case presented in Fig.5a: C_{OSC} = 101.8 pF, C_T = 105,4 pF, V_{SUP} = 20 V and R_0 =1.2 kΩ,

b) for the case presented in Fig.5b: C_{OSC} = 327 pF, C_T = 268.8 pF, V_{SUP} = 12 V and R_0 = 208 Ω.

As seen from Fig.4, a satisfactory agreement between the calculations and measurements of the dependencies of the period of the output signal on the regulation voltage, for both the temperatures, has been achieved. It is worth noticing that the period time decreases nearly tenfold in the range of the regulation. Increasing the temperature pushed the characteristics to the left direction, which is especially important in the range of V_{reg} changing from 1.2 V to 2 V, where the values of T_S corresponding to the selected value of V_{reg} can differ from each other by over 30%.

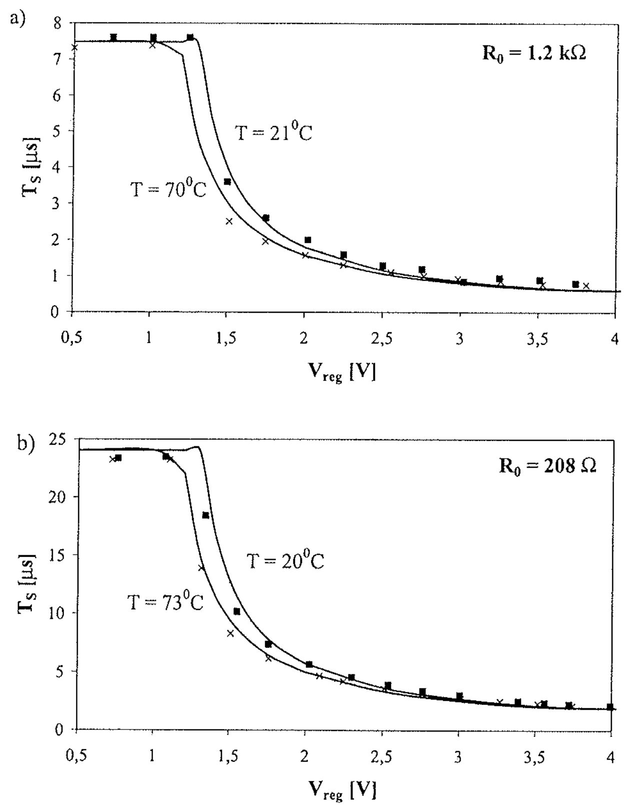

Fig.4. Calculated (lines) and measured (squares) dependencies of the period time on the regulation voltage

The shape of the obtained characteristics qualitatively agrees with the results corresponding to the other values of RC elements, which confirms the correctness of the proposed model.

In turn, in Fig.5, the results of the measurements and simulations of MC34066 operating in the test circuit (Fig.4) for the changed values of the external elements, which are C_{OSC} = 327 pF, C_T = 268.8 pF, R_0 = 208 Ω and for two temperatures T_1 = 20^{0}C and T_2 = 73^{0}C are presented.

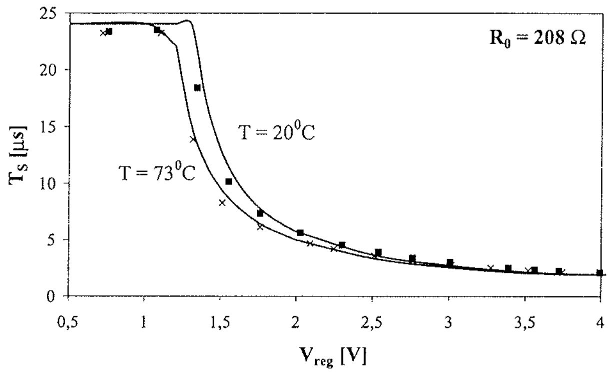

Fig.5. Measured and calculated dependence of T_S on V_{reg}

As seen, also in this case a good agreement between the calculation and measurement results for both the temperatures in the whole range of the regulation voltage V_{reg}, was achieved. The shape of the obtained characteristics qualitatively agrees with the results corresponding to the other values of RC elements, which confirms the correctness of the proposed model.

In Fig.6 the measured and calculated dependences of the supply current I_{SUP} on the control voltage V_{reg} at fixed values of the supply voltage V_{CC} and the load resistance R_0 are presented. The investigations have been performed for the following values of the external elements: C_{OSC} = 330 pF, R_{OSC} = 91 kW, C_t = 270 pF i R_t = 14 kΩ, T = 20^{0}C.

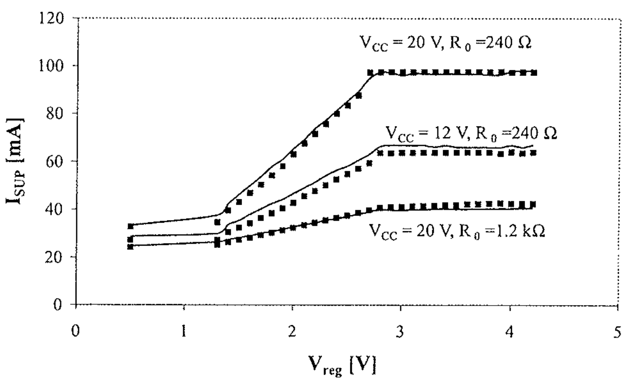

Fig.6. The dependence of the controller supply current on the regulation voltage

As seen, the results of the measurements and calculations fit very well.

From the dependences illustrated in Fig.6 it appears that I_{SUP} current value depends strongly on the V_{CC} and R_0 values. Decreasing R_0 and increasing V_{CC} cause the I_{SUP} to increase. On the other hand, the biggest value of I_{SUP} corresponds to the biggest values of V_{reg}, that is for the highest frequencies of the control signal. I_{SUP} increases linearly in the range of V_{reg} changing from 1.3 V to 2.7V. So, this is the range in which the pulse time duration t_W and period T_S keep constant values.

Fig.7 illustrates the mode of operation of the soft-start block for C_{SS} = 1 nF, C_{OSC} = 327 pF, C_T = 268.8 pF, R_{OSC} = 89.45 kΩ, R_T = 14.86 kΩ, V_{CC} = 12 V and R_0 = 208 Ω. In the figure, solid and dashed lines denote the simulation results of the considered controller obtained with the soft-start circuit taken into account and without it, respectively.

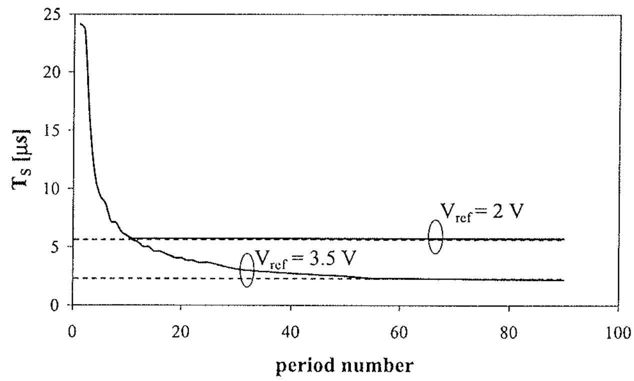

Fig. 7. The dependence of the interval between two successive pulses on the period number

As seen, at the steady-state the values of T_S period corresponding to both the considered situations are practically the same, whereas immediately after the controller switching-on the soft-start circuit causes the interval between two successive pulses of the output signal to lengthen even tenfold. Such properties of the investigated controller are convenient for the principle MC34066 operation available in the catalogue data /14/.

In Fig.8 the calculated dependence of the device inner temperature on the voltage V_{reg} corresponding to the characteristics from Fig.7, is presented. As seen, the inner temperature depends on the supply voltage and the load resistance. For the maximum allowable value of V_{CC} and at R_0 = 240 Ω the inner temperature tends to its maximum value given in the catalogue.

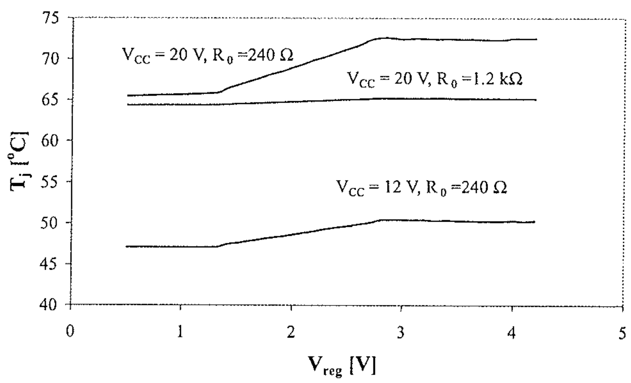

Fig.8. The calculated dependence of the inner temperature on the regulation voltage

5. Conclusions

In the paper the new electrothermal macromodel of ZCS controller dedicated for PSPICE is proposed. The basis for this macromodel preparation were the measurements of MC34066 characteristics. The macromodel has been verified experimentally in the test circuit worked out by the authors.

The model presented in Chapter 4 assures a good agreement with experimental results in the wide range of temperatures, the supply voltage, the load resistance, as well as the external RC elements. It is worth mentioning that this agreement is achieved both for on-time and off-time modes of MC34066.

/1/ N. Mohan, T.M. Undeland, W.P. Robbins, *Power Electronics: Converters, Applications, and Design* (New York, John Wiley &Sons, 1995).

/2/ M. Kazimierczuk, D. Czarkowski, *Resonant Power Converters* (New York, Wiley&Sons, 1995).

/3/ R.W. Ericson, D. Maksimovic, *Fundamentals of Power Electronics* (Norwell, Kluwer Academic Publisher, 2001).

/4/ Switch-reg.lib, *SPICE library*, 1998.

/5/ Ch.P. Basso, *Switch-Mode Power Supply SPICE Cookbook* (New York, McGraw-Hill, 2001).

/6/ K. Górecki, J. Zarębski, A New SPICE Macromodel of ZVS Resonant Converter Controller. *6th International Seminar on Power Semiconductors ISPS'2002*, Prague, 2002, pp. 195-198.

/7/ K. Górecki, J. Zarębski, The SPICE Macromodel of MC34066 Controller. *6th International Conference on Unconventional Electromechanical and Electrical Systems UEES'04*, Alushta, 2004, Vol. 2, pp. 525-530.

/8/ Speakman Z.: A model for the failure of bipolar silicon integrated circuits subjected to electrostatic discharge. 12th Annual Proceedings Reliability Physics, 1974, p. 60.

/9/ Stojadinovic N.: Failure physics of integrated circuits. A review. Microelectronics and Reliability, 1983, Vo. 23, No. 4, p. 609.

/10/ J. Bielefeld, G. Pelz, H.B. Abel, G. Zimmer, "Dynamic SPICE-Simulation of the Electrothermal Behavior of SOI MOSFET's", *IEEE Transactions on Electron Devices,* Vol.42, No.11, 1995, pp.1968-1974.

/11/ Chih-Ju Hung, P. Roblin, S. Akhtar, "Distributed B-spline electrothermal models of thyristors proposed for circuit simulation of power electronics". *IEEE Transactions on Electron Devices,* Vol.48, No.2, 2001, pp.353-366.

/12/ Schurack E., Latzel T., Rupp W., Gotwald A.: Nonlinear Effects in Transistors Caused by Thermal Power Feedback : Simulation and Modeling in SPICE. IEEE Int. Symp. on Circuits and Systems - ISCAS'92, San Diego 1992, p. 879.

/13/ J. Zarębski, K. Górecki, SPICE Modelling of PWM Controllers. *IEEE International Power Electronics Congress CIEP'2002,* Guadalajara, 2002, pp. 61-65.

/14/ MC34066, MC33066 High Performance Resonant Mode Controllers. *Catalogue data, ON Semiconductor*, 2000.

/15/ J. Zarębski, Modelling, Simulations and Measurements of Electrothermal Characteristics in Semiconductor Devices and Electronic Circuits. Proceedings of Gdynia Maritime Academy, Gdynia, 1996 (in Polish).

/16/ K. Górecki, J. Zarębski, K. Posobkiewicz, The Electrothermal Macromodel of the Monolithic Voltage Regulator LT1073 for SPICE. *10th IEEE International Conference on Electronics, Circuits and Systems ICECS 2003*, Sharjah, 2003, pp. 1113-1116.

Dr. Krzysztof Górecki
Prof. Janusz Zarębski
Gdynia Maritime University
Department of Marine Electronics
Morska 83, 81-225 Gdynia, POLAND,
Tel. ++48 58 6901448, ++48 58 6901599, fax ++48 58 6217353
E-mail: gorecki@am.gdynia.pl, zarebski@am.gdynia.pl

Prispelo (Arrived): 07. 10. 2005; Sprejeto (Accepted): 30. 01. 2006

LEAD-ACID BATTERY STATE-OF-CHARGE ESTIMATION FOR INDUCTION MOTOR FORKLIFT TRUCKS

Kristjan Baša[1], Andrej Žemva[2]

[1]Iskra Avtoelektrika d.d., Šempeter pri Gorici, Slovenia

[2]University of Ljubljana Faculty of Electrical Engineering, Ljubljana, Slovenia

Key words: lead-acid battery, secondary battery, state-of-charge, estimation, forklift trucks, pulse-width modulation, battery current reconstruction, induction motor

Abstract: While the automobile industry of electrically powered cars is still in its infancy, the industry vehicles, such as forklift trucks and other material handling equipment, have been in production for several decades. The use of electrically powered trucks imposes the problem of fuel-gauges, as they are not equipped with a reservoir enabling simple measurement of the fuel content. Knowing the battery state-of-charge is essential in preventing stranding and ensuring full-range exploitation of the battery power as well as informing the driver about the truck working hours time when battery charging should be done.

New electric trucks emerging in the market use AC motors for traction, necessitating phase current measurement. By using the existing hardware for phase current measurement, the battery current can be calculated thus reducing the cost of an additional hardware needed for battery current measurement. This paper addresses also the technique for correct battery current reconstruction from phase currents.

The paper presents two techniques enabling accurate estimation of the remaining battery capacity. During battery discharging, the ampere-hours taken from the battery are integrated and when the battery is not loaded, the open-circuit voltage measurement is made. A new technique to reduce the rest period needed to take the measurement of the open-circuit voltage is imposed to further improve the battery state of charge algorithm. Using both methods, i.e. the ampere-hours and open-circuit voltage, simplifies the overall state-of-charge estimation irrespectively of different battery sizes, battery ageing and temperature changes.

Ugotavljanje napolnjenosti svinčevih baterij v aplikacijah paletnih viličarjev s pogonom na indukcijski motor

Kjučne besede: svinčeva baterija, akumulator, stanje napolnjenosti, viličar, pulzno-širinska modulacija, rekonstrukcija baterijskega toka, izmenični motor

Izvleček: Medtem ko je avtomobilska industrija vozil na električni pogon še v povojih, je proizvodnja industrijskih vozil, kot so paletni viličarji in druga vozila za delo z blagom, v teku že več desetletij. Z uporabo električnih vozil se porodi problem merilnikov goriva, ker nimamo na vozilu rezervoarja, kjer bi lahko opravili preprosto meritev polnosti. Vedenje o napolnjenosti baterije je ključno, če nočemo, da nas vozilo pusti na cedilu, a da hkrati izkoristimo vso energijo, ki nam jo nudi akumulator. Poznavanje napolnjenosti baterije informira voznika o delovnih urah, ki jih električno vozilo še lahko opravi, in opozori, kdaj je potrebno baterijo napolniti.

Nova električna vozila, ki se pojavljajo na trgu, poganjajo motorji na izmenični pogon, kjer je za pravilno krmiljenje potrebno meriti fazne tokove. Z uporabo obstoječega elektronskega vezja za merjenje faznih tokov je možno izmeriti in izračunati baterijski tok. S tem se zmanjša strošek dodatnega elektronskega vezja, ki bi bil potreben za merjenje baterijskega toka. Ta članek predlaga metodo za pravilno rekonstrukcijo baterijskega toka iz merjenih faznih tokov.

Za točno ocenjevanje napolnjenosti baterije sta predstavljeni dve metodi. Med praznjenjem baterije se sešteva poraba amper ur in, ko baterija ni obremenjena, se opravi meritev napetosti odprtih sponk. Predstavljena je nova metoda za zmanjšanje potrebnega časa počitka baterije po uporabi, ki izboljšuje algoritem ugotavljanja napolnjenosti baterije. Uporaba obeh metod izboljšuje skupno oceno o napolnjenosti baterije in je neodvisna od kapacitete baterije, efekta staranja in temperaturnih sprememb.

1 Introduction

All vehicles used today in the field have limited power sources, which consequently limit its operational hours. To ensure their proper operation, enough energy to power them, has to be made available in the system. Whether this energy is directly measurable or not, the driver has to be informed by some means of the actual energy still in the vehicle. Drivers of combustion-engine driven vehicles are accustomed to checking the gas gauge so as to estimate operational hours the vehicle can run. Measurement of the remaining gasoline available in the vehicle is simply a measurement of the level of fluid in the tank. The gauge usually shows the level as a portion of the full tank. On the other hand, electrically powered vehicles lack this simplicity of the fuel gauge and determination of the available energy in the battery pack is quite an ample task. In majority of cases industrial vehicles are powered by secondary lead-acid batteries addressed in this paper. This type of the batteries has been a successful commercial commodity for more than a century. The reasons for this wide use are mostly their low price, simple manufacturing and good performance and life cycle characteristics /3/. In the same way, the fuel gauges show the percentages of the tank fullness and the battery state-of-charge indicators show the percentage of the remaining battery capacity. This helps the driver to estimate how long the vehicle will operate and when charging of the battery is necessary. The accuracy of these indicators is essential in preventing stranding and ensuring full-range exploitation of the battery power. The battery state-of-charge (SOC) is a complex non-linear function of the discharge current, ambient temperature, battery age and other parameters /4/. In practice, direct measurement of some of these parameters is either impossible or too expensive. There are several practical methods available to monitor lead-acid batteries. All of them use one or more measurement data to estimate the remaining capacity in the battery. Most of the methods implemented in the market use either the simple open-voltage /6/ or coulometric method (ampere-hour measurement) or a combination of the two /5/. Other techniques are specific gravity, voltage under load /2/ and various battery model-based methods /1/, /7/. The specific gravity method directly indicates SOC by showing the acid concentration in the electrolyte transformed during discharge.

The method presented in this paper is a combination of the open-circuit and ampere-hours measurement /4/. A monitoring technique based on the open-circuit voltage, which was originally used in the forklift truck, is improved with battery current measurement. An improved technique drastically reducing the stabilizing time of the battery voltage is developed to predict the open-circuit voltage. The proposed algorithm optimizes the overall accuracy due to the constant measurement of ampere-hours drawn from the battery. At the same time, it adapts to different operating conditions, battery ageing and quality of battery service. Battery-powered material-handling trucks use different types of the traction motors. In the past, mainly separately excited DC motors were used. Today, with new technologies evolving and fast signal processors availability, induction traction motors are widely used. For control purposes, phase currents of the AC induction motors have to be known. To reduce the cost and additional hardware for battery current measurement, the paper describes techniques to reconstruct the battery current of the induction motor from the measured phase currents /8/. All high power devices on the electric truck contribute to the total energy consumption and have to be taken into account. The main truck controller collects these data and computes the total battery current.

2 Battery capacity

The term battery capacity describes the amount of usable energy stored in the battery. There are several principles to define it. The theoretical capacity is the total power that can be drawn from a battery. This value depends on the amount of the electrolyte and not on the material in the plates of a new battery /3/. The electrolyte in the lead-acid battery is a solution of sulphuric acid and water. This concentration is defined as a specific gravity, a measure of density, which is the ratio of the mass of the mixture of sulphuric acid and water to pure water. The relationship between the state-of-charge and specific gravity is linear as shown in Figure 1 /3/.

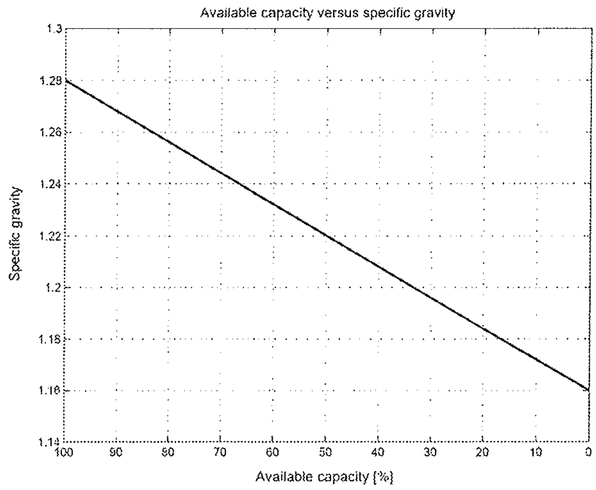

Figure 1. Relationship between the available capacity and specific gravity for a typical traction secondary lead-acid battery

The usable capacity defines the ampere-hours available in the battery at a certain discharge rate. A battery rated at 400 Ah at C/5 rated current means that the battery can be discharged at 80 amperes in 5 hours. This capacity varies depending on the discharge current. The above battery discharged at 200A will last only 1.6 hour, giving only 320Ah. Peukert /9/ empirically defined the relationship between the available capacity *Ca* and the discharge current I as:

$$C_a = KI^{n-1} \tag{1}$$

where constants n and K depend on the temperature, concentration of the electrolyte, and the structure of lead-acid batteries. It should be noted that the usable capacity does not take the recuperation effect into account, because it is derived under continuous, constant current discharge conditions /4/. This means that with intermittent rest periods between discharges, the electrolyte has more time to diffuse and thus increases the total capacity of the battery. Since the usable capacity is defined as practical capacity, most commercially available battery indicators show usable capacity. The recommended usable capacity is generally only 80% of the rated usable capacity to insure the maximum battery life /3/.

3 Battery SOC measurement

In a certain way SOC differs from the usable capacity showing the percentage of the available total capacity rather than indicating the amount of ampere-hours available from a cell. As already mentioned above, there exist several measuring techniques to estimate the battery SOC /6/.

1) specific gravity measurement, 2) open-circuit voltage measurement, 3) battery voltage under load measurement, 4) ampere-hours measurement, and other combinations of these four basic techniques. The specific gravity measurement method is impractical for real applications, since the battery has to be opened and rested for several hours after use.

3.1 Open circuit voltage method

The open-circuit voltage of a secondary lead-acid battery is directly related to the battery SOC. This method is particularly suitable for automated battery monitoring since it enables to measure the voltage directly from the battery terminals and no special sensors are required. The nominal voltage of the lead-acid cell is 2V. The open-circuit voltage is a direct function of the electrolyte concentration, ranging from 2.125V for a cell with 1.28 of the specific gravity to 2.05 V with 1.21 of the specific gravity /6/. The open-circuit voltage depends also on temperature of the electrolyte but the temperature coefficient is about 0.2mV/C and can be neglected in real applications where operating conditions do not change for more than 50 °C, which is less than 1% of the total battery capacity. Thus, the relationship between the open-circuit voltage and specific gravity is linear within the usable battery capacity range. The battery open-circuit voltage being linearly dependent on specific gravity, which is a direct SOC indicator, the state-of-charge can be defined by the ratio of difference of actual open-circuit voltage V_{OCV} to empty battery open-circuit voltage V_{empty}, to difference of full battery open-circuit voltage V_{full} to empty battery open-circuit voltage V_{empty}:

$$SOC_{OCV} = \frac{\hat{V}_{OCV} - V_{empty}}{V_{full} - V_{empty}} \qquad (2)$$

The open-circuit voltage must stabilize before a reliable measurement can be made. This stabilization process can take from 30 minutes to several hours depending on battery design, former discharge current and SOC.

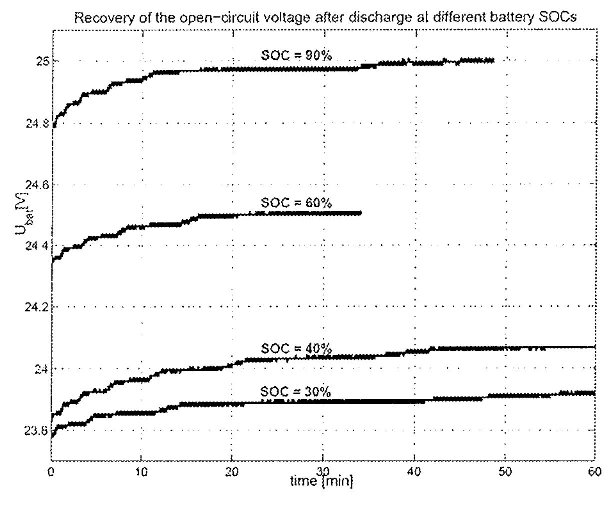

Figure 2. Recovery of the open-circuit voltage at different battery SOCs

Figure 2 shows a typical recovery process of the battery open-circuit voltage at different SOCs.

Estimating the open-circuit voltage shortly after the load has been disconnected from the battery can solve the problem of the long stabilization period after each discharge cycle. A period of 7 minutes was established as appropriate by the method presented in /4/. The proposed method is based on experimentally determined time required by the battery voltage to fully stabilize. Interpreting this time in a logarithmic scale, very constant values were obtained for different types of batteries and discharge rates prior to the recovery process. Since 7-minute period of rest can be quite long for some truck drivers, the time needed to calculate the open-circuit voltage should be reduced. To have it further reduced, the proposed method takes into account the current battery SOC of the battery and the battery current prior to the recovery process.

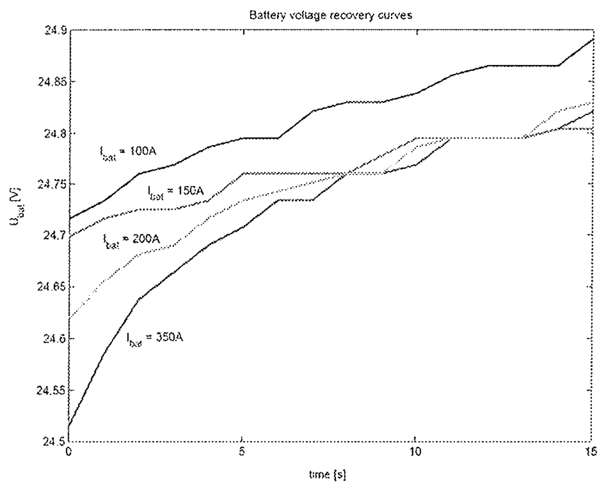

Figure 3. Battery open-circuit voltage recovery curves after different battery current loads

The higher current, before the rest period takes place, has a strong impact on the recovery curve of the open-circuit voltage as it can be seen from Figure 3. Taking this into account, the asymptote of the recovery curve can be adapted. The dependency was found to be linearly related to the current. At the same time, the total ampere-hours drawn from the battery after the last rest period affect the recovery curve, since with greater loads the battery takes more time to stabilize than with smaller loads.

3.2 Ampere-hour method

Under-load measurement of the battery current and integrating it over the time constitutes the ampere-hours measurement method. This method is widely used since it is simple to implement and gives satisfactory results for constant-load states conditions. The coulometric measurement gives a continuous indication of the battery ampere-hours and by knowing the battery capacity the current battery

SOC_{Ah} can be calculated by the ratio /1/ of the actual battery capacity $C_a - \int I_{bat}dt$ to total battery capacity C_a:

$$SOC_{Ah} = 1 - \frac{\int I_{bat}dt}{C_a} \tag{3}$$

This technique provides a relatively accurate SOC indication, but is prone to the accumulation error resulting from inaccurate current measurement and other factors that are not taken into account. In its most basic form, the battery capacity is assumed to be constant, but in reality the capacity varies with the discharge current, type of discharge, battery age and temperature. As these effects are not taken into account, this method can be regarded as accurate only for short time lasting states. Its second drawback is that the total battery capacity has to be known. To neglect the lack of knowledge of the battery capacity, the proposed method uses the open-circuit voltage result SOC_{OCV} and ampere-hours consumed C_{meas} to estimate the total battery capacity $\hat{C}_a$ (4).

$$\hat{C}_a = \frac{C_{meas}}{SOC_{OCV}} \tag{4}$$

Each of the techniques discussed above has its own drawbacks. However, by combining the open-circuits voltage and ampere-hours measurement, it is possible to get very accurate results. The ampere-hours measurement is used

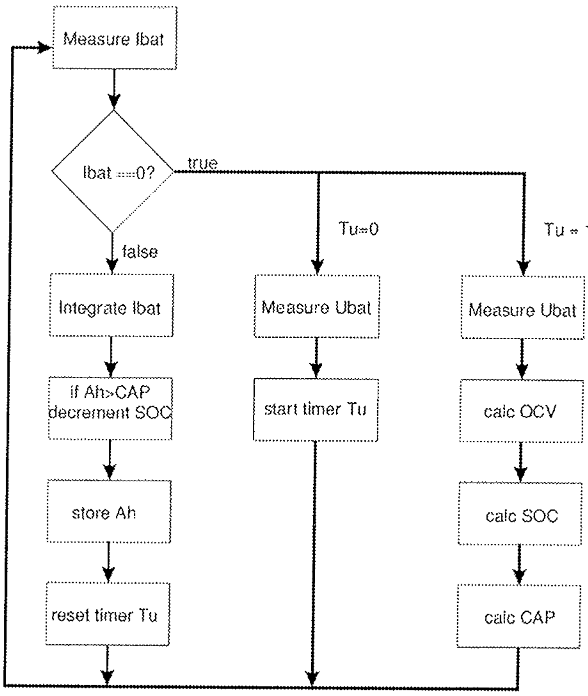

Figure 4. Measurement algorithm scheme

when the truck is operating and current is drawn from the battery. This informs the driver of the current ampere- hours consumption. When the truck is at rest and no power is drawn from the battery for long enough periods, the open-circuit voltage measurement takes place and estimates the battery SOC (Figure 4). On the basis of SOC calculated from the open-circuit voltage, the total battery capacity correction is made (4), which influences the ampere-hours SOC estimation (3).

4 Battery current reconstruction

The forklift truck is a material-handling vehicle powered by a lead-acid battery. The whole system is composed of several electrical devices. The main truck controller is a four-phase inverter controlling an induction motor and DC pump. besides this, it handles the system logic and drives all hydraulic components. The electrically powered aided steering (EPAS) is a separate device controlling a permanent magnet motor, tiller card is a driver command board and graphic display is the system output device informing the driver of the system status. Only the main truck controller and EPAS system are the major power consumption devices and their current has to be taken into account. Since EPAS is a separate device, the information of its current load is sent to the main truck controller through a system communication channel.

In order to correctly calculate the ampere-hours drawn from the battery, an accurate current measurement unit is needed. This usually involves shunt resistor measurement or more sophisticated equipment such as toroidal coils and Hall sensors. Both techniques require expensive electronic parts that have to be added to the system. Furthermore, it complicates the electrical wiring of the truck, which adds an additional cost to the truck. Since the main truck controller already measures the current of the traction induction motor and the current drawn by the DC pump motor, it can calculate also the battery current. The hydraulic pump is a PWM driven serial excited DC motor, so its current can be calculated from the measured DC motor current flowing in the phase i_{phase}. By knowing the applied frequency $1/T_{period}$ and duty cycle T_{on} of PWM modulation, also the battery current I_{DC} can be reconstructed by:

$$I_{DC} = i_{phase} \frac{T_{on}}{T_{period}} \tag{5}$$

More problems arise in the case of traction motor battery current reconstruction. The traction motor is a three-phase symmetrically wounded induction motor driven by a three-phase voltage source inverter (Figure 5). It is possible to

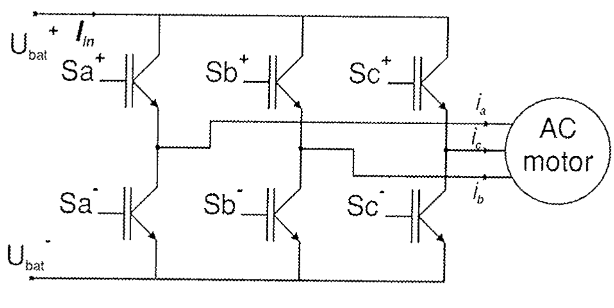

Figure 5. Three-phase inverter

calculate the current drawn from the battery by knowing the phase currents and the switching state of the three-phase inverter. Due to the discrete nature of the output phase voltage, only seven distinct voltage vectors can be generated. Each voltage vector within the sequence corresponds to the state of the VSI power switches. These states determine the way in which phase currents are mirrored by the dc-link current (Table 1).

$I_{in} = 0$	(Sa, Sb, Sc) = (0,0,0)
$I_{in} = i_a$	(Sa, Sb, Sc) = (1,0,0)
$I_{in} = -i_a$	(Sa, Sb, Sc) = (0,1,1)
$I_{in} = i_b$	(Sa, Sb, Sc) = (0,1,0)
$I_{in} = 0$	(Sa, Sb, Sc) = (0,0,0)
$I_{in} = i_a$	(Sa, Sb, Sc) = (1,0,0)
$I_{in} = -i_a$	(Sa, Sb, Sc) = (0,1,1)
$I_{in} = i_b$	(Sa, Sb, Sc) = (0,1,0)

Table 1. Inverter states and line currents

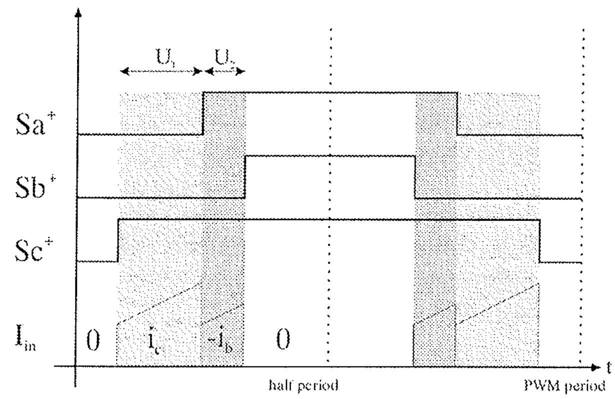

Figure 6. Signals controlling the upper transistors in a three-phase inverter

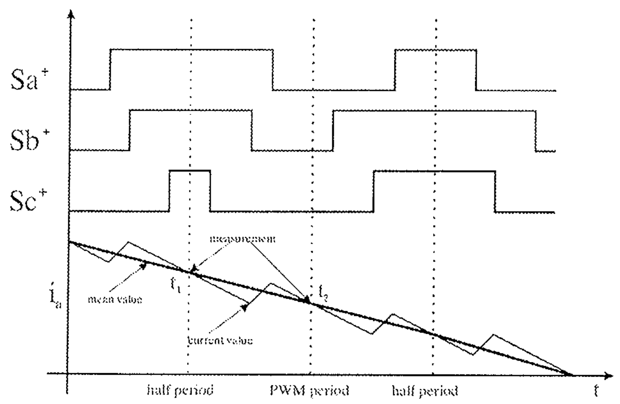

Figure 7. Correct measurement of phase currents in symmetric PWM

A signal processor placed on the main controller board drives the phase inverter and does all on board calculations for induction motor control. The VSI state is known at any time in the workflow. The same processor measures also induction motor phase currents. To avoid measurement errors due to the ripple current caused by PWM modulation of the sinusoidal phase current, symmetrical PWM modulation is implemented. The measurement of the phase current takes place at a half period when all upper transistors are switched on and at periods where all lower transistors are switched on and there is no battery current flowing into the inverter (Figure 6). The average phase current is calculated based on two measurements at times t1 and t2 (Figure 7).

In each sampling period, the correct sector has to be determined and the length of the U1 and U2 stator voltages has to be calculated (Figure 6). Determining the actual sector the inverter is in; the correct direction of the line current can be defined. When this is known, the average battery current can be calculated for that period:

$$\bar{I}_{in} = \frac{i_{phase1}(Sa,Sb,Sc)\cdot U_1 + i_{phase1}(Sa,Sb,Sc)\cdot U_2}{T_{half\_period}} \qquad (6)$$

The sampling frequency of phase currents for battery current reconstruction is 50Hz.

5 Measurement results

In order to evaluate the proposed method of the battery SOC estimation algorithm, several measurements were made in field. They were carried out on a forklift truck powered by a 24V lead-acid battery manufactured by Fiamm (12 cells, 375Ah at C/5). The battery was fully charged before each discharge cycle with a laboratory charger. The cycle tests were done under various working conditions. The truck was accelerating, decelerating, lifting load and driving on different slopes to match normal operating conditions.

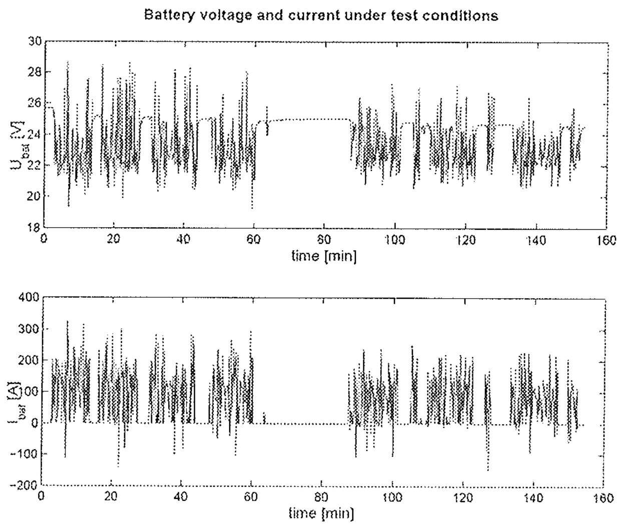

Figure 8. Battery current and voltage under test conditions

Thus, the battery was not discharged at a constant but at a time-varying rate (Figure8). During discharge, the ampere-hours were measured with a BRUSA BCM 400 ampere meter and logged every 10 minutes. At the same time, the estimated SOC based on ampere-hours calculated within the main truck controller were logged on a laptop computer connected to the main truck controller over a serial communication interface. The measured ampere-hours were then compared to ampere-hours calculated by the truck main controller. As can be seen in Figure 9, the accumulation error increases at the end of the discharge cycle, where the error between the measured and calculated ampere-hours rises to 2%. These results show reliability due to the known battery capacity and quite new battery pack used in the test. In old batteries, this error can increase, since they can no longer provide the rated capacity. In a separate discharge cycle open-circuit voltage estimation tests were made. After each discharge cycle, the battery was put to rest to fully stabilize in order to measure the actual open-circuit voltage (Table 2). After each 5% of discharge, a rest period of two hours took place to allow for correct measurement of the open-circuit voltage. As demonstrated in graphs 9 and 10, the proposed technique of the SOC measurement gives very satisfying results, as the error between the actual and estimated SOC never exceeds 5% (Figure 10). To provide for a comparison, values obtained with the old algorithm are plotted in Figure 10. As it can be seen, by using the new algorithm, accuracy is improved by more than 15% compared to the old one. This is mainly due to continuous measurement of battery consumption in terms of ampere-hours drawn form the battery.

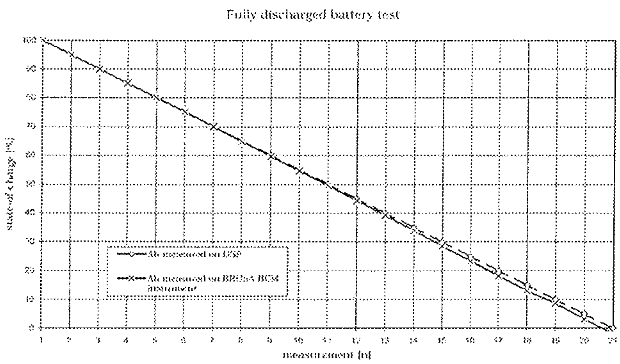

Figure 9. SOC measurement results based on Ah measurement

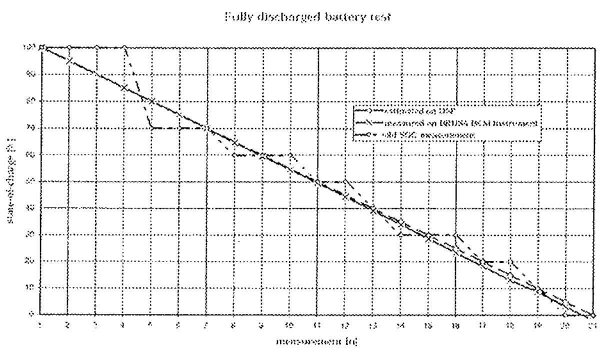

Figure 10. SOC measurement results improvements

Estimated Voltage	Estimated SOC	Error
23,78	0,19	0,01
23,74	0,172	-0,008
23,78	0,19	0,01
23,85	0,225	0,045
23,74	0,172	-0,008
23,75	0,175	-0,005
25,25	0,925	0,035
25,21	0,907	0,018
25,14	0,872	-0,018
25,14	0,872	-0,018
25,25	0,925	0,035

Table 2. Estimated open circuit voltage after different loads were disconnected from the battery at 18% and 89% of actual SOC respectively.

6 Conclusion

This paper addresses issues related to the battery SOC estimation of lead-acid powered forklift trucks. It shows that the use of the coulometric method for calculating SOC allows continuous monitoring of the battery pack also when the truck is running. Combining this method with the open-circuit voltage method improves the overall accuracy as shown by the obtained measurement results. The proposed open-circuit voltage estimation method shortens the time needed to accurately calculate the battery SOC and provides more flexibility to the truck driver and truck work-cycle performance. Its additional advantages are that there is no need for the battery capacity to be known, its age is not important, and the ambient operating conditions are not restrictive. Other fields of use are in solar modules, repeaters, and other remote equipment.

The paper also describes a simple technique to reconstruct the battery DC current from three-phase induction motor currents. It gives very good results and reduces the cost of additional hardware needed for accurate battery current measurement.

7 References

/1/ S. Pang, J. Farrell, J. Du, and M. Barth, "Battery state-of-charge estimation", *Proc. of the American Control Conference*, Vol. 2, pp. 1644-1649, June 2001.

/2/ C.Y. Tseng , C.F. Lin, "Estimation of the state-of-charge of lead-acid batteries used in electric scooters", *Journal of Power Sources*, Article in Press, 2005.

/3/ D. Linden, *"Handbook of Batteries"*, USA: McGraw-Hill, 2nd ed. 1995.

/4/ Aylor, J.H., A. Thieme, and B.W. Johnson, "A Battery State-of-Charge Indicator for Electric Wheelchairs", *IEEE Transactions on Industrial Electronics*, Vol. 39, No. 5, pp. 398-409, 1992.

/5/ P. Sinclair, R. Duke and S. Round, "An Adaptive Battery Monitoring System for an Electric Vehicle"

/6/ K. Marsh, Ed., *"Curtis Battery Book One"*, Curtis Instruments Inc., Mt. Kisco, 1971.

/7/ B. Vairamohan, "State of Charge Estimation for Batteries", *Master Thesis in Electrical Engineering, University of Tennessee*, December 2002.

/8/ Texas Instruments, "Three-phase current measurements using a single line resistor on the TMS320F240", *Literature Number: BPRA077*, May 1998.

/9/ W. Peukert, "An equation for relating capacity to discharge rate", Electrotech, Z. 18, 1897.

Kristjan Baša,
Iskra Avtoelektrika d.d., Polje 15, 5290 Šempeter pri Gorici
Andrej Žemva
University of Ljubljana Faculty of Electrical Engineering
Tržaška 25, 1000 Ljubljana, Slovenia

Prispelo (Arrived): 09. 01. 2006; Sprejeto (Accepted): 30. 01. 2006

MAGNETIC FORCE ON THE WELDING ARC

J. Tušek, I. Škrbec

Faculty of Mechanical Engineering, Ljubljana, Slovenia

Key words: magnetic force, welding arc, deflection of the arc, arc blow, undercuts, triple-wire electrode

Abstract: The article states causes, effects and methods of preventing welding arc deflection in welding, surfacing and other processes involving welding arcs. The first part of the article gives a short survey of literature reporting on effects of various kinds of magnetic fields on the welding arc, on material transfer, and on the welding processes itself. Some fundamental theoretical principles of physics covering magnetic and electromagnetic fields, which affects the welding arc directly or indirectly, are described.

Then two main causes for arc blow effect are indicated. These are an electromagnetic field, which generates due to welding current flow, and permanent magnetic field, which generates in work pieces due to various reasons.

Two macro sections of surfacing welded with triple - wire electrode and with different voltage are shown, which effects on the arc blow.

Magnetne sile na varilnem obloku

Kjučne besede: magnetna sila, varilni oblok, odklanjanje obloka, plesanje obloka, obrobne zajede, trižična elektroda

Izvleček: Članek obravnava vzroke, posledice in metode za preprečitev odklanjanja obloka pri varjenju, navarjanju in pri drugih akttivnostih z varilnim oblokom. V prvem delu članka je podan kratek pregled literature, ki poroča o različnih vplivih magnetne sile na varilni oblok, prehajanje materiala in na celoten process. Opisani so nekateri osnovni teoretični oziroma fizikalni principi magnetnih in elektromagnetnih polj, ki direktno ali indirektno vplivajo na varilni oblok. Prikazana sta dva najznačilnejša pihalna učinka (odklanjanje obloka) varilnega obloka. To sta elektromagnetno polje, ki se generira zaradi prevajanja električnega toka in permanentno magnetno polje, ki zaradi različnih vzrokov nastane v varjencih.

Prikazana sta dva maro obrusa navarov, varjena s trižično elektrodo z različno obločno napetostjo, kar vpliva na odklanjaje varilnih oblokov.

1 Introduction

In the practice of arc welding, weld defects such as weld surface irregularities and undercuts occur. Welders most often neither know the causes of their appearance nor methods for preventing these defects. These defects are very often caused by arc deflection which is due to effect of magnetic and electromagnetic forces. Electromagnetic forces are produced by welding current flow, while magnetic forces are due to inhomogeneous magnetic field in the work piece, a welded structure or even in the filler material.

The welding arc is a process of electric discharge in a gas through which an electric current flow. Carriers of electric current in the welding arc are electrons and ion, also called plasma. Each current conductor is surrounded by an electromagnetic field. Owing to changes in conductor diameter, also electromagnetic field density varies. By arc welding electromagnetic field is very often inhomogeneous, which results in electromagnetic effects.

2 A short literature survey on research in the field of magnetic forces on the welding arc

In the literature of the last decade it is hard to find an article reporting on magnetic field effects on the welding arc. An exception seems to be reference /1/, in which a general survey of arc deflection due to magnetic field effects and cures to this can be found.

Investigations on magnetic field influence on the welding arc, on material transfer, and on weld shape began in the sixties, but they were most intensive in the seventies and the eighties /2-6/.

In all the references stated, the main purpose was to investigate the feasibility of arc deflection, its restriction, and its control during welding. Fewer reports are dealing with prevention of influences exerted by the magnetic field, which was generated by welding current flow through the electrode, the arc and the work piece.

Between the electric current and magnetic field there are certain effects which are comprised in the term "Lorentz force". This force, which is a vectorial product of electric current and magnetic flux density, can deflect the arc or move it along a certain area /7,8/. In this way the arc can be controlled.

In literature reports on investigations on the influence of a longitudinal magnetic field on the melting rate and the welding process /9,16/. Owing to the outside magnetic field effects electric resistance in the arc increases, a lower current is flowing through the arc while wire feed speed is kept constant. The melting rate can thus be increased by 50 % /10/.

Problems due to arc blow effect are not thoroughly investigated in the literature.

3 Some theoretical principles of physics

A magnetic field exists between poles of permanent magnets or around current-carrying wires. We can visualize it with the help of lines of force. In case of a straight current - carrying wire, the lines of force form concentric circles (Fig.1a). If the wires is wound in the form of a coil consisting of several loops, the lines of force get more concentrated and run through the coil.

In a relatively long coil, the lines of force are parallel to each other, which means that there is a homogeneous magnetic field in the coil (fig.1b). Magnetic field intensity can be measured by a magnetometer. It is dependent on electric current intensity flowing through the coil, on the number of loops, and on the coil length.

$$H = \frac{I \cdot N}{l} \qquad \left[\frac{A}{m}\right]$$

I [A] - current intensity

N [/] - number of loops

L [m] - coil length

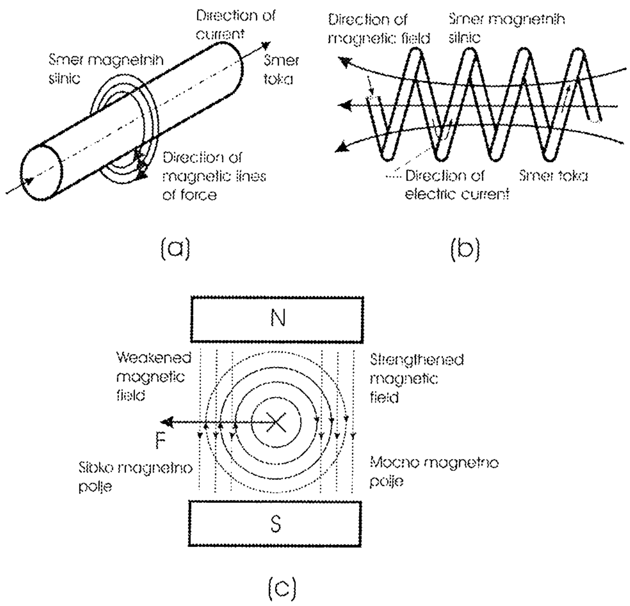

Figure 1: *Correlation between electric current and magnetic field;* ***a*** *- Magnetic field around a current-carrying wire,* ***b*** *- Magnetic field pattern in a relatively long coil carrying direct current;* ***c*** *- Direction of force, visualized by magnetic lines of force, is dependent on electric current.*

The magnetic field intensity in the middle of an infinite current - carrying wire is calculated by dividing electric current intensity with the wire diameter. The magnetic field intensity at a certain distance from the wire is calculated by dividing with "$2\pi r$", where "r" is the distance perpendicular to the wire.

Magnetic flux density is a vector of which the direction is a tangent to a magnetic line of force. It is defined at a point as a force F at that point which the homogeneous magnetic field exerts on a small length of wire that carries an electric current.

$$F = B \cdot I \cdot L \qquad \left[\frac{Vs \cdot A \cdot m}{m^2}\right] = \left[\frac{N}{m}\right]$$

B [T = Vs/m^2] - magnetic flux density

I [A] - current intensity

L [m] - conductor length

$$B = \mu \cdot H \qquad \left[\frac{Vs \cdot Am}{m^2 \cdot Vs}\right] = \left[\frac{Aa}{m}\right]$$

μ [Vs/Am] - permeability

It was already in 1845 that Faraday found out that an inhomogeneous magnetic field exerts a force on all the substance in the magnetic field in the direction of the field gradient. The magnetic force is thus exerted if the magnetic field is inhomogeneous.

Figure 3 shows a simple and well - known case, i.e. Principle of the effect of a magnetic force. The magnetic force is acting in the direction from a higher concentration of magnetic lines of force to their lower concentration.

In welding, the cross section through which electric current is flowing varies because the current flows not only through the welding wire, but also through a molten drop, the welding arc, the molten pool, and the work piece. Variations in the conduction cross section entail variations in current distribution density, and consequently in magnetic flux density, which means that the magnetic field is inhomogeneous. Another case in welding is when magnetic lines of force run through various media having specific magnetic permeability which causes a non-uniform distribution of magnetic lines of force, which generates magnetic forces.

4 What is magnetic arc blow and where does it arise

In all welding process in which electric arc or electron beam is used energy by the motion of electrically charged particles. Carriers of electric current in solid conducting materials are electrons, while in gaseous materials, i.e. arc, these are electrons and positively or negatively charged ions. During welding, the cross section, the shape, and the physical condition of the conductor vary; consequently the direction of action of the electromagnetic force varies as well. The welding arc possesses a magnetic field of its own, which is unsymmetrical due to the difference in magnetic permeability, which causes arc deflection.

Such cases are shown in Figure 2. In the first case (Figure 2a), the electromagnetic force is deflecting the arc due to a stronger magnetic density at point "A". Magnetic flux density is dependent on welding parameters as well as on the location of fixation of welding cables. In both cases (Figures 2b and 2c), magnetic arc blow can be eliminated by setting two or more welding cables at various location on the work piece so that the welding current flows from the arc through the work piece in various directions. Figure 2b shows the magnetic arc blow occurring, during welding, at the edge of the work piece. Magnetic flux density in the vicinity of the arc is asymmetrical due to various media, which induces an electromagnetic force which deflects the arc. In practice, this problem can be solved by inclining the electrode, by a choice of suitable welding parameters or by a special metal prolongation which makes magnetic flux easier and forms a symmetrical magnetic field round the arc.

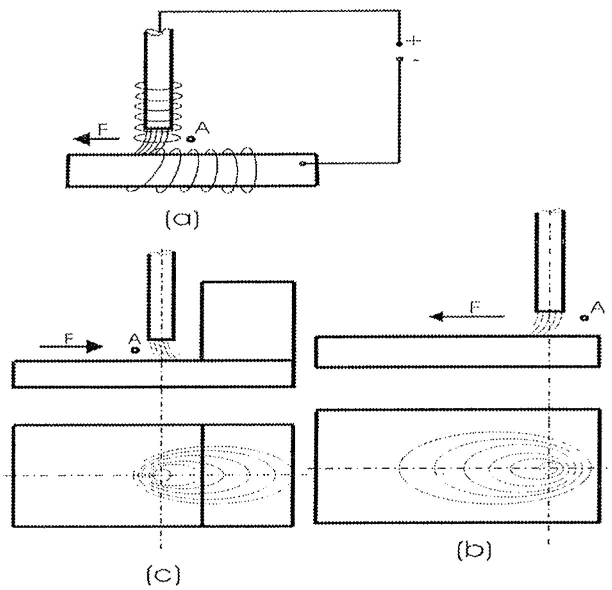

Figure 2: *Magnetic force on the arc welding;*
F *- Direction of the magnetic force,*
a *- Direction of arc deflection is dependent*
b *- on direction of welding current flow, Magnetic arc blow occurring during welding at the edge of workpiece,*
c *- Magnetic arc blow occurring during welding along the wall of metal plate.*

Magnetic arc blow occurs also during welding along the wall (Figure 2c) or in the narrow gap in the groove. The magnitude of arc deflection is affected also by the shape of the weld groove, the level of the magnetization of individual work piece, and total magnetic field intensity which may increase by a factor 10 if two work pieces are brought closer together. Fig. 3 shows influences of the groove shape on the distribution of magnetic density or magnetic lines of force in the weld groove.

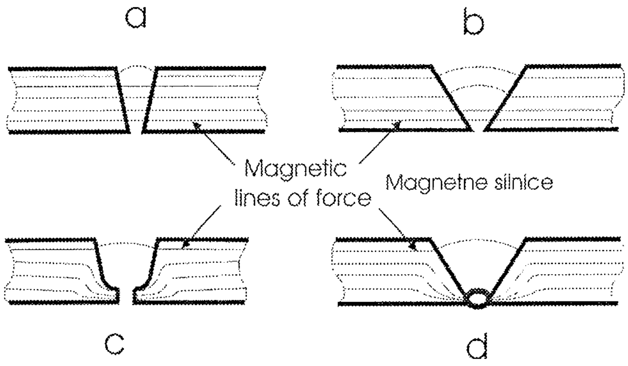

Figure 3: *Influence of groove shape on magnetic field intensity which is proportional to density of magnetic lines of force in the weld groove.*

It can be described as follows:

- Magnetic field intensity in the narrow gap is relatively strong, but distributed across the whole area of the groove.
- In the wider grove, the magnetic field is weaker than in the narrow one and concentrated in the weld root.
- In the U groove, magnetic field density is even higher and may be increased if two work pieces are brought closer together.
- The root pas having been welded, magnetic field density in the weld groove reduces.

Magnetic field density and magnitude of electrodynamic force which deflects the arc and causes undesired effects differ from one welding process to another. Practical experiences show that magnetic flux density of up to 2 mT does not induce magnetic arc blow. Magnetic flux densities of 2 mT up to 4 mT usually induce deflection, but for the majority of welding process, this is still acceptable and quality weld can be made. At higher magnetic flux densities, however, certain measures should be taken.

It should be stressed once again, however, that the magnetic field intensity measured at the tip of the work piece may rise by up to 10 times if the workpieces are joined together.

When several work pieces are joined, not only magnetic field density, but also other magnetic field properties, such as magnetic induction, permeability, remanence, coercive, and magnetostriction, changes as well.

5 Influence of the welding process on magnetic arc blow

Magnetic arc blow is different in different welding processes. Higher arc voltage causes electrons in the arc to travel faster and turn less in the magnetic field. Consequently arc deflection is weaker and the arc is more stable. The welding arc burning under higher pressure then atmospheric is more prone to deflection since electrons in the arc are slower. Arc deflection is stronger in TIG welding then in MAG/MIG welding or manual arc welding, because in TIG welding, arc voltage is usually lower.

It happens, however, very often that arc deflection causes difficulties in welding with multiple-wire electrode or in welding with several electrodes.

In welding with multiple-wire electrode, the wires are supplied from single power source, which means that in the wires different or the same direct currents may flow and welding parameters can not be changed for each individual wire. If the current is flowing through the wires paralelly in the same direction, the wires and the arcs attract each other (Figure 4), which may result in weld surface irregularities and undercuts /11/.

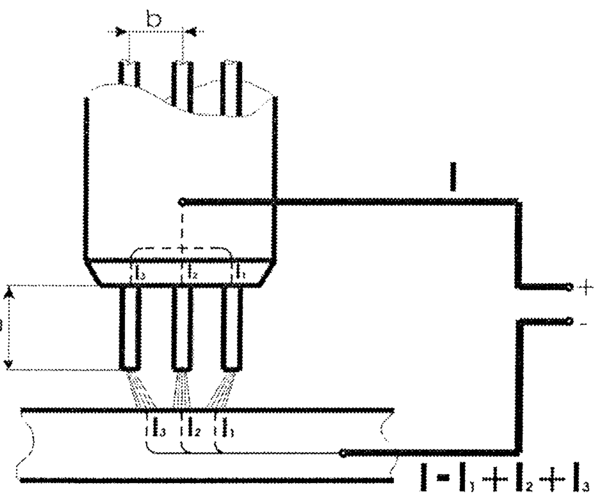

Figure 4: *Welding arcs attract each other in welding with multiple-wire electrode with direct current due to electromagnetic forces;* **L** *- wire extension length,* I_1, I_2, I_3 *- current intensity in the wires*

The choice of suitable welding parameters, wire-to-wire distance, wire extension length, and wire arrangement in the contact tip are, therefore, of utmost importance in welding with multiple-wire electrode /12,13,14/.

Figure 5 shows macrosections of two submerged-arc surfacing welded with triple-wire electrode, the wires being arranged in the direction transverse to the welding direction. In both cases, all welding parameters, with the exception of welding voltage, were kept constant. The wire used had a diameter of 2 mm, wire extension length was 28 mm, wire-to-wire distance 7 m, welding speed 30 cm/min, current intensity 195 A/wire and arc voltage 35 V in the first case (left) and 20 V in the second case (right). As stated, the only varying parameter was arc voltage. The figure and the welding parameters confirm the fact that the welding arc with lower voltage is more sensitive to magnetic arc blow because electrons in the arc are slower. Together with the arc (Figure 4), also droplets deflect from the ideal direction perpendicular to the work piece. They detach from the wires and travel in the direction of the arc. This affects the surfacing shape (Figure 5, right). In welding of the surfacing as shown in figure 4 (left), the welding parameters selected are ideal. High arc voltage creates stable arcs, there is no magnetic arc blow among them, therefore, the droplets detached travel from the wire to the weld in perpendicular direction. The weld shape is uniform and without undercuts.

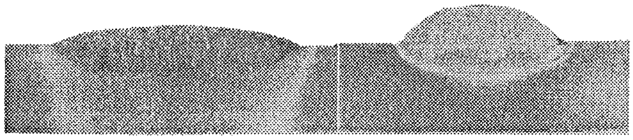

Figure 5: *Macrosections of submerged-arc surfacings welded with triple-wire electrode, wires being arranged in the direction transverse to welding direction. Welding parameters:* ***I*** *= 3 x 195 A,* **d_0** *= 2 mm,* **L** *= 28 mm,* **b** *= 7 mm,* **v_v** *= 30 cm/min,* **U** *= 35 V -* ***left***, **U** *= 20 V -* ***right.***

In welding with several electrode heads, each wire is supplied from a separate power source and has separate driving and regulation systems. This means that different currents of different intensity and voltage may flow in individual wires. It is recommended to use in practical welding cases, as regards the first wire, direct current with low arc voltage and high current intensity. As regards the other wires, alternating current with a somewhat higher arc voltage and somewhat lower current intensity should be used. The alternating currents in the wires should be phase-delayed in order to prevent mutual electromagnetic influence.

The electromagnetic force between two or more arcs in welding with several electrodes supplied with alternating current can be calculated according to the following equation:

$$F_i = \frac{\mu_o \cdot I_i^2}{2 \cdot \pi \cdot b \cdot \cos\Phi_{ij} \cdot \cos\Phi_{jj}}$$

F_i - electromagnetic force exerted on i[th] arc

μ_o - magnetic permeability in the air

I_i - effective value of welding current in the i[th] arc

Φ_{ij}, Φ_{jj}- angle of inclination of electrode (Figure 6)

b - distance between arcs

6 Causes of magnetic field generated in workpieces

We have been mainly talking about magnetic arc blow which occurs due to an electromagnetic field. But arc deflection and magnetic arc blow may occur also due to a magnetic field existing in workpieces or in a welded structure as a whole.

It is well known that only ferromagnetic materials, such as iron, cobalt, nickel, and their alloys, can be magnetised. Some materials are more easy to magnetise and more difficult to demagnetise. It is usual to distinguish between magnetically hard and soft materials. Magnetically soft materials are relatively easy to magnetise, but only to certain degree. Magnetically hard materials are more difficult to magnetise, but they remain magnetised.

For ferromagnetic materials, it can be stated that there is a correlation between magnetic hardness and metallurgical hardness.

There are different causes of magnetisation of workpiece. Ferromagnetic workpieces can get magnetised from the earth's magnetic field or other local magnets, such as various magnetic clamps used in mechanical or other treatments of the workpiece, devices for magnetic inspection, high-frequency welding units, and welding cables running along the workpieces.

Various electrical connection cables, tack welds and other means of tacking can cause local magnetisation or intensity magnetic field in the welding structure.

It has already been mentioned (Figure 2) that the welding current (particularly direct current) may provoke arc blow, which is often the case and causes difficulties in welding.

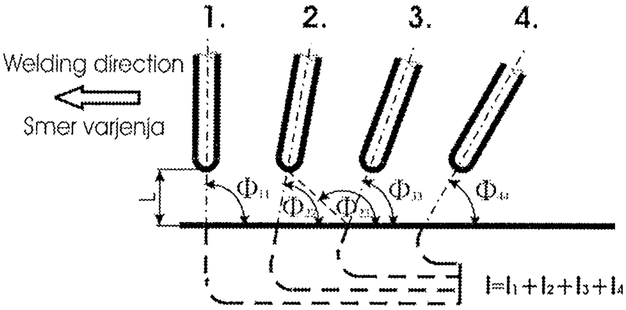

Figure 6: *Schematic representation of a system for welding with four electrodes, including data required for calculation of electromagnetic force; Φ_{ij}, Φ_{jj} - angle of inclination of electrode, I_1, I_2, I_3, I_4 - current intensity in the wires*

7 Measures for reducing problems caused by magnetic arc blow

In practice, several more or less efficient methods for reduction or even elimination of the influence of the magnetic field on arc deflection during arc welding is known. For reduction of magnetic field concentration in the root area of the weld preparation, special leather bags filled with iron powder can be used. They permit a uniform distribution of magnetic lines of force across the weld groove. For demagnetisation of larger structures, strong power sources producing current intensities over 20 kA can be used. These devices are very expensive, but they do not always guarantee success.

Success can be achieved in a simple and cost-effective way by current-carrying welding cables wrapped around the weld preparation. But first it is necessary to establish magnetic field intensity and its direction in the weld groove.

In the magnetic field intensity in the weld groove does not exceed 4 mT, the effect of magnetic arc blow can be prevented by the selection of appropriate welding parameters. This can be achieved by welding with larger electrode - wire diameters and by suitable weld preparation (Figure 3) so that the arc burns in a proper distance from the magnetic field.

Stronger magnetic fields can be eliminated, as already mentioned, by wrapping current-carrying welding cables around the work piece.

It is known, magnetic field intensity and its direction are depended upon the number of loops, current intensity, and current direction, coil length, and kind of the material. Therefore, this operation should be carried out as carefully as possible in order not to produce an opposite effect.

For demagnetisation of a 2 mm thickness, 50 Hz alternating current can be used. For demagnetisation of greater thickness's, direct current should be used.

In welding of larger structures, such as pipes and hollow sections, the structures as a whole can not be demagnetised, but local demagnetisation around the weld groove should be achieved.

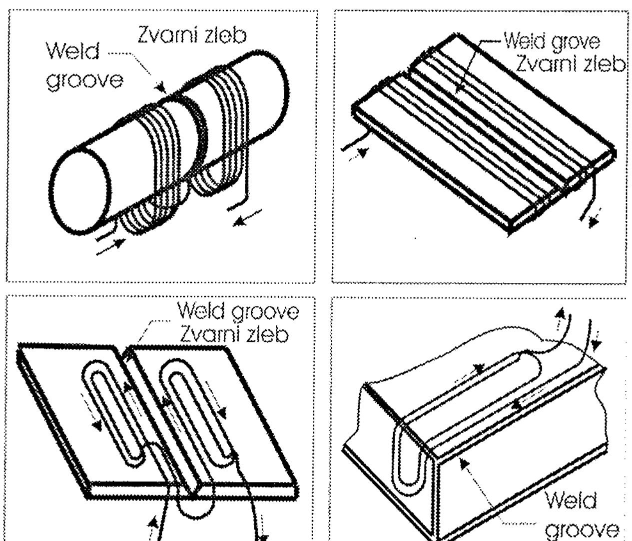

Figure 7: *Some alternative variants of electric cable arrangement to demagnetise weld groove, i.e. welded joint.*

 Informacije MIDEM 36(2006)1, str. 44-50

The magnetic field intensity in the parent metal and in the vicinity of the weld groove can be reduced by using an auxiliary welding equipment which supplies direct current which can be set to values lower than that of the welding current, i.e. even down to 10 A. The electric cables should be wrapped around the workpiece in the direction parallel to the weld groove as shown in Figure 7. The number of turns depends on the magnetic field intensity existing in the weld groove. It is recommended to wrap up ten turns of cable around the groove. The direction of electric current in the cable is also very important.

If the current does not flow in the correct direction, the magnetic field in the workpiece does not reduce, but increases. The direction of the current and the effect of demagnetisation can easily be established by a welding wire (if it is not austenitic) or more accurately by a measuring instrument.

With the correct selection of demagnetisation parameters, demagnetisation should be complete in 5 seconds.

Figure 8 shows a practical application of the demagnetisation method described. At the weld, that part of the root run is marked where the magnetic field was eliminated. Those parts where the magnetic field was not eliminated from the weld preparation are visible as well.

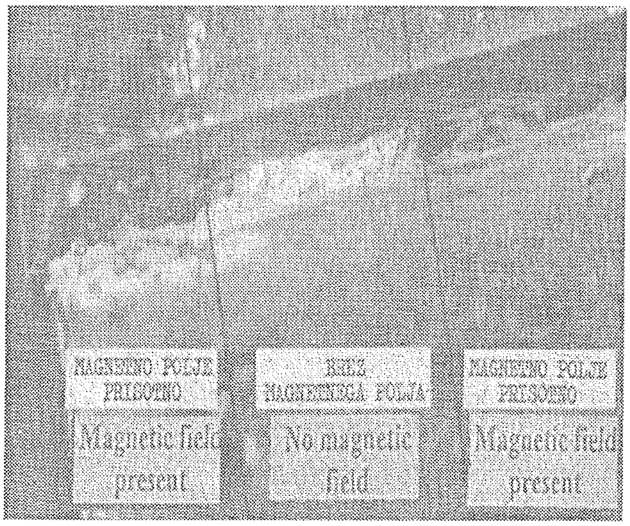

Figure 8: *Root run welded in the presence of magnetic field (left, right) and in its absence (centre).*

8 Conclusions

In the article, causes for generation of magnetic arc blow in arc welding are stated. There are usually two causes for arc deflection, i.e. magnetic arc blow, namely the electromagnetic field produced by the welding current and the magnetic field existing in one or more workpieces.

Magnetic arc blow causes weld defects, such as undercuts and weld surface irregularities. Magnetic arc blow should, therefore, be eliminated or its effect prevented. For this purpose, the article states several methods.

The generation of magnetic arc blow due to welding current can be prevented by application of several welding cables disposed, in an optimum manner, across the workpiece or with various metal prolongations which produce an electromagnetic field around the welding arc homogeneous as possible.

If an electromagnetic field is existing in the workpiece, prevention of magnetic arc blow generation is much more difficult because arc blow may arise all of a sudden, and demagnetisation of the workpiece is not easy. The article describes how the magnetic field in the workpiece or in the weld groove can be eliminated and secure favourable conditions for quality welding.

9 References

/1/ P.J. Blakeley: Magnetic arc blow - causes and remedies. Welding and Metal Fabrication, vol. 59, 7: 401-404, 1991.

/2/ F. Erdmann-Jesnitzer, W. Schröder & J. Schubert: Beobachtung zur Wrikung von Magnetfeldern beim Lichtbogenschweiâen. Werkstatt und Betrieb, vol. 94, 8: 506-508, 1961.

/3/ F. Erdmann-Jesnitzer, K. Leloiditis & D. Rehfeldt: Anwendung der Lichtbogentechnik bei Draht - und Rohrfertigung. Metall, vol. 25, 8: 892-895, 1971.

/4/ H. B. Basler & F. Erdmann-Jesnitzer: Možnosti zunanjega učinkovanja na električni varilni oblok. Varilna tehnika, vol. 23, 3-4: 59-66, 1974.

/5/ G. K.Hicken & C. E. Jackson: The Effects of Applied Magnetic Fields on Welding Arcs. Welding Research Supplement, vol. 45, 11: 515-524, 1966.

/6/ D. Rehfeldt: Ein Beitrag zur Steuerung des Lichtbogens und des Materialübergangs bei Elektroschweiâverfahren. Fortschrittberichte der VDI Zeitschriften. Reihe 2, Nr. 34, VDI - Verlag GmbH Düsseldorf 1977.

/7/ G. B.Serdjok: Vrašenie svaročnoj dugi na koncentričeski elektrodah pri magnitnom upravlenii. Svaročnoe proizvodstvo, vol. 36, 10: 1-3, 1965.

/8/ I. M. Kovalev: Otklonenie svaročnoj dugi v poperečnom magnitnom pole. Svaročnoe proizvodstvo, vol. 36, 10: 4-6, 1965.

/9/ A. M. Boldyrev, V. A. Birzhev & A. V. Chernykh: Increasing the melting efficiency of electrode wire in welding in a longitudinal magnetic field. Welding International, vol. 4, 7: 746-748, 1990. Selected from Svaročnoe proizvodstvo, vol. 36, 4: 18-19, 1989.

/10/ I. R. Packevič, A. V. Zernov & V. S. Serafimov: Vlijanie prodolnogo magnitnogo polja na plavlenie i perenos elektrodnogo metalla. Svaročnoe proizvodstvo, vol. 44, 7: 8-9, 1973.

/11/ J. Tušek: Raziskava procesov pri varjenju in navarjanju z dvojno in trojno elektrodo pod praškom. Disertacija, D 133, Univerza v Ljubljani, Fakulteta za strojništvo. Ljubljana 1991.

/12/ V. Kralj & J. Tušek: Current distribution in wires in welding with double-wire electrode. IIW/IIS Doc. 212-843-93. Glasgow 1993.

/13/ J. Tušek: Melting characteristics of wire by submerged arc welding with double and triple electrode. IIW/IIS, Doc. 212-772-90. Montreal 1990.

/14/ J. Tušek: Submerged arc welding with double and triple-wire electrode. The International Journal of the Joining of Materials, vol. 6, sept.: 105-110, 1994.

/15/ F. Kawabata et al: Aplication of Four Electrode Submerged Arc Welding Process to Large Diameter Pipe Manufacture. IIW/IIS - Public Session "Welding and allied processes, energy and economy". Ljubljana 1982.

/16/ A. Neumann, K. J. Matthes & S. Smarzynski: Einfluss des vertikalen Magnetfelds beim SG (CO_2) - Schweissen. Schweissechnik, Berlin, vol. 29, 8: 356-359, 1979.

Associated Prof. Dr. Janez Tušek univ. dipl. ing.
Igor Škrbec - student
Faculty of Mechanical Engineering
University in Ljubljana, Aškerčeva 6, 1000 Ljubljana
Email: janez.tusek@fs.uni-lj.si; janez.tusek@tkc.si

Prispelo (Arrived): 24. 09. 2005; Sprejeto (Accepted): 30. 01. 2006

THE EXPANDED UNCERTAINTY - EITHER THE COVERAGE FACTOR 1.96 OR THE 95% CONFIDENCE INTERVAL

[1]France Pavlovčič, [2]Janez Nastran

[1]Ministry for environment and spatial planning, Environmental Agency of the Republic of Slovenia

[2]University of Ljubljana, Faculty of electrical engineering

Key words: coverage factor, shape coefficient, probability distribution, confidence interval, uncertainty.

Abstract: Measurements are nowadays permanent attendants of our life. Scientific research, health, medical care and treatment, industrial development, safety and even global economy depend on accurate measurements and tests, and many of these fields are under the legal metrology because of their severity. But, how trustworthy are the results of measurements, on which very important and even vital things of our life depends. The producers of measuring equipment, devices and sensors are going along narrowing the uncertainty intervals by technical means, and emphasize their reliability also by statistical interpretation of measuring results. When expressing the uncertainty of their products, they use multiples of standard deviations to increase customers' trustfulness in their products. Are they really achieving such a good statistical confidence as it is expected by the higher multiples of standard deviation? The technique of estimating the expanded uncertainty is based on the coverage factors, by which the standard uncertainty is multiplied. These coverage factors depend on degree of freedom, which is the function of the number of implied repetitions of measurements, and therefore the reliability of the results is increased. The standard coverage factor is 1.96, and under certain circumstances, the obtained expanded uncertainty has the 95% statistical probability. The statistical probability of the expanded uncertainty is calculated due to the coverage factor, presuming the probability distribution is normal or Gaussian. The number of influential quantities which contribute their parts to the combined uncertainty increases, and they are dealt very ex-actly by sophisticated mathematical models. This attitude of dealing with the uncertainties is defined and described by some standards and guides. The present paper describes the reverse method of estimating the expanded uncertainty with the 95% probability. The algorithm of this model is based on the 95% confidence interval of any distribution of statistically acquired data (the A-type uncertainty) or any given distribution (the B-type uncertainty), and the coverage factor is determined due to this confidence interval. The coverage factor is determined by the 95% confidence interval of the actual probability distribution. The expanded uncertainty, which is the product of this coverage factor and the standard uncertainty in this case too, is estimated to have 95% statistical probability. In general, it is not possible to achieve the 95% confidence interval by using the standard coverage factor 1.96, even if it is increased due to degree of freedom, which compensates only the lack of the repeated measurements. The addition theorem is established, and it has the mathematical properties, which are in accordance with the standards and guides. The model is introduced in procedures carried out in the calibration laboratory.

Razširjena negotovost – ali krovni faktor 1.96 ali interval s 95% zaupanjem

Kjučne besede: krovni faktor, koeficient oblike, porazdelitev verjetnosti, interval zaupanja, negotovost.

Izvleček: Meritve so stalne spremljevalke našega življenja. Znanstvene raziskave, zdravje, medicinska nega in zdravljenje, industrijski razvoj, varnost in celo svetovno gospodarstvo so odvisni od zanesljivih meritev in testov. Veliko teh področij je vključenih v zakonsko meroslovje zaradi svoje posebne pomembnosti. Kolikšno zaupanje pa imajo rezultati meritev, od katerih so odvisna tako pomembna in celo življenjsko važna področja našega življenja? Izdelovalci merilne opreme, naprav in senzorjev napredujejo v smislu zoževanja intervalov negotovosti s tehničnimi sredstvi ter tudi poudarjajo svojo zanesljivost s statistično razlago merilnih rezultatov. Kadar izražajo negotovost svojih merilnih sistemov, uporabljajo večkratnike standardne negotovosti, da povečajo zaupanje odjemalcev svojih izdelkov. Ali res dosegajo tako dobro statistično zaupanje kot je pričakovati z večjimi večkratniki standardne negotovosti? Tehnika ocenjevanja razširjene negotovosti temelji na krovnih faktorjih, s katerimi je pomnožena standardna negotovost. Krovni faktorji so odvisni od stopnje prostosti, ki je funkcija števila izvedenih ponovitev meritev, s tem pa je povečana zanesljivost rezultatov. Standardni krovni faktor je 1.96 in pod posebnimi pogoji ima dobljena razširjena negotovost 95% statistično zaupanje. Statistična verjetnost razširjene negotovosti je izračunana glede na krovni faktor, če predpostavljamo normalno ali Gaussovo porazdelitev verjetnosti. Število vplivnih veličin, ki prispevajo svoje deleže h kombinirani negotovosti, se povečuje in le-te so zelo točno obravnavane z visoko razvitimi matematičnimi modeli. Ta pristop obravnavanja negotovosti je definiran in opisan v nekaterih standardih in vodilih. Pričujoči članek opisuje obratno metodo ocenjevanja razširjene negotovosti s 95% zaupanjem. Algoritem tega modela temelji na intervalu s 95% zaupanjem katerekoli porazdelitve statistično pridobljenih podatkov (A-tip negotovosti) ali katerekoli dane porazdelitve (B-tip negotovosti), pri čemer je krovni faktor določen glede na ta interval zaupanja. Krovni faktor je določen z intervalom 95% zaupanja dejanske porazdelitve verjetnosti. Razširjena negotovost, ki je tudi v tem primeru zmnožek tega krovnega faktorja in standardne negotovosti, ima po oceni 95% statistično zaupanje. V splošnem ni mogoče doseči interval s 95% zaupanjem s standardim krovnim faktorjem 1.96, tudi če je povečan v odvisnosti od stopnje prostosti, ki vračuna v razširjeno negotovost le pomanjkanje števila ponovljenih meritev. Operacija seštevanja je določena tako, da ima matematične zakonitosti v skladu s standardi in vodili. Model je uporabljen v postopkih, izvajanih v kalibracijskem laboratoriju.

1. Introduction

The expanded uncertainty is calculated according to the standard EA-4/02 /1/ as the multiplication of the standard coverage factor 1.96 with the standard uncertainty when the degree of freedom is approaching to infinite value. This standard also points out the necessity to determine the confidence interval of the 95% coverage probability and to calculate expanded uncertainty due to this interval. That means, that the probability of the measurement readings being inside the confidence interval is 95% and the probability of being outside the confidence interval is 5%. The coverage factor 1.96 and the 95% confidence interval coincide only with the normal (Gaussian) probability distribution. It is the same with very often used combination of the coverage factor 2 and the 95.45% confidence interval. In the cases of multiple standard deviations, when the probability of the measuring results being inside the confidence interval is very close to unit, it is more convenient to talk about the probability of the measuring results being outside the confidence interval. Some producers of measuring devices state the expanded uncertainty on the basis of 3, 4, 5 and 6 times of the standard uncertainty and associated this expanded uncertainty with the probability of the measurement readings being outside the confidence interval as 2.7‰, 63 ppm, 0.57 ppm and 2 ppb respectively. But this is valid only with the normal distribution. To see the problem, we must be aware of dealing with several kinds of distributions not only with the normal distribution. Namely, the distributions of the B-type uncertainties are mostly not normal, for instance the temperature drift, the time drift and the resolution have the rectangular distribution. Sometimes also the A-type uncertainties do not match with the normal distribution as they are result of regulated quantities, or are affected by the resolution of measuring device. In the latter case the probability distribution consists of two Dirac functions, one at the lower measurement reading and the other at the upper measurement reading regarding the resolution. If the distribution is unknown the coverage factor is calculated from Chebyshev's inequality /2/ and is 4.472 for the 95% confidence interval or the 5% probability of being outside that interval. From this point of view, regardless of the shape of the distribution, the 4 times of the standard uncertainty does not mean the 63 ppm probability of measurement readings being outside the confidence interval, but a lot more, and consequently it means a much lower probability of being inside the confidence interval. The uncertainty, the extended or the standard one, does not stand by itself, but contributes its portion to a combined uncertainty. The probability distribution, which corresponds to the combined uncertainty, is the convolution of the contributing probability distributions. The convolution of two rectangular distributions gives the trapezoidal distribution, or in some cases the triangular distribution, and the next rectangular distribution convoluted to the trapezoidal or to the triangular distribution results in the distribution with the square dependent tails, and the further rectangular distributions lead to the distribution with the polynomial dependent tails. By further convolutions, the resulted distribution tends toward the normal distribution. Nevertheless there are some not "well-behaved probability distributions" as quoted by the standard /1/ to cause the coverage probability of less than 95% by using standard coverage factor. Hence we are to deal with so defined polynomial D(delta)-shaped distributions because these distributions very closely describe the cases with the large probability around the mean values of measured quantity with some excessive, but still reliable values. The tails of such distributions are fatter than the tails of the normal distribution and the coverage factor must be greater than 1.96 to achieve the 95% confidence interval. The main distributions dealt in this paper are shown in Tab. 1.

Taking into consideration Tab. 1 we established that all these probability distributions are involved in nearly every measurement. Namely, there are several sources of uncertainties with the rectangular probability distributions, and when combined the resulted probability is either trapezoidal, triangular. The rectangular, trapezoidal and triangular probability are discussed in the standard EA-4/02 /1/ and further on U-shaped distribution is dealt in NIS3003 /3/ used with sinus wave measuring signal, but the other distributions and further convolutions of these distributions are rarely described in literature. There is an algorithm of combining the normal distributions and the rectangular distributions only, described in the literature /4/. The symmetrical impulse measuring signal is very common in measuring systems, for instance the measurement of the contact resistance, the temperature measurement of the resistance temperature sensors with the DC current and several measurements where the influence of hysteresis is being avoided. This measuring signal gives the symmetrical Dirac shaped distribution. The reason why we chose the polynomial Δ-shaped distribution is to show that there exist the probability distribution with the coverage factor greater than 1.96 to achieve the 95% confidence interval, and that such distributions are very commonly involved in uncertainty calculations although we do, or do not, admit it.

DISTRIBUTION SHAPE	DISTRIBUTION NAME	SOURCE
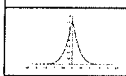	polynomial Δ-shaped distribution	concentrated values around average with some excessive values
	normal or Gaussian distribution	random errors
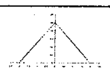	triangular distribution	convolution of two equal rectangular distributions
	trapezoidal distribution	convolution of two rectangular distributions
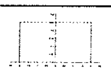	rectangular distribution	time and temepreture drift, resolution (B-type)
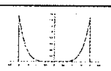	U-shaped distribution	sine wave measuring signal
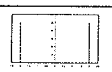	symmetrical Dirac shaped distribution	symmetrical impuls maesuring signal, resolution affect (A-type)

Tab. 1: Various distributions and their sources.

2. The contributing distributions

The measured signal is continuous function depended on one independent variable, such as time or a counter. Its range has the supremum and the infimum, which are the bounds of the domain of definition of the corresponding distribution. The upper and the lower bounds are finite values. Amplitude is defined as the maximum of the absolute values of the difference between the non-weighted mean value of the measured signal throughout its whole definition interval and the lower and the upper bounds respectively. This kind of distributions is represented by the following equation:

$$\int_{-\infty}^{+\infty} p(X) \cdot dX = \int_{-A}^{+A} p(X) \cdot dX = 1 \qquad (1),$$

where the amplitude A is the minimal value that corresponds this equation.

We are looking for the coverage factor $\hat{K}$ of any distribution, applied to the standard deviation, which gives the 95% confidence interval as follows:

$$\int_{-\hat{K}\cdot\sigma}^{+\hat{K}\cdot\sigma} p(X) \cdot dX \geq 0.95 \qquad (2),$$

at the infinite degree of freedom.

There are upper limits of this coverage factor as follows:

- any, even unknown distribution corresponds to Chebyshev's inequality /2/, therefore:

$$\hat{K} \leq \left.\sqrt{\frac{1}{1-P}}\right|_{P=0.95} = \sqrt{20} \qquad (3);$$

- any, even unknown distribution with the finite upper and lower bounds corresponds to Eq. (1), therefore according to Eqs (1) and (2), the upper limit of the coverage factor is:

$$\hat{K} \leq \frac{A}{\sigma} \qquad (4);$$

where the equality is present only, when the cover factor $\hat{K}_1$ of the 100% confidence level is considered.

The coverage factor of each known distribution is calculated by using the Eq. (2). The results of the calculation for the dealt distributions are presented in Fig. 1 as the function (2), which is calculated for the 95% probability level. The upper limits are also shown in this figure: the maximum of the function (2) for the 95% probability level of an unknown distribution due to Chebyshev's inequality and the function (1) for the 100% probability level. The functions (1) and (2) in Fig. 1 make the boundary of the area of the probability levels from 95% up to 100%. There is also the position of Gaussian distribution marked in Fig. 1.

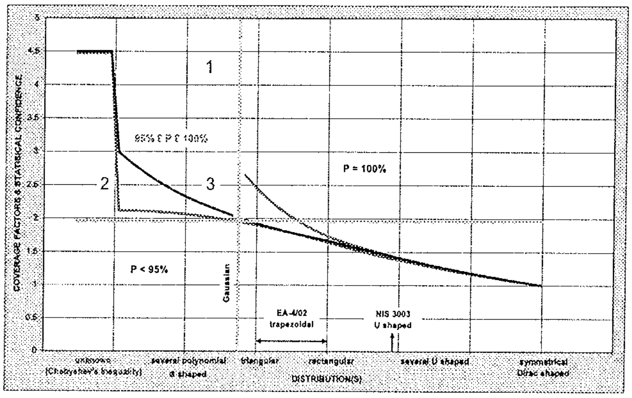

Fig. 1: The cover factors of several distributions and statistical confidence of the acquired data interval.

Legend:

1 ... the cover factors of the 100% confidence level,

2 ... the cover factors of the 95% confidence level,

3 ... the statistically determined cover factors of the 95% confidence level using the presented model.

There is no problem to determine the coverage factor of the probability distribution defined by the probability density $p(X)$ described by the analytic function, by the tabled values or by the geometrical definition. But, detemining the coverage factor out of statistically acquired data, we have to astablished a model, which solution gives results within the mentioned area with the probability levels from 95% up to 100%. The solution given by the presented model is one of many possible solutions, and it is shown in Fig. 1 as the function (3).

3. The kurtosis and Modelling the coverage factor

The kurtosis is the parameter of the descriptive statistics, which gives information about the probability distributions of acquired data that are created by our measurements. It is the classical measure of nongaussianity, and it expresses the similarity to the normal or Gaussian distribution. The distribution shape is quantified by it, but the mapping of the set of the shapes to the set of their numerical values is surjection. There is no rule to get the distribution shape out of the kurtosis. From the kurtosis, it can be concluded only that:

- a certain distribution is peaked around its mean and have the fat tails (could be the polynomial Δ-shaped distributions in this paper) - leptokurtic distributions;
- it is flat (could be the rectangular distribution) or even concave (could be the U-shaped distribution) with the thin tails or without them - platykurtic distributions;
- it could be very similar to the normal distribution - mesokurtic distributions.

The kurtosis is the fourth standardized moment $\boldsymbol{k_4}$ about the mean, and is defined as the quotient of the fourth moment m_4 about the mean and the fourth power of the standard deviation σ and it is:

$$k_4 = \frac{m_4}{\sigma^4} \quad (5).$$

When the probability distribution is the analytic function with the finite bounds of its domain, the fourth moment about the mean or, as it is also named, the fourth central moment is:

$$m_4 = \int_{-\infty}^{+\infty} (X - \bar{X})^4 \cdot p(X) \cdot dX = \int_{-A}^{+A} (X - \bar{X})^4 \cdot p(X) \cdot dX \quad (6),$$

and when it is acquired through non-weighted data, it is:

$$m_4 = \frac{1}{n} \cdot \sum_{i=1}^{n} (X_i - \bar{X})^4 \quad (7).$$

The standard deviation is respectively to Eqs (6) and (7) as follows:

$$\sigma = \sqrt{\int_{-\infty}^{+\infty} (X - \bar{X})^2 \cdot p(X) \cdot dX} = \sqrt{\int_{-A}^{+A} (X - \bar{X})^2 \cdot p(X) \cdot dX} \quad (8),$$

$$\sigma = \sqrt{\frac{1}{n} \cdot \sum_{i=1}^{n} (X_i - \bar{X})^2} \quad (9).$$

The kurtosis of the normal distribution is k_{4g} = 3, the kurtoses of leptokurtic distributions are greater than 3 and of platykurtic are less than 3. The kurtoses of mesokurtic distributions are about 3.

Some earlier methods of determining the coverage factor of the 95% confidence interval by processing the measured signal were developed for the purpose of the calibration laboratory /5/, /6/. The first one a little bit underestimates the coverage factors of leptokurtic and overestimates the ones of platykurtic distributions, but the second method overestimates the coverage factor of all distributions.

The basis of the present modelling of the coverage factor of the 95% confidence interval is the kurtosis, because it is the statistical parameter that quantifies the shape of the analysed probability distribution. The coverage factor is basically the square root of the ratio between the kurtosis k_4 of the analyzed distribution and the kurtosis k_{4g} of the normal distribution, corrected by the empirical coefficient κ and multiplied with the coverage factor of the normal distribution at the infinite degree of freedom:

$$\hat{K}_{basic} = K(\nu)\big|_{\nu=\infty} \cdot \kappa \cdot \sqrt{\frac{k_4}{k_{4g}}} = 1.96 \cdot \kappa \cdot \sqrt{\frac{k_4}{3}} \quad (10),$$

where the empirical coefficient is:

$$\begin{aligned} \kappa = 1 \quad &\Leftarrow \quad \frac{k_4}{3} = \frac{m_4}{3 \cdot \sigma^4} = 1 \\ \kappa = 1.1 \quad &\Leftarrow \quad \frac{k_4}{3} = \frac{m_4}{3 \cdot \sigma^4} \neq 1 \end{aligned} \quad (11).$$

The empirical coefficient is necessary to correct the basic coverage factors of mesokurtic distributions with the finite bounds of their domain. This is not the case with the normal distribution, because it has the infinite domain. The range of any dealt measured signal has finite bounds, and so does the domain of the corresponding probability distribution, even it is nearly normal. Hence, the "normal" distribution with the finite bounds at ($2.8\times\sigma$) has the kurtosis of 2.5 and the rounded value of the empirical coefficient is 1.1 to obtain the standard coverage factor. Therefore the empirical coefficient is unit 1 only with the normal distribution over the infinite domain. This coefficient has two values due to comparison of two kinds of distributions: the set of distributions with the finite bounds of their domain and the one with the infinite bounds of its domain - the normal distribution. Using this coefficient, we get the standard coverage factor of 1.96 for normal distribution over the finite and over the infinite its domain. In some later software, we introduced in the calibration laboratory, the ratio of the actual kurtosis against the normal kurtosis of 2.5 $(=\sqrt{2\cdot\pi})$ instead against 3 is used, and empirical coefficient is unit 1 in this case. However the latter case affects only the B-type uncertainty associated with the normal distribution.

Considering the upper limits of the coverage factor due to Eqs (3) and (4) the coverage factor of the probability distribution with the finite bounds of its domain actually is:

$$\hat{K} = K(\nu) \cdot \min\left(\kappa \cdot \sqrt{\frac{k_4}{3}}\ ,\ \frac{A}{1.96 \cdot \sigma}\ ,\ \frac{\sqrt{20}}{1.96}\right) = K(\nu) \cdot C \quad (12),$$

and the shape coefficient of the probability distribution is:

$$C = \min\left(\kappa \cdot \sqrt{\frac{m_4}{3 \cdot \sigma^4}}\ ,\ \frac{A}{1.96 \cdot \sigma}\ ,\ \frac{\sqrt{20}}{1.96}\right) \quad (13).$$

This coverage factor at the infinite degree of freedom is graphically shown as the function (3) in Fig. 1. Its values are in the lower range of the area indicating the confidence interval of 95% up to 100%, which is very good. The advantage of this coverage factor $\hat{K}$ is, that it consists of two multiplicands: the first one - $K(\nu)$ is dependant on degree of freedom, as it is generally known as the coverage factor, and the other - C depends on the shape of the probability distribution, mainly on the kurtosis and we named it as the shape coefficient.

4. The convolution and the addition algorithm

When combining several probability distributions in uncertainty calculations the resulted probability distribution is the convolution of all participant distributions. The convolution of two probability distributions is:

$$p_{1\wedge 2}(X)=p_1(X)\otimes p_2(X)=\int_{-\infty}^{+\infty} p_1(\tau - X)\cdot p_2(\tau)\cdot d\tau \qquad (14).$$

The each distribution contributes the amplitude, the standard deviation and the fourth moment about the mean to the resulted amplitude A_Σ, the resulted standard deviation s_Σ and the resulted fourth moment $m_{4\Sigma}$, as follows for the N convoluted distributions:

$$p_\Sigma(X)=p_1(X)\otimes p_2(X)\otimes \ldots \otimes p_i(X)\otimes \ldots \otimes p_N(X) \qquad (15),$$

$$A_\Sigma = \sum_{i=1}^{N} A_i \qquad (16),$$

$$\sigma_\Sigma^2 = \sum_{i=1}^{N} \sigma_i^2 \qquad (17),$$

$$m_{4\Sigma} = \sum_{i=1}^{N} m_{4i} + 6\cdot \sum_{i=1}^{N-1}\left(\sigma_i^2 \cdot \sum_{j=i+1}^{N} \sigma_j^2\right) \qquad (18).$$

Using Eqs (5) and (13) to (18), the resulted shape coefficient is obtained:

$$C_\Sigma = \min\left(\frac{\sqrt{\sum_{i=1}^{N} C_i^2 \cdot \sigma_i^4 + 2\cdot \sum_{i=1}^{N-1}\left(\kappa_i \cdot \sigma_i^2 \cdot \sum_{j=i+1}^{N} \kappa_j \cdot \sigma_j^2\right)}}{\sum_{i=1}^{N} \sigma_i^2}, \frac{\sum_{i=1}^{N} A_i}{1.96\cdot \sqrt{\sum_{i=1}^{N} \sigma_i^2}}, \frac{\sqrt{20}}{1.96}\right) \qquad (19),$$

where the empirical coefficient κ_i is:

$$\begin{aligned} \kappa_i &= 1 \quad \Leftarrow \quad C_i = 1 \\ \kappa_i &= 1.1 \quad \Leftarrow \quad C_i \neq 1 \end{aligned} \qquad (20).$$

The addition of the shape coefficients is commutative and associative and the resulted shape coefficient is a member of the same set of values as the participant shape coefficients in the evaluating process, which all are the necessary mathematical conditions for the applied methods of determining the combined uncertainties as it is prescribed by the standard /7/ as universality, internal consistency and transferability.

5. conclusions

The presented method of evaluating the expanded uncertainty of the measurand on the basis of the 95% confidence interval has the following features:

- it is universal /7/, because this algorithm is applicable to all kinds of measurements, to the A and B-type of the uncertainty evaluation and to all type of input data distribution;
- it is internally consistent /7/, which mathematically means being commutative and associative, so that combined uncertainty is independent of grouping and decomposing the contributing components;
- it is transferable /7/, which mathematically means that the resulted shape coefficient and the participant shape coefficients are the members of the same set of values or are fitting the same function, so the one result can be directly used as a component in evaluating the uncertainty of another measuring process;
- the expanded uncertainty is obtained by multiplying the standard deviation or the combined uncertainty, which is appropriate, by the coverage factor /1/ and the shape coefficient, so that the expanded uncertainty is estimated to have the 95% confidence level:

$$\begin{aligned} U\big|_{P=95\%} &= K(\nu)\cdot C\cdot \sigma \\ U_c\big|_{P=95\%} &= K(\nu_{eff})\cdot C_\Sigma \cdot u_c \end{aligned} \qquad (21),$$

therefore the intervals $\pm U$ or $\pm U_c$ about the measuring result are the 95% confidence interval;

- the convolution of many normal distributions gives normal distribution and so does the resulted shape coefficient; further on, the convolution of great number of whatever distributions leads to mesokurtic distribution and even to normal distribution and so also does the resulted shape coefficient, hence the central limit theorem is met by this method /1/;
- the expanded uncertainty depends on its effective degrees of freedom - Eq. (21) so that the proper reliability is achieved /1/;
- the expanded uncertainty estimated by this method - Eq. (21) takes into account the effective degree of freedom of the output estimates and the non-normality or non-gaussianity of the probability distributions and so far meets regulations /1/ about the 95% confidence interval.

References

/1/ *EA-4/02: Expression of the Uncertainty of Measurement in Calibration*, European cooperation for Accreditation, Publication Reference, December 1999.

/2/ Korn, G.A., Korn, T.M.: *Mathematical Handbook for scientists and engineers*, McGraw-Hill Inc., 2nd edition, 1968.

/3/ *NIS3003: The expression of Uncertainty and Confidence in Measurement for Calibrations*, NAMAS Executive, National Physical Laboratory, Teddington, Middlesex, TW110LW, England, Edition 8, May 1995.

/4/ Korczynski, M.J., Hetman A.: *Direct method of coverage interval calculation: advantages and disadvantages*, International Workshop: From Data Acquisition to Data Processing and Retrieval, Republic of Slovenia, Ministry of Education, Science and Sport, Metrology Institute and European Thematic Network, Advanced Mathematical and Computational Tools in Metrology, Ljubljana, Sep. 13-15, 2004.

/5/ Pavlovčič, F., Groselj, D.: *Ugotavljanje in razširjanje merilne negotovosti medija s procesiranjem Gaussovega naključnega signala* (Engl. *An establishment and a propagation of a measuring uncertainty of a medium by processing Gaussian random signal*); V: ZAJC, Baldomir (ed.). *Zbornik šeste Elektrotehniške in računalniške konference ERK '97, 25. - 27. september 1997, Portorož, Slovenija*. Ljubljana: IEEE Region 8, Slovenska sekcija IEEE, 1997, pp. 415-418.

/6/ Pavlovčič, F.: *A dynamic modelling of measuring uncertainty of industrial and environmental media us-ing a signal processing technique*; In: ILIĆ, Damir (ed.), BORŠIĆ, Mladen (ed.), BUTORAC, Josip (ed.). XVII IMEKO World Congress, June 22-27, 2003, Dubrovnik, Croatia. *Metrology in the 3rd millennium: proceedings*. Zagreb: HMD - Croatian Metrology Society, 2003, p. 1663.

/7/ *Guide to the expression of uncertainty in measurement*, International Organisation for Standardisa-tion, 1st edition, 1995.

Asst Prof. Dr France Pavlovčič, univ.dipl.ing.
Ministry for environment and spatial planning,
Environmental Agency of the Republic of Slovenia,
Vojkova 1b, SI - 1000 Ljubljana, Slovenia
tel.: +386 (0)1 4784 098,
fax: +386 (0)1 4784 054,
E-mail: france.pavlovcic@gov.si

Prof. Dr Janez Nastran, univ.dipl.ing.
University of Ljubljana, Faculty of electrical engineering,
Tržaška 25, SI - 1000 Ljubljana, Slovenia
tel.: +386 (0)1 4768 282,
fax: +386 (0)1 4264 647,
E-mail: janez.nastran@fe.uni-lj.si

Prispelo (Arrived): 24. 11. 2005; Sprejeto (Accepted): 30. 01. 2006

Poročila s konferenc
Conference reports

Posvet o meritvah 10. in 11. novembra 2005
v Kolarjevi predavalnici na IJS

Namen posveta:

Zavod TC SEMTO (Tehnološki center za sklope, elemente, materiale, tehnologije in opremo za elektrotehniko), Center odličnosti Materiali za elektroniko naslednje generacije ter drugih prihajajočih tehnologij in Center odličnosti za napredno procesiranje, tehnologije in materiale za keramične elektro in elektromehanske naprave SICER (EU 5OP) so želeli seznaniti partnerje v TC, kot tudi širše okolje z novostmi na tem pomembnem področju, novostmi in usmeritvami v opremljenosti in možnostmi storitev, ki jih lahko posamezen laboratorij ponudi tudi navzven.

Izkušnje drugih nas lahko spodbujajo pri našem iskanju rešitev.

Program posveta:

Uvod:

- pozdrav in otvoritev
- Rudi Zorko, METREL: uvod (pomen in pristop k meritvam v razvoju in meritvam v proizvodnji) rudi.zorko@metrel.si
- Ivan Skubic: Meroslovni sistem Republike Slovenije mirs@gov.si
- Matjaž Lindič, SIQ: vzdrževanje merilnih naprav, kalibracije, sledljivost, .. (standardi, predpisi, dobra praksa, akreditacije). matjaz.lindic@siq.si

Karakterizacija materialov:

- Slavko Bernik, IJS: Vrstična elektronska mikroskopija (SEM) in mikroanaliza slavko.bernik@ijs.si
- Miran Čeh, IJS: Transmisijska elektronska mikroskopija (TEM) (HR, Z kontrast) miran.ceh@ijs.si
- Anton Zalar, Janez Kovač, IJS: Spektroskopija Augerjevih elektronov (AES) anton.zalar@ijs.si
- Janez Kovač, Anton Zalar, IJS: Rentgenska fotoelektronska spektroskopija (XPS/ESCA) in rentgenska mikroskopija janez.kovac@ijs.si
- Matjaž Godec, IMT: Integrirane tehnike za karakterizacijo površin, mej zrn in faz, nano in mikrostrukture ter mikroteksture kovinskih materialov in kompozitov matjaz.godec@imt.si
- Janez Holc, IJS: Optični profilometer janez.holc@ijs.si
- Barbara Malič, IJS: Uporaba termične analize za karakterizacijo materialov v elektroniki barbara.malic@ijs.si
- Janez Jamnik, Marjan Bele; KI: Impedančna spektroskopija janez.jamnik@ki.si
- Miha Škarabot, IJS: Mikroskopija na atomsko silo (AFM) miha.skarabot@ijs.si

Merjenje električnih in magnetnih veličin:

- Uroš Aljančič FE-LMSE: enosmerna karakterizacija polprevodniških elementov; CV meritve s podporo LAB View-a; Meritve življenskih dob nosilcev v polprevodniških elementih; meritve plastnih upornosti; meritve kritičnih dimenzij; meritve debeline tankih plasti in lomnega količnika; meritve koncentracije prašnih delcev; merive hrapavosti in debeline tankih plasti uros.aljancic@fe.uni-lj.si
- Janez Trontelj (ml.), FE-LMFE: Meritve mikrosistemov na 200 mm veliki Si rezini na novi opremi (CO) janez.trontelj1@guest.arnes.si
- Matjaž Vidmar, Leon Pavlovič, FE-LSO: Meritve parametrov anten (30 MHz do 18 GHz); meritve RF spektra do 50 GHz; meritve v časovnem prostoru z vzorčevalnim osciloskopom; meritve RF moči in frekvence; meritve S11, S12, S21, S22 do 18 GHz s pomočjo vektorskega in skalarnega analizatorja vezij leon.pavlovic@fe.uni-lj.si
- Dušan Fefer, FE-LMM (akreditiran za merjenje gostote magnetnega pretoka - nacionalni referenčni etalon): Predstavitev merilne opreme za merjenje in generiranje referenčnih enosmernih in izmeničnih magnetnih polj; merilna sledljivost do nacionalnih in mednarodnih etalonov. Dusan.fefer@fe.uni-lj.si
- Vladimir Bregar, Iskra Feriti: Karakterizacija dielektričnih in feromagnetnih materialov v območju 40 MHz do 18 GHz. Vladimir.bregar@ijs.si
- Darko Belavič, Hyb: Meritve gauge faktorja pri debeloplastnih uporih darko.belavic@ijs.si
- Zvonko Trontelj, FMF: Kaj nudi Center za magnetne meritve - Cmag zvonko.trontelj@fmf.uni-lj.si

Merjenje električnih in magnetnih veličin, avtomatizacija merjenja:

- Aleš Štagoj, Iskra Zaščite: Predstavitev VN laboratorija Iskra Zaščite ales.stagoj@iskrazascite.si

- Darko Koritnik, ICEM: Močnostni električni preizkusi darko.koritnik@icem-tc.si
- Franc Koplan, Mitja Pregelj,Magneti : Merilni sistem za 100% sortiranje AlNiCo in SmCo magnetov f.koplan@magneti.si
- Leopold Knez, Iskra TELA: Elektromagnetne meritve leopold.knez@iskra-tela.si
- Janko Mole, Merilne možnosti v Metrelu janko.mole@metrel.si

Merjenje neelektričnih veličin - optičnih, mehanskih, vakuuma, ...:

- Andrej Pregelj, TC Vakuum: Meritve v vakuumskih sistemih in njihovo vzdrževanje andrej.pregelj@guest.arnes.si
- Janez Šetina IMT: akreditiran laboratorij za metrologijo tlaka - nacionalni etaloni (7 mbar do 2000 bar) janez.setina@imt.si
- Boštjan Batagelj, FE-LSO: Meritve optičnega spektra telekomunikacijskih valovnih dolžin; meritve lastnosti optičnega vlakna (slablenje, pasovna širina, disperzija, nelinearnosti); meritev pogostosti bitnih napak v telekomunikacijski zvezi bostjan.batagej@fe.uni-lj.si
- Grega Bizjak, FE-LFR-laboratorij za razsvetljavo in fotometrijo: meritve svetlobno-tehničnih veličin: svetlobni tok, svetilnost, osvetljenost, svetlost, barva svetlobe grega@leo.fe.uni-lj.si
- Marko Topič (Janez Krč), FE-LPSO: Merjenje totalne, spekularne in difuzne optične prepustnosti in odbojnosti vzorcev s spektroskopom Perkin Elmer Lambda 950 ; meritve kotne porazdelitve razpršene svetlobe na vzorcih s hrapavimi površinami z računalničko krmiljenim sistemom z vrtlivo roko; merjenje spektralne občutljivosti fotodetektorjev in sončnih celic z monokromatorjem; merjenje šumnih karakteristik fotodetektorjev z FFT spektralnim analizatorjem marko.topic@fe.uni-lj.si , marko.topic@yahoo.com
- Branko Cvetković, Iskra TELA: Merjenje dolžin in merjenje kotov z inkrementalnimi in absolutnimi merilnimi dajalniki branko.cvetkovic@iskra-tela.si
- J.Bojkovski , I.Pušnik, V.Batagelj, D.Hudoklin, J.Drnovšek, FE - LMK- Laboratorij za metrologijo in kakovost: Zagotavljanje sledljivosti na mednarodni nivo in diseminacija vrednosti na podrocju termometrije-izkušnje nacionalnega etalona za termodinamsko temperaturo T. Jovan.bojkovski@fe.uni-lj.si, janko.drnovsek@fe.uni-lj.si

Pripravili smo broširan povzetek, ki je bil udeležencem na razpolago. Prispevke smo objavili na spletni strani Zavoda TC SEMTO www.zavodtcsemto.si.

Poslanstvo Zavoda TC SEMTO je, da pospešuje:

- da se obstoječe znanje in raziskovalna ter merilna oprema čim bolje izkoristi - vnovči
- da se napori in vlaganja ne podvajajo, ampak maksimalno izkoristijo
- da zadržimo le ključne procese in kupimo preostalo tam, kjer je to kvalitetno in ceneje
- da se medsebojno informiramo o potrebah in ponudbi znanja in storitev
- da se informiramo o strateških ciljih ter skupaj usmerjamo napore in sredstva v našemu prostoru potrebna znanja in vlaganja.

S tem poslanstvom Zavod TC SEMTO deluje že od leta 2000 in prispeva k zbliževanju strokovnjakov iz RR institucij in industrije. S tem namenom organizira tudi nekaj posvetovanj letno. Zavod TC SEMTO je soustanovitelj Centra odličnosti Materiali za elektroniko naslednje generacije ter drugih prihajajočih tehnologij. Člani Zavoda TC SEMTO aktivno delujejo tudi v strokovnem društvu MIDEM. Zavod TC SEMTO aktivno sodeluje pri pripravi slovenske tehnološke platforme NaMaT (Napredni materiali in tehnologije), ki je osnova za sodelovanje z evropsko tehnološko platformo EuMaT. Več o zavodu lahko preberete na spletni strani www.zavodtcsemto.si

Zavod TC SEMTO je odprt tudi za ostale institucije in industrijo.

Igor Pompe

OBISK UNSW IN SODELOVANJE NA SPIE SIMPOZIJU O MIKRO IN NANO STRUKTURAH

Obisk Avstralije se je izkazal kot uspešna strokovna in življenjska izkušnja. Osnovni namen potovanja je bilo sodelovanje na SPIE simpoziju z naslovom »Microelectronics, MEMS, and Nanotechnology«. Posvetovanje je bilo v Brisbanu na queenslandski univerzi za tehnologijo, (Queensland Univ. of Technology, QUT) v času od 11. do 15. 12. 2005. Poleg udeležbe na simpoziju smo izkoristili to potovanje tudi za obisk univerze v Sydneyu (University of New South Wales, UNSW). UNSW je ena od vodilnih izobraževalnih in raziskovalnih univerz v Avstraliji s preko 40000 študentov, od tega več kot 9000 študentov prihaja iz 120 različnih dežel. UNSW je tudi ena od vodilnih avstralskih raziskovalnih inštitucij z več kot 70 raziskovalnimi centri in dvanajstimi, od vlade financiranimi združenimi raziskovalnimi centri, ki pokrivajo področja biomedicine, informacijskih tehnologij in materialov, ter še ostale veje znanosti kot so ekonomija, socialna politika, zgodovina itd.. V zadnjem času je UNSW največ investirala v ključne novodobne discipline (»hi-tech«), vključno s sončnimi celicam (oddelek prof. Greena je eden od vodilnih na tem področju), kvantno računalništvo (nanotehnologije), fotoniko in telekomunikacije. Priložnost za obisk se nam je ponudila zato, ker smo imeli že predhodno vzpostavljene dobre kontakte s prof. Kwokom, ki je vodja nam sorodnega raziskovalnega laboratorija za mikrosisteme (Microsystems (MEMS)) na fakulteti za Elektrotehniko in telekomunikacije pri UNSW. Ukvarjajo se s tehnologijo in načrtovanjem elementov in sistemov, ki pokrivajo interdisciplinarna področja, pri tem pa imajo poleg lastnega mikroelektronskega laboratorija tudi dostop do moderne nanotehnološke opreme. Njihovi projekti so vpeti v raziskave optičnih stikal za planarne steklene valovode, MEMS bazirane optične povezave med čipom in sistemom v ohišju, elektrod za znotraj očesne vsadke, fizikalne inercijske senzorje (optični akcelerometer, giroskop, itd.). Poleg naštetega se ukvarjajo še z mikrotehnologijami in raziskavami novih materialov za mikroobdelavo. Na samem sestanku smo izmenjali predstavitve naših in njihovih aktivnosti, ugotovili ključna področja skupnega zanimanja ter začrtali program nadaljnjega sodelovanja. Ogledali smo si tudi njihova mikro/nano-tehnološka laboratorija, ter z odgovornim osebjem tehnoloških laboratorijev izmenjali izkušnje in odprli debato o trendih nadaljnjega razvoja na tem področju.

Uspešno zaključeni obisk na UNSW smo nadaljevali v Brisbane na QUT, kjer je potekal SPIE simpozij. QUT je po velikosti približno tako velika kot UNSW in je znana po tem, da so njihovi programi zelo fleksibilni, z možnostjo izmenjave programov s tujimi univerzami ter da na njihovi univerzi letno diplomira največ študentov v Avstraliji. Poleg fakultet in šol za okolje, menedžment, kreativno industrijo, izobraževanje, zdravje, informacijsko tehnologijo, pravo in humanistiko, imajo še štiri inštitute in znanstveno raziskovalni center.

Simpozij je bil razdeljen v pet tehničnih sklopov, ki so potekali paralelno:

- Mikroelektronika: načrtovanje, tehnologija in zapiranje v ohišja
- BioMEMS in nanotehnologije
- Elementi in procesne tehnologije za mikroelektroniko, MEMS, in fotoniko
- Fotonika: načrtovanje, tehnologije in zapiranja v ohišja
- Kompleksni sistemi

Mi smo sodelovali s prispevkom »Silicon dry-etching profile control by RIE at room temperature for MEMS application« v sklopu Elementi in procesne tehnologije za mikroelektroniko, MEMS, in fotoniko. V našem sklopu je bilo predstavljeno 35 ustnih referatov in 39 referatov z posterji, približno toliko prispevkov pa je bilo tudi v ostalih sklopih. Velika večina tujih (neavstralskih) avtorjev je prihajalo z »bližnjih« univerz in inštitucij Singapurja, Tajvana, Hongkonga in Japonske. Predstavljena so bila dela, ki so se ukvarjala s posameznimi tehnološkimi segmenti ter tehnologijami, potrebnimi za izdelavo naprednih miniaturnih mikrosenzorjev, kot tudi končne realizacije elementov. Predstavljeni so bile tudi različni pristopi in metode za karakterizacijo materialov in elementov v mikro- in nano-elektroniki. Za nas so bile zanimive tudi ostale sekcije, predvsem v sekciji BioMEMS in nanotehnologije, kjer so bili predstavljeni nekateri za nas zanimivi prispevki s področja mikrofluidike, mikro/nanomanipulacije ter biomedicinskih mikroelementov, senzorjev in biosenzorjev. Simpozij je bil uspešen tudi s stališča navezave novih stikov z udeleženci konference v smislu možnosti znanstvenega sodelovanja. Tako upamo, da nam bo že to leto uspelo pridobiti tudi katerega od uglednih predavateljev tega simpozija kot vabljenega predavatelja na konferenco Midem 2006.

Uspešno strokovno pot smo zaključili še z dvema tednoma dopusta. Kajti, le redko se ti ponudi priložnost, da lahko spoznavaš deželo in ljudi, ki živijo tam spodaj (Down Under). Poleg ogleda glavnih atrakcij in čudovitih peščenih plaž mest Sydneya in Brisbana smo si ogledali še mesta Alice Springs in Cairns. Prvi leži v notranjosti dežele, kjer je puščava, drugi pa se nahaja v severovzhodnem obalnem delu, kjer je podnebje že subtropsko. V bližini teh dveh krajev smo si ogledali njihove znamenitosti kot so Ayers Rock, Olgas, Kings Canyon, Cape Tribulation in veliki koralni greben.

Potovanje v Avstralijo je odlično uspelo tako v strokovnem kot »posvetnem« smislu.

Ljubljana, 24. 01. 2006

Danilo Vrtačnik, Slavko Amon

Seminar "The thick and thin of ceramic based interconnections"

1. December 2005, Dovenport House Conference Centre, Greenwich, London

1. decembra 2005 je bil v Angliji (London, Greenwich) organiziran seminar pod naslovom "The thick and thin of ceramic based interconnections". Organizator je bila angleška sekcija IMAPS (International Microelectronics and Packaging Society). "Interconnections" bi se lahko prevedlo kot "povezave"," thick and thin" pa se nanaša na debeloplastno in tanko plastno tehnologijo povezav v hibridnih vezjih ali modulih. Mimogrede, pri naslovu seminarja je še besedna igra. Fraza "Through thick and thin" pomeni nekaj podobnega kot, da vstrajaš skozi slabo in dobro. Registriranih je bilo med 50 in 60 udeležencev.

Če, seveda precej subjektivno, ocenim predstavljene referate, sta bila eden ali dva "reklamna". Vendar so bile tudi "propagandne" predstavitve predstavljene kot "resni" referati, poleg same "reklame" so bili podani tudi rezultati preiskav, kar jih lahko kvalificira kot aplikativne prispevke. V glavnem pa so bili prispevki dober pregled današnje uporabe keramičnih materialov v elektroniki, predvsem hibridni elektroniki.

Večina prispevkov je obravnavala uporabo keramike v taki ali drugačni "vlogi" ali v povezavah v vezjih ali pa kot nosilce vezij. V poročilu bom na kratko predstavil samo nekatere, za nas zanimive, referate.

S. Muckett (Mozaik, Anglija) je v referatu z naslovom "Use of ceramic interconnect in the automotive sector" najprej predstavil znane probleme, ki jih ima elektronika v avtomobilih, predvsem v motorjih. To so predvsem visoke temperature, nizke temperature (parkirano vozilo pozimi), vibracije in agresivno okolje. Vezja morajo biti zato testirana pri temperaturah med -40°C in 150°C. LTCC (low temperature co-fired ceramics) tehnologija izdelave kompleksnih večplastnih vezij močno prodira v avtomobilsko elektroniko. Vendar ta tehnologija zaradi razmeroma steklastih LTCC materialov in s tem povezanih nizkih koeficientov termičnih prevodnosti ni dobra za močnostna vezja. Zato je, za posebne namene, predavatelj napovedal "povratek" starejših, sicer zelo zanesljivih, vendar zelo dragih večplastnih modulov, kjer so v večplastnih strukturah na osnovi Al_2O_3 zapečeni prevodniki na osnovi kovin z visokim tališčem. Po drugi strani pa je tudi LTCC precej dražji od običajnih tiskanih vezij, zato bo uporabljan tam, kjer boljša kvaliteta upraviči višjo ceno. Podatek; nemška avtomobilska industrija vgradi v avtomobile okrog 200 miljonov keramičnih vezij na leto, v boljših avtomobilih pa je že za okrog 2000 dolarjev elektronike.

G. Thompson (TT Electronics Welwin, Anglija) je v predstavitvi z rahlo provokativnim naslovom "What's all the fuss about ceramics?"predstavil keramiki alternativne substrate in aplikacije, ki so jih razvili v njihovi firmi. Ena od glavnih prednosti substratov na osnovi Al_2O_3 je njihova visoka toplotna prevodnost, ki je nekaj deset krat višja od toplotne prevodnosti tipičnih tiskanih vezij. Avtor misli, da bodo predvsem za zahtevne pogoje delovanja avtomibilske elektronike počasi prevladali substrati na osnovi jekel, pokritih z dielektriki, ali substrati na osnovi aluminija. Na Al substratih je nanešen razmeroma debel sloj, okrog 50 um, Al_2O_3, kot izolacijska plast. V diskusiji je povedal, da je plast nanešena z anodno oksidacijo, ni pa hotel komentirati, kako naredijo tako debel sloj - verjetno poslovna skrivnost. Upore v vezjih lahko izdelajo s komercialnimi debeloplastnimi uporovnimi materiali na kovinskih substratih, na anodiziranih aluminijastih sibstratih pa ne, ker jih omejuje tališče kovinskega aluminija (660°C).

Q. Reynolds (Heraeus, Anglija) je v referatu "A European perspective for hybrid and component materials" predstavil pregled zahtev oz. direktiv RoHS (Restriction of the use of certain hazardous substances in electrical and electronic equipment), WEEE (Waste electrical and electronic equipment) in ELV (End of life vehicle). Direktiva RoHS predpisuje, da sme homogen material vsebovati pod 0,1% Pb, Hg in šest valentnega kroma ter pod 0,01 % Cd. Homogen material je definiran kor material, ki se ne more mehansko ločiti v več materialov. Kot primer: spajka na pospajkanem tiskanem vezju je homogen material, pospajkano plošča vezja pa ne. Obstaja pa še vedno veliko izjem, kjer bi, predvsem svinec, težko izločili, ne da bi se karakteristike materiala zelo poslabšale ali pa cena zelo narasla. Najbolj znana izjema so avtomobillski akumulatorji. Neaktere druge izjeme so piezoelektrična keramika na osnovi svinčevih oksidov, svinčeva stekla v televizijskih zaslonih (ščitijo pred mehkimi rentgenskimi žarki), veliki računalniki - serverji (pri teh ne morejo tvegati, da nove plošče tiskanih vezij ali komponente ne bi zanesljivo delale), "velike inštalacije"(eden od primerov so dvigala, ki morajo na vsak način delati varno, elektronika na naftnih poljih itd.) in podobno. Pomembna izjema je elektronika in sploh oprema za vojsko in varnostne službe. Določene izjeme so tudi za avtomobilsko elektroniko, ker morajo za posamezne tipe avtomobilov proizvajalci zagotavljati prave rezervne dele in komponente, tudi če vsebujejo svinec, za obdobje vsaj 10 let. Opozoril pa je tudi, da so vse direktive podvržene občasnim revizijam, ki v glavnem manjšujejo dovoljene izjeme.

F. Anderson (Coors Tek, USA)je zelo podrobno (mogoče celo preveč) predstavil substrate na osnovi Al_2O_3, ki jih pod tržnim imenom "Superstrate" razvijajo in tržijo že slabih 30 let. To je bila ena od predstavitev, ki so uspešno pomešale reklamo in vtis, da gre za resen referat. Povprečna velikost Al_2O_3 zrn pri superstrate substratih je precej pod 1 um, kar tudi pomeni zelo gladko površino. Kvaliteto kontrolirajo predvsem z meritvami električnih karakteristik in njihovim sipanjem. Predavatelj je povedal, da so njihovi substrati idealni za debele filme, vendar se zaradi visoke cene v glavnem uporabljajo za tankoplastno tehnologijo. Kako dosežejo drobno zrnato keramiko po sintranju, seveda ni hotel povedati ne v referatu in ne v sledeči diskusiji. Problem je, da že majhen dodatek tekoče faze (stekla) sicer omogoči sintranje keramičnih substratov pri nižji temperaturi, vendar tekoča faza hkrati spodbudi rast večjih zrn. Razvili so tudi nove Al_2O_3 substrate z še bolj "gladko" površino p žgabju brez mehanske obdelave, ki naj bi bila boljša za tanko filmske radio-frekvenčne aplikacije. Vendar je cena teh okrog 20 do 25 krat višja (vprašanje, nekako ne ravno zaželjeno, je bilo postavljeno med diskusijo) kot cena običajnih Superstrate substratov.

J. Forbes (Selex, Anglija) je predstavil referat z naslovom "Ceramic interconnections in MW modules - users prespective". Selex je zelo veliko multi nacionalno podjetje, ki je nastalo z združitvijo Galileo Avionica and BAE Systems Avionics sredi leta 2005. Med ostalim razvijajo in izdelujejo sonzorje in radarske sisteme, predvsem za vojaško letalsko industrijo. Letalski radarji so sestavljeni iz 120 do 1500 mikro valovnih modulov. Te se običajno izdela v tankoplastni tehniki in nato pritrdi na plošče tiskanega vezja z ožičenjem - bondiranjem. To je zahteven in predvsem drag process. Predavatelj je opisal raziskave in razvoj novih, bolj preprostih in cenejših sistemo na osnovi tankih in debelih filmov. Zahtevane frekvence so med 8 in 12 GHz, širina prevodnih linij v komponentah pa okrog 10 um. Zato pri uporabi debeloplastnih materialov uporabljajo foto občutljive paste, ki se jih lahko zjedka na take dimenzije. Testirali so različne substrate z višjo toplotno prevodnostjo in kaže, da so se odločili za AlN, ki ima s 160 W/m okrog sedemkrat višjo toplotno prevodnost kot običajno uporabljan Al_2O_3. Problem pri tem materialu pa je, da velika večina komercialnih prevodnikov in uporov ni kompatibilna z njim. Zato nanesejo preko AlN substrata plast dielektrika, ki se z njim "ujema",. Ker je toplotna prevodnost steklastih dielektrikov bistveno nižja (dva do tri velikostne rede) od prevodnosti AlN, s tem seveda poslabšajo toplotne karakteristike. Na koncu si je, kot "uporabnik", zaželel debeloplastnih materialov, kompatibilnih z izbranimi substrati. V diskusiji je povedal, da bi bili verjetno za uporabne debeloplastne materiale, predvsem upore, pripravljeni plačati tudi deset krat več, kot stanejo komercialne paste.

Ostali referati, ki tukaj niso opisani, so obravnavali med ostalim računalniški paket za design tri dimenzionalnih MCM (Multi chip module) struktur (cena tega je približno 20000 $), tanke filme za aplikacije z visoko stopnjo integracije in precej splošno predstavitev o keramiki v mikroelektroniki.

Marko Hrovat
Institut Jožef Stefan, Jamova 39, 1000 Ljubljana

Povzetki magisterijev in doktorskih disertacij v letu 2005
MS and PhD Abstracts, year 2005

MAGISTERIJI v letu 2005

Naslov naloge: **Hibridni oscilator za digitalno zemeljsko televizijo**

Avtor: **KOSI Andrej**

Univerza v Mariboru, Fakulteta za elektrotehniko, računalništvo in informatiko

Povzetek

S hitrim razvojem elektronskih naprav se pojav!ja potreba po vedno bolj zmogljivih in kakovostnejših nastavljivih frekvenčnih virih. Namen magistrske naloge je izdelava in preizkus kakovostnega nastavljivega frekvenčnega vira. Področje, kjer bi lahko takšen ftekvenčni vir uporabili, je digitalna televizija. V zadnjih letih digitalna televizija zbuja vedno večje zanimanje. Pri prehodu na digitalno televizijo je eden ključnih elementov kakovosten oscilator nastavljive frekvence. Predstavljene so različne možnosti za izvedbo takšnega oscilatorja. Med različnimi možnosti smo izbrali tako imenovani hibridni oscilator za praktično izvedbo. Izraz hibridni oscilator združuje dva različna pristopa, in sicer sintezator z neposredno sintezo signala in fazno sklenjeno zanko. V magistrski nalogi sta predstavljena sintezator z neposredno sintezo signala in fazno sklenjena zanka. Predstavljeni so najpomembnejši sklopi, njihovo delovanje in praktični izračuni. Na podlagi vseh spoznanj smo izdelali prototip hibridnega oscilatorja za frekvenčno področje UHF. Opravili smo meritve, s katerimi smo izmerili lastnosti hibridnega oscilatorja. Prikazani so glavni problemi pri izvedbi hibridnega oscilatorja in možne rešitve teh.

Naslov naloge: **Raziskava električnih razmer v omejevalniku toka s tekočo kovino**

Avtor: **KOPRIVŠEK Mitja**

Univerza v Mariboru, Fakulteta za elektrotehniko, računalništvo in informatiko

Povzetek

Nizkonapetostna stikalna tehnika je širok nabor različnih aparatov, naprav in postrojev, ki se uporabljajo za izpolnjevanje različnih funkcij v električnih tokokrogih. V uvodu so prikazani različni stikalni principi, ki se uporabljajo v različnih stikalnih aparatih. Poudarek je na instalacijskih odklopnikih in taljivih varovalkah. V nadaljevanju je prikazano izpopolnjevanje zaščitne funkcije pri čemer je še posebno opredeljena vloga električnega obloka kot stikalnega elementa. Osrednji del je namenjen raziskavi električnih razmer v omejevalniku toka s tekočo kovino. Prikazana je primerjava električnih razmer v taljivi varovalki in omejevalniku s tekočo kovino. V sklepnem delu so podane smernice za nadaljnje raziskave na področju omejevalnikov toka.

Naslov naloge: **Enofazno galvansko ločeni usmernik s korekcijo faktorja moči**

Avtor: **KOLMAN Ludvik**

Univerza v Mariboru, Fakulteta za elektrotehniko, računalništvo in informatiko

Povzetek

V nalogi je predstavljen enostopenjski galvansko ločeni močnostni pretvornik s korekcijo faktorja moči. Opisana je izvedba prevodnega pretvornika z enim transistorskim stikalom, oziroma s prevodnim pretvornikom. Prevodni pretvornik z enim stikalom se uporablja za moči do 250W. Nad 1kW, pa se uporablja izvedba z dvojnim stikalom. V osnovi je enostopenjsko galvansko ločeni pretvornik s korekcijo faktorja moči izpeljan iz pretvornika navzdol. Uporablja se princip delovanja pretvornika navzgor s korekcijo faktorja moči ter zvezo med vhodno omrežno napetostjo in omrežnim tokom. Na tej osnovi je izdelan tudi stikalni regulator. Za shranite v energije in galvanske ločitve je uporabljen transformator in izhodni filter. Tako zastavljen pretvornik zadosti napetostnim in tokovnim zahtevam. Eksperimentalni rezultati za predlagano shemo 3500 W galvansko ločenega prevodnega pretvornika z enim stikalom kažejo vzpodbudne rezultate. Primerjava doseženih rezultatov z rezultati v literaturi, potrjuje uporabnost te vezave.

Naslov naloge: **Povezljive naprave in omrežni sistemi s področja hišne avtomatizacije**

Avtor: **Laura Klančnik**

Univerza v Ljubljani, Fakulteta za elektrotehniko

Povzetek

Magistrska naloga obravnava različne pristope k razvoju inteligentnih povezljivih naprav ter omrežij za potrebe hišne avtomatizacije.

Nekaj poglavij je posvečenih razlagi standardov, ki so bistven del razvoja omrežnih sistemov. Opisana sta dva komunikacijska standarda, ki izstopata na področju hišne avtomatizacije: LonWorks (de facto standard z 20 letno tradicijo), Konnex (novejši vseevropski standard, ki je še v procesu nastajanja).

Osnova za to nalogo je delo pri projektu Povezljivi aparati Gorenje, zato si posebno pozornost zasluži tudi CECED specifikacija, ki pokriva standardizacijo sporočil pri komunikaciji v omrežju gospodinjskih naprav.

Vedno bolj se poudarja pomembnost razvoja odprtih sistemov in omrežij. Uporaba OSGi standarda na strani hišnega strežnika omogoča ravno to - koeksistenco in interoperabilnost različnih standardov in komunikacijskih medijev v enem omrežju.

Na koncu naloge so vsa pridobljena znanja združena v različne možne izvedbe sistemov.

To magistrsko delo je ustvarjeno tudi z namenom njegove uporabe kot izhodiščne literature za pridobivanje osnovnih znanj s področja hišne avtomatizacije in lažje razumevanje dejanskih specifikacij omenjenih standardov, saj trenutno za to področje še ne obstaja literatura v slovenskem jeziku.

Naslov naloge: **Karakterizacija in analiza delovanja bralne elektronike amorfnosilicijevih detektorjev ultravijoličnega sevanja**

Avtor: **Andrej Žunič**

Univerza v Ljubljani, Fakulteta za elektrotehniko

Povzetek

Namen magistrske naloge je, na podlagi karakterizacije različnih konceptov bralne elektronike, določiti optimalen pretvornik za praktično realizacijo senzorskega sistema zaznavanja ultravijoličnega sevanja. O primernosti realizacije posameznega pretvornika bi se odločali na podlagi izmerjenih vhodnih območij pretvornikov, nelinearnosti, dinamičnih in šumnih lastnosti ter enostavnosti pretvorbe izhodne električne veličine v UV indeks in minimalno eritemalno dozo sevanja, ki določa zgornjo mejo zdravega izpostavljanja sončnim žarkom.

V uvodnem poglavju je opisana združljivost tankoplastnih polprevodniških tehnologij in mikroelektronskih tehnologij za naročniška integrirana vezja (ASIC). Za tankoplastne detektorje iz amorfnega silicija, ki so občutljivi v ultravijoličnem, vidnem in infrardečem spektru, so opisane zahteve, dogajanje znotraj plasti in njihove lastnosti. Narejen je tudi kratek pregled namensko integriranih vezij od njihovega začetka, ki sega v 80. leta. do današnjih dni.

V drugem poglavju na kratko, kolikor je potrebno za opravljanje meritev. opišemo delovanje posameznih pretvornikov: *I-f* pretvornika, ki izhodni tok detektorja pretvarja v frekvenco izhodnega signala pretvornika; *I-U* pretvornika, ki izhodni tok detektorja pretvarja v napetost na izhodu pretvornika; A-D pretvornika, ki analogni signal prevaja v digitalni izhodni signal; in *I-I* pretvornik, ki služi zgolj za zaščito bralne elektronike na vhodu vseh dosedanjih pretvornikov. Sledi opis načrtovanja oz. določitve debelin posameznih plasti UV detektorja. Bralna elektronika je načrtovana tako, da je možna direktna depozicija UV detektorja na njeno vrhnjo plast, zato smo opisali zaporedje nanosa plasti detektorja *pin* na bralno elektroniko in postopek plazemsko vzbujene kemijske parne depozicije (PECVD). Za točne meritve je potrebno zagotoviti ustrezne merilne pogoje. zato smo na koncu opisali postopek realizacije testne ploščice, na kateri so potekale vse meritve.

Poglavje o karakterizaciji je najobširnejše, ker je v njem zajeta glavnina raziskovalnega dela, zato je razdeljeno na štiri podpoglavja. Večinoma se posvečamo določanju električnih lastnosti pretvornikov. Zaradi različnih zahtev, kaj se tiče vzbujanja in oblike izhodnega signala, so bile za posamezen pretvornik izbrane različne merilne metode. Zato na začetku opišemo merilne metode za posamezen pretvornik, ki se med seboj razlikujejo tudi za določanje statičnih, dinamičnih kakor tudi šumnih lastnosti.

Nato za posamezen pretvornik podamo rezultate meritev, ki vključujejo statične, dinamične in šumne lastnosti. Pri statičnih lastnostih je podano merilno območje, izmerjena prenosna karakteristika, njen lineariziran potek in nelinearnost. Z dinamičnimi lastnostmi smo opisali obnašanje pretvornika pri sinusnem vzbujanju, vendar je bilo pri *I-f* pretvomiku to neizvedljivo, ker je pretvornik nelinearen sistem. V tem primeru smo podali le relacije med amplitudo vhodnega toka, frekvenco vhodnega signala in referenčno napetostjo pretvornika. Šumne lastnosti določajo prag pretvornika in posredno celotnega UV senzorja. zato jim je potrebno posvetiti posebno pozornost. Pri *I-f* pretvomiku smo pomerili odvisnost gostote močnostnega spektra tokovnega šuma od vhodnega toka in prišli do ugotovitve, da le-ta raste z vhodnim tokom. Ker je *I-U* pretvornik linearen sistem. smo zanj izdelali šumni model, ki ga sestavljata ekvivalentni tokovni šumni izvor in ekvivalentni napetostni šumni izvor. Pri *I-U* pretvorniku smo torej določili gostoto močnostnega spektra tokovnega in napetostnega šuma, ki nam skupaj podajata pravo sliko o šumnih lastnostih pretvornika. Napetostni prispevek upada z večanjem vhodne upornosti, za razliko od tokovnega, ki je neodvisen od upornosti na vhodu. Gostota močnostnega spektra tokovnega šuma analogno-digitalnega pretvornika vsebuje komponento kvantizacijskega šuma, ki smo ga zmanjšali z nizkopasovnim Butterworth-ovim filtrom različnih mejnih frekvenc. Raven spekter dobimo, če uporabimo filter drugega reda z mejno frekvenco pri 600 Hz.

V nadaljevanju 3. poglavja opišemo UV detektor z njegovimi optičnimi, električnimi, optoelektronskimi. dinamičnimi in šumnimi lastnostmi. Z optično analizo. s katero smo želeli doseči čim večjo občutljivost detektorja v UV spektru, smo iz primerjave lastnosti struktur *nip in pin* zaključili. da ima iz optičnega stališča boljše lastnosti slednja. Prav tako se je izkazala očitna prednost uporabe *strukture pin* v substrat konfiguraciji, kjer sta plasti *p* in *n* izdelani iz a-SiC:H s širšo optično režo, Pri čemer naj bo, zaradi dobrega kvantnega izkoristka, debelina prednje plasti *p* čim tanjša. Debelina plasti *i* pa je pogojena z razmerjem med absorbirano svetlobo v UV in vidnem. spektru. Primerjava potekov spek-

tralne občutljivosti različnih detektorskih struktur je pokazala, da je z linearno kombinacijo široko- in ozko-pasovnega detektorja dosežemo dobro korelacijo z dejanskim UV indeksom.

Na koncu opišemo koncept karakterizacije celotnega UV sistema, ki bo opravljena. ko bodo odpravljene težave z depozicijo UV detektorja na bralno elektroniko. Za karakterizacijo bi potrebovali ustrezen UV izvor s poznanim spektrom in referenčni senzor UV indeksa.

Končni cilj razvoja UV senzorja je izdelati cenovno sprejemljiv senzor UV indeksa. ki bi integriral UV indeks vse do minimalne eritemalne doze sevanj. ki predstavlja zgornjo mejo zdrave izpostavitve sončnim žarkom. Ker se izhodi pretvornikov med seboj razlikujejo, smo za vsakega od njih predvideli posebno logiko za določanje eritemalne doze sevanja. Ko bi uporabnik dosegel minimalno eritemalno dozo sevanja, bi ga na to opozoril pisk piezo piskača.

DOKTORSKE DISERTACIJE v letu 2005

Naslov disertacije: **Akcijska logika dreves izvajanj z operatorjem unless**

Avtor: **MEOLIČ Robert**

Univerza v Mariboru, Fakulteta za elektrotehniko, računalništvo in informatiko

Povzetek

Doktorska disertacija definira in raziskuje akcijsko logiko dreves izvajanj z operatorjem unless (ACTLW). ACTLW je izjavna temporalna logika razvejanega časa. Izhaja iz logike ACTL, ki je bila vpeljana leta 1990 in je ena od uveljavljenih temporalnih logik za izražanje lastnosti modelov, ki temeljijo na dogodkih. ACTLW je fleksibilnejša od ACTL, saj ne vsiljuje uporabe notranjega dogodka T pri izražanju lastnosti. ACTLW je tudi nekoliko izraznejša od ACTL, saj vsebuje temporalni operator unless (W), katerega pomena v ACTL ni možno v celoti izraziti. Nasprotno pa lahko vse formule ACTL izrazimo z uporabo operatorjev ACTLW. ACTLW omogoča učinkovito izvedbo preverjanja modelov s podobnimi algoritmi kot pri preverjanju modela s CTL, kar je pomembna izboljšava glede na logiko ACTL. Doktorska disertacija podaja definicijo logike ACTLW, izpeljave vseh standardnih temporalnih operatorjev in algoritme za globalno preverjanje modela z ACTLW s simboličnim računanjem. Predstavljeni so tudi algoritmi za tvorjenje diagnostike pri ACTLW, za tvorjenje lineamih prič in protiprimerov pri ACTLW ter za tvorjenje avtomatov prič in proti primerov pri ACTLW. Doktorska disertacija je v celoto zaokrožena z vzorci formul ACTLW in dvema večjima praktičnima primeroma: verifikacijo več različnih algoritmov za medsebojno izključevanje in verifikacijo dveh asinhronih vezij za porazdeljeno medsebojno izključevanje.

Naslov disertacije: **Novi postopki implementacije adaptivnih digitalnih sit s programirnimi vezji**

Avtor: **OSEBIK Davorin**

Univerza v Mariboru, Fakulteta za elektrotehniko, računalništvo in informatiko

Povzetek

V doktorski disertaciji se ukvarjamo s sistemi za digitalno obdelavo signalov in njihovo implementacijo. Pri sistemih digitalne obdelave signalov ločimo med izvedbo s signalnim procesOljem, ki temelji na uporabi programske opreme in izvedbo v strukturi programirnih logičnih vezji, ki temelji na uporabi aparaturne opreme. Izvedba s programirnimi vezji je zanimiva zaradi možnosti sočasnega izvajanja več aritmetičnih operacij. V doktorski disertaciji smo predstavili nove strukture funkcij za digitalno procesiranje signalov, ki so primerne za implementacijo v programirna vezja. Omejili smo se na funkcije, ki jih uporabljajo sistemi adaptivnih digitalnih FIR sit. Med različnimi adaptivnimi algoritmi za nerekurzivna digitalna sita smo zaradi enostavnega izračuna izbrali algoritem najmanjših srednjih kvadratov (LMS - least-means-squares) z nespremenljivo adaptivno konstanto. Omenjen algoritem smo uporabili v podsistemu za izračun koeficientov digitalnega sita. Algoritem temelji na dveh glavnih funkcijah: funkciji izračuna zmnožka produkta dveh vektorjev in funkciji izračuna vsote dveh vektorjev. Pri razvoju novih struktur teh funkcij v sistemih adaptivnih nerekurzivnih digitalnih sit s programirnimi vezji smo naredili modele na različnih nivojih. Z modeli na višjih nivojih smo opisali delovanje sistema adaptivnega digitalnega sita s plavajočo vejico. Z modeli na nižjih nivojih pa smo opisali delovanje sistema adaptivnega sita implementiranega v programirna vezja s celoštevilsko aritmetiko. Za izračun koeficientov smo z novimi strukturami funkcij zmanjšali aparaturno kompleksnost podsistema. Zato smo predlagali vhodno polje, ki bo aparaturno poenostavilo implementacijo polja množilnikov. Omenjeno vhodno polje se običajno uporablja pri nerekurzivnih digitalnih sitih v strukturi porazdeljene aritmetike. Za dodatno aparaturno poenostavitev implementacije smo predlagali uporabo enakega vhodnega polja tudi za medsebojno povezavo polja zaporednih množilnikov s poljem zaporednih seštevalnikov v enotni podsistem za izračun koeficientov. Predlagali smo tudi nov način implementacije LMS algoritma z nespremenljivo adaptivno konstanto (NLMS - normalized LMS) v programirna vezja s katerim bomo v celoti izkoristili procesno moč aparaturne opreme sistema. V novih strukturah smo podali ocene natančnosti izvajanja aritmetičnih operacij po naslednjih kriterijih: srednjega kvadratičnega odstopanja, porazdelitvene funkcije odstopanja in razmerja moči signal šum. Sistem adaptivnega FIR sita smo implementirali v dve programirni vezji družine XC4000E. Sistem ima 16 koeficientov, dolžina registrov za zapis vhodno-izhodne besede in notranje strukture je 16 bitov. Opisan sistem adaptivnega sita smo uporabili za izločanje motilnega signala iz koristnega signala. Pri tem smo s simulacijskimi rezultati v realnem okolju dosegli izboljšanje razmerja signal šum v poprečju za 12dB.

Naslov disertacije: **Zasnova večstoritvenega posrednika v telekomunikacijskih omrežjih naslednje generacije**

Avtor: **ALJAŽ Tomaž**

Univerza v Mariboru, Fakulteta za elektrotehniko, računalništvo in informatiko

Povzetek

Disertacija temelji na ugotovitvi, da trenutno uveljavljena arhitektura omrežij naslednje generacije ne more v celoti zagotoviti funkcionalnosti dopolnilnih storitev, ki jih omogoča signalizacija SS7 (ang. Signaling System No. 7) v klasičnem telefonskem omrežju, kar še posebej velja za tiste storitve, ki se nanašajo na identiteto uporabnika (telefonsko številko, ime ipd.), omejujejo njihovo komunikacijo in jo zakonito prestrezajo. V doktorski disertaciji predlagamo dopolnitev arhitekture omrežij naslednje generacije z novim omrežnim elementom, imenovanim večstoritveni posrednik (ang. Multi-Service Mediatar -MSM), za katerega smo zasnovali ustrezno arhitekturo in ključne protokole. Novi omrežni element omogoča tudi v telekomunikacijskih omrežjih naslednje generacije delovanje dopolnilnih storitev signalizacije SS7 in zakonito prestrezanje prometa v novi tehnologiji na enak način kot v klasičnih telefonskih omrežjih. Predlagana rešitev je popolnoma primerna za promet v realnem času, kot je prenos govora prek paketnega omrežja - VoIP, in minimalno vpliva na druge ključne arhitekturne gradnike omrežij naslednje generacije. Teoretične raziskave smo podkrepili s simulacijami na nivoju paketov IP telekomunikacijskega omrežja naslednje generacije z vključenim večstoritvenim posrednikom. S simulacijo smo preverili delovanje novega omrežnega večstoritvenega posrednika in določili njegovo minimalno zmogljivost obdelave paketov na sekundo, ki še zagotavlja primerno delovanje celotnega omrežja za različne oblike prometa VoIP.

Naslov disertacije: **Uporaba površinske mikroobdelave optičnega vlakna v senzorski tehniki in fotoniki**

Avtor: **CIBULA Edvard**

Univerza v Mariboru, Fakulteta za elektrotehniko, računalništvo in informatiko

Povzetek

Cilj disertacije je uvedba površinske mikroobdelave s selektivnim jedkanjem optičnega vlakna v aktualno področje MEMS in MOEMS tehnologij z realizacijo vrste miniaturnih senzorjev tlaka in raztezka ter mikroleč na vrhu optičnega vlakna. Predstavljeni senzorji delujejo na principu Fabry-Perot interferometra, ki omogoča visoko občutljivost in kompaktno miniaturno zasnovo senzorske strukture. Z namenom ocenitve možnosti in omejitev pri realizaciji senzorjev v takšni izvedbi smo izpeljali prenosno funkcijo Fabry-Perot interferometra z upoštevanjem geometrijskih lastnosti senzorske strukture. Kot prvo je prikazana izvirna tehnologija izdelave miniaturnega senzorja tlaka za biomedicinske in industrijske aplikacije. Senzor uporablja polimerno membrano, postavljeno v notranjost votlega distančnika, izdelanega z jedkanjem stopničnega mnogorodovnega vlakna v HF kislini. Zunanje dimenzije senzorja tako ne presegajo premera standardnega optičnega vlakna. Izdelani in preizkušeni so senzorji z elastično poliuretansko membrano ter senzor z membrano iz polistirena. Senzor s poliuretansko membrano zagotavlja visoko občutljivost in je zato primeren za biomedicinske aplikacije, kjer se zahteva merilno območje pod 40 kPa, senzor s polistirensko membrano pa je zaradi večjega modula elastičnosti primeren za merjenje višjih tlakov za različne industrijske aplikacije (do 1200 kPa). Posebnost senzorja v primerjavi z obstoječimi rešitvami je v izjemni občutljivosti, kjer smo dosegli ločljivost manj kot 10 Pa, ob sočasnem zmanjšanju zunanjih dimenzij na premer optičnega vlakna. Naslednji prispevekje realizacija senzorja raztezka, primernega za točkovne ali kvazi- porazdeljene meritve. Izpopolnjena tehnologija izdelave na osnovi selektivnega jedkanja vrha gradientnega optičnega vlakna v HF kislini z namenom pridobitve konkavne poglobitve in posebnim postopkom varjenja z enorodovnim vlaknom omogoča doseganje dovolj nizkih transmisijskih izgub senzorja, kar omogoča vezavo večjega števila senzorjev v kvazi-porazdeljen sistem. Dodatno je razvit originalni postopek za nastavitev delovne točke senzorja, s čimer zagotovimo linearen odziv senzorja na merjen raztezek in ponovljivost izdelave, kar je še posebej primerno za enostavno procesiranje signalov kvazi-porazdeljenega sistema z optičnim reflektometrom (OTDR). Pomembna lastnost senzorja raztezka je možnost samokompenzacije temperaturnega raztezka merjenca z uporabo dodatnega kompenzacijskega senzorja. Kot tretji prispevek predstavljamo originalno zasnovo in tehniko izdelave miniaturnega senzorja tlaka s SiO_2 membrano, za katerega je v primerjavi s senzorjem tlaka s polimerno membrano sicer značilna nižja občutljivost, odlikujejo pa ga visoka temperaturna (do 700°C) in kemična obstojnost. Bistvenega pomena je možnost doseganja poljubne občutljivosti senzorja v območju tlakov 0-40 kPa pa vse do nekaj sto MPa. Četrti prispevek je originalna zasnova in iznajdba postopka za izdelavo posebne senzorske strukture, ki omogoča pretvorbo merjenega tlaka, ki deluje na vlakno v radialni smeri, v vzdolžni raztezek. Na ta način smo dosegli možnost kvazi-porazdeljene meritve tlaka, kjer so posamezni senzorji locirani vzdolž enega optičnega vlakna. Takšna zasnova omogoča enostavno instalacijo kvazi-porazdeljenega senzorja na merilno mesto ter preprosto metodo procesiranja signalov z uporabo optičnega reflektormetra (OTDR). Kot zadnji primer uporabe površinske mikroobdelave vrha optičnega vlakna smo prikazali izvirno zasnovo in tehniko izdelave mikroleče na vrhu optičnega vlakna, uporabne za različne namene. Sem spadajo kolimacija in fokusiranje svetlobe na izhodu optičnega vlakna, povečanje sklopne učinkovitosti vlakna s svetlobnimi viri, detektorji ali drugim optičnim vlaknom, za uporabo v mikrooptiki itd. Posebnost

rešitve je v enostavnosti in prilagodljivosti postopka, ki s pomočjo razvitega simulacijskega algoritma jedkanja vrha vlakna omogoča realizacijo mikroleče z raznovrstnimi optičnimi lastnostmi. V primerjavi z obstoječimi rešitvami na tem področju mikroleča hkrati izpolnjuje zahteve po mehanski kompaktnosti, ustrezni poravnavi mikroleče z optičnim vlaknom, temperaturni in kemični obstojnosti itd.

Naslov disertacije: **Transport elektronov po minipasu polprevodniških superrešetk**

Avtor: **Uroš Merc**

Univerza v Ljubljani, Fakulteta za elektrotehniko

Povzetek

Polprevodniške superrešetke so nanometrske heterostrukture, zgrajene z izmenjujočim se periodičnim nanašanjem dveh polprevodniških materialov z različnima energijskima režama. Delovanje superrešetk temelji na resonančnem tuneliranju, ki je posledica interference valov v strukturah z dvema ali več potencialnimi barierami. Namen tega dela je bil predstaviti in nadgraditi fizikalno sliko delovanja struktur z resonančnim tuneliranjem. Pretežno smo se ukvarjali z modeliranjem in karakterizacijo struktur, pri čemer je bil poglavitni poudarek na novih, še ne poznanih lastnostih. Raziskave smo pričeli s strakturami z dvema in tremi barierami, ki predstavljajo uvod v raziskave superrešetk. Pri slednjih nas je se posebej zanimal transport elektronov po minipasu, preden le-ta razpade na diskretna lokalizirana energijska stanja. Prednost struktur, katerih osnovni princip delovanja temelji na resonančnem tuneliranju, je ta, da imajo njihove tokovno-napetostne karakteristike negativno diferencialno prevodnost. To je lastnost, ki omogoča izvedbo številnih novih in zanimivih načinov uporabe struktur, še posebej s področja optoelektronike.

Ker znašajo debeline plasti raziskovanih struktur tipično le nekaj nanometrov, je bilo potrebno celotno analizo delovanja izvajati z vidika kvantne mehanike in posledičnim reševanjem Schrodingerjeve valovne enačbe. Na podlagi teoretičnih osnov smo razvili dva kvantnomehanska numerična modela. Prvi je bil model matrik sipanja (model odprtih sistemov) in smo ga uporabljali za določanje prepustnostnih spektrov in valovnih funkcij elektronov z energijami višjimi od prevodnega pasu emitorja. Na ta način smo lahko nazorno analizirali princip nastanka energijskih minipasov in raziskovali vpliv električnega polja na resonančne vrhove. V model matrik sipanja smo vključili tudi zelo pomembno odvisnost efektivne mase elektrona od njegove energije. Drugi model je bil model lastnih vrednosti in lastnih vektorjev sistema (model zaprtih sistemov), in smo ga uporabljali za določanje lege energijskih nivojev in pripadajočih valovnih funkcij, ne glede na lego nivojev. Na osnovi obeh modelov smo raziskovali fizikalne pojave in sklepali o načinu delovanja struktur.

V disertaciji smo natančno raziskali vpliv električnega polja na resonančne vrhove prepustnostnih spektrov številnih struktur z različnim številom period. Na ta način smo lahko sklepali o lokalizaciji in delokalizaciji elektronov na posameznih energijskih nivojih. V nadaljevanju smo poskušali ugotoviti, ali koherentne lastnosti diod z resonančnim tuneliranjem z dvema barierama veljajo tudi za diode s tremi barierami. Pri tern smo raziskovali vpliv temperature in Fermijeve energije na tokovno-napetostno karakteristiko, ki smo jo določali na osnovi prepustnostnih spektrov. Naš namen je bil izdelati diodo s tremi barierami z izboljšanimi lastnostmi glede na diodo z dvema barierama, Raziskava je vključevala diode s protiodbojno zaščito, ki poveča vrhnjo tokovo gostoto in omogoča izvedbo struktur z višjimi barierami.

Primerjali smo različne hitrosti elektronov v superrešetkah in izpeljali skupinsko hitrost elektronov, ki temelji na modelu neskončnih struktur in se navadno uporablja kot hitrost elektronov v navadnih superrešetkah. Pokazali smo. da je zato, ker je transport elektronov določen z resonančnim tuneliranjem, dejanska hitrost elektronov hitrost tuneliranja, ki se jo določi s prepustnostnim spektrom, in se razlikuje od skupinske hitrosti. V disertaciji smo hitrost tuneliranja določili na dva načina: iz Lorentz-ove oblike resonančnih vrhov in iz faznih časov. Naše ugotovitve so pokazale, da je hitrost tuneliranja močno odvisna od robnih vrednosti in je neodvisna od dolžine strukture. Za razliko od skupinske hitrosti smo z uporabo hitrosti tuneliranja lahko določili tudi hitrost elektronov v različnih tipih superrešetk.

Poleg hitrosti je za transport elektronov po minipasu ključnega pomena tudi širina minipasu. V tern delu je izvirno predstavljena odvisnost širine minipasu od električnega polja. Zvezo med njima smo določili na osnovi lege energijskih nivojev in izvirnega določanja lokalizacijske dolžine elektronov neposredno iz valovne funkcije. Dobljeno odvisnost širine minipasu smo aproksimirali z analitično funkcijo in jo uporabili za nadgradnjo znamenitega Esaki-Tsu-jevega modela, ki določa zvezo med hitrostjo sipanih elektronov in električnim poljem. S primerjavo izračunanih rezultatov z izmerjenimi rezultati drugih raziskovalnih skupin smo pokazali, da je dejanska prostorska amplituda Bloch-ovih oscilacij določena z lokalizacijsko dolžino elektronov, in je manjša od amplitude, določene z disperzijsko relacijo.

Naslov disertacije: **Optimizacija analognih elektronskih vezij z dinamičnim izbiranjem algoritmov**

Avtor: **Andrej Nussdorfer**

Univerza v Ljubljani, Fakulteta za elektrotehniko

Povzetek

Doktorska disertacija obravnava dvostopenjsko kombinirano optimizacijsko metodo. Zaradi računske zahtevnosti optimizacijskih problemov je velik poudarek na raz-

voju računsko učinkovitejših optimizacijskih metod, Med drugimi je zelo razširjen večstopenjski pristop optimizacije. Pri tern pristopu skuša kombiniran algoritem izkoristiti dobre lastnosti sestavnih metod ob izogibanju slabih lastnosti le-teh.

Velik pomen pri optimizaciji ima tudi kriterijska funkcija sama. Posebej pri inženirskih optimizacijskih problemih je lahko kvaliteta rešitve zelo odvisna od lastnosti kriterijske funkcije. V splošnem so kriterijske funkcije optimizacijskih problemov nelineame funkcije parametrov problema, kar otežuje analitično obravnavo le-teh. Zaradi želje po robustnosti rezultatov je bil vpeljan zapis kriterijske funkcije s kazenskim in kompromisnim področjem ter princip ogljiščnih točk. Tak zapis se je v praksi izkazal za zelo uspešnega. V disertaciji je pokazana analitična obravnava take kriterijske funkcije. pri čemer so predstavljene določene uporabne lastnosti takega zapisa. Te namreč nakazujejo možnost razvoja učinkovitejših večstopenjskih optimizacijskih algoritmov.

Na podlagi pokazanih lastnosti sta bili izbrani sestavni optimizacijski metodi, to sta Box-ova metoda omejenih simpleksov in metoda področja zaupanja. Za metodo področja zaupanja je poleg algoritma pokazana teoretična obravnava in močni konvergenčni teoremi. Za Box-ovo metodo omejenih simpleksov pa je prikazan le algoritem sam, saj za to metodo ni konvergenčnih teoremov, oziroma so ti zelo šibki in omejeni na majhno skupino funkcij.

Vsaka večstopenjska metoda vsebuje tudi mehanizem za preklop med metodami. Pokazano je nekaj primerov takih kombiniranih metod. Opisana je tudi izbrana preklopna strategija.

Sestavni deli kombinirane optimizacijske metode so nato združeni v celovit algoritem. Ta algoritem je tudi implementiran in preizkušen na nizu optimizacijskih primerov. Ti primeri gredo od optimizacije analitičnih funkcij do realnih optimizacijskih problemov. Rezultati optimizacijskih poskusov so pokazali, da je predstavljena kombinirana optimizacijska metoda učinkovitejša od obeh posameznih sestavnih metod.

Nazadnje so pokazane pomanjkljivosti kombinirane metode ter nakazane možnosti za nadaljnjo izboljšavo.

Informacije MIDEM
Strokovna revija za mikroelektroniko, elektronske sestavine dele in materiale

NAVODILA AVTORJEM

Informacije MIDEM je znanstveno-strokovno-društvena publikacija Strokovnega društva za mikroelektroniko, elektronske sestavne dele in materiale - MIDEM. Revija objavlja prispevke s področja mikroelektronike, elektronskih sestavnih delov in materialov. Ob oddaji člankov morajo avtorji predlagati uredništvu razvrstitev dela v skladu s tipologijo za vodenje bibliografij v okviru sistema COBISS.
Znanstveni in strokovni prispevki bodo recenzirani.

Znanstveno-strokovni prispevki morajo biti pripravljeni na naslednji način:
1. Naslov dela, imena in priimki avtorjev brez titul, imena institucij in firm
2. Ključne besede in povzetek (največ 250 besed).
3. Naslov dela v angleščini.
4. Ključne besede v angleščini (Key words) in podaljšani povzetek (Extended Abstract) v anglešcčini, če je članek napisan v slovenščini
5. Uvod, glavni del, zaključek, zahvale, dodatki in literatura v skladu z IMRAD shemo (Introduction, Methods, Results And Discsussion).
6. Polna imena in priimki avtorjev s titulami, naslovi institucij in firm, v katerih so zaposleni ter tel./Fax/Email podatki.
7. Prispevki naj bodo oblikovani enostransko na A4 straneh v enem stolpcu z dvojnim razmikom, velikost črk namanj 12pt. Priporočena dolžina članka je 12-15 strani brez slik.

Ostali prispevki, kot so poljudni cčlanki, aplikacijski članki, novice iz stroke, vesti iz delovnih organizacij, inštitutov in fakultet, obvestila o akcijah društva MIDEM in njegovih članov ter drugi prispevki so dobrodošli.

Ostala splošna navodila
1. V članku je potrebno uporabljati SI sistem enot oz. v oklepaju navesti alternativne enote.
2. Risbe je potrebno izdelati ali iztiskati na belem papirju. Širina risb naj bo do 7.5 oz.15 cm. Vsaka risba, tabela ali fotografija naj ima številko in podnapis, ki označuje njeno vsebino. Risb, tabel in fotografij ni potrebno lepiti med tekst, ampak jih je potrebno ločeno priložiti članku. V tekstu je treba označiti mesto, kjer jih je potrebno vstaviti.
3. Delo je lahko napisano in bo objavljeno v slovenščini ali v angleščini.
4. Uredniški odbor ne bo sprejel strokovnih prispevkov, ki ne bodo poslani v dveh izvodih skupaj z elektronsko verzijo prispevka na disketi ali zgoščenki v formatih ASCII ali Word for Windows. Grafične datoteke naj bodo priložene ločeno in so lahko v formatu TIFF, EPS, JPEG, VMF ali GIF.
5. Avtorji so v celoti odgovorni za vsebino objavljenega sestavka.

Rokopisov ne vračamo. Rokopise pošljite na spodnji naslov.

Uredništvo Informacije MIDEM
MIDEM pri MIKROIKS
Stegne 11, 1521 Ljubljana, Slovenia
Email: Iztok.Sorli@guest.arnes.si
tel. (01) 5133 768, fax. (01) 5133 771

Informacije MIDEM
Journal of Microelectronics, Electronic Components and Materials

INSTRUCTIONS FOR AUTHORS

Informacije MIDEM is a scientific-professional-social publication of Professional Society for Microelectronics, Electronic Components and Materials - MIDEM. In the Journal, scientific and professional contributions are published covering the field of microelectronics, electronic components and materials.
Authors should suggest to the Editorial board the classification of their contribution such as : original scientific paper, review scientific paper, professional paper...
Scientific and professional papers are subject to review.

Each scientific contribution should include the following:
1. Title of the paper, authors' names, name of the institution/company.
2. Key Words (5-10 words) and Abstract (200-250 words), stating how the work advances state of the art in the field.
3. Introduction, main text, conclusion, acknowledgements, appendix and references following the IMRAD scheme (Introduction, Methods, Results And Discsussion).
4. Full authors' names, titles and complete company/institution address, including Tel./Fax/Email.
5. Manuscripts should be typed double-spaced on one side of A4 page format in font size 12pt. Recommended length of manuscript (figures not included) is 12-15 pages
6. Slovene authors writing in English language must submit title, key words and abstract also in Slovene language.
7. Authors writing in Slovene language must submit title, key words and extended abstract (500-700 words) also in English language.

Other types of contributions such as popular papers, application papers, scientific news, news from companies, institutes and universities, reports on actions of MIDEM Society and its members as well as other relevant contributions, of appropriate length , are also welcome.

General informations
1. Authors should use SI units and provide alternative units in parentheses wherever necessary.
2. Illustrations should be in black on white paper. Their width should be up to 7.5 or 15 cm. Each illustration, table or photograph should be numbered and with legend added. Illustrations, tables and photographs must not be included in the text but added separately. However, their position in the text should be clearly marked.
3. Contributions may be written and will be published in Slovene or English language.
4. Authors must send two hard copies of the complete contributon, together with all files on diskette or CD, in ASCII or Word for Windows format. Graphic files must be added separately and may be in TIFF, EPS, JPEG, VMF or GIF format.
5. Authors are fully responsible for the content of the paper.

Contributions are to be sent to the address below.

Uredništvo Informacije MIDEM
MIDEM pri MIKROIKS
Stegne 11, 1521 Ljubljana, Slovenia
Email: Iztok.Sorli@guest.arnes.si
tel.+386 1 5133 768, fax.+386 1 5133 771